SEDIMENTOLOGY AND DIAGENESIS OF LOWER TO MIDDLE CAMBRIAN CARBONATE PLATFORM, SHADY DOLOMITE, VIRGINIA

by

Roger Joseph Barnaby

Dissertation submitted to the Faculty of the

Virginia Polytechnic Institute and State University

in partial fulfillment of the requirements for the degree of

DOCTOR OF PHILOSOPHY

in

Geology

APPROVED:

J. F. Read, Chairman

J. R. Craig

L. Glover III

J. D. Rimstidt

A. K. Sinha

August, 1989

Blacksburg, Virginia

ABSTRACT

Drill cores through the Lower to Middle Cambrian Shady Dolomite carbonate platform (600 to 1200 m thick) in the Austinville, Virginia, region allow the evolution of the carbonate platform from a gently sloping ramp, to a high relief, rimmed shelf to be documented. The Shady Dolomite forms the initial carbonate foundation for the overlying Cambrian-Ordovician carbonate shelf sequence, which persisted for about 30 m.a. until it was destroyed by incipient collision during the Early Ordovician.

The Shady Dolomite records several episodes of dolomitization during burial, coeval with late Paleozoic deformation. Rare relict cores of zone 1 dolomite were replaced and overgrown by zone 2A dolomite, the dominant replacement phase. After replacement dolomitization, the sequence was subjected to dissolution and fracturing, followed by Pb-Zn mineralization, zones 2B, 3 and 4 dolomite cement, sphalerite, quartz, and calcite.

Zone 1 dolomite apparently has similar isotopic and trace element composition as zone 2A dolomite. Zone 2A dolomite ($\delta^{18}O$ = -10.2 to -7.0 ‰ PDB; $\delta^{13}C$ = +1.0 to +1.6 ‰ PDB) is depleted in ^{18}O and enriched in ^{13}C relative to marine cements ($\delta^{18}O$ = -7.5 to -6.1; $\delta^{13}C$ = +0.2 to +0.8), reflecting precipitation at elevated temperatures from fluids in equilibrium with the host limestone. Zone 2B dolomite cement has identical $\delta^{18}O$ values as zone 2A dolomite, indicating precipitation from similar fluids for the two dolomite generations. The Mn and Fe contents of zones 2A and 2B dolomite likely reflect a pH control over the fluid Mn and Fe chemistry; their similar low total Sr and nonradiogenic $^{87}Sr/^{86}Sr$, imply that Sr was largely derived from the limestone precursor.

Zones 3 and 4 dolomite cements ($\delta^{18}O$ = -13.8 to -11.3; $\delta^{13}C$ = -0.7 to +0.9) are depleted in ^{18}O relative to previous dolomites, recording hotter fluids. Zone 3 dolomite is depleted in Fe, due to pyrite precipitation whereas zone 4 dolomite cement has relatively

high Mn and Fe contents. Zones 3 and 4 dolomite cements and later calcite are enriched in total Sr and have high $^{87}Sr/^{86}Sr$, indicating late radiogenic Sr-enriched brines.

Fluid inclusions indicate that zones 2A and 2B dolomite precipitated from warm (100 - 175°C), saline (23 - 26 wt.% NaCl equiv.) fluids, followed by later hotter (175 - 225°C) more saline (30 - 33 wt.% NaCl equiv.) fluids. Pressure solution of the Knox Group dolomites during overthrusting provided much of the Mg^{2+} for dolomitization, this Mg^{2+} was transported by regional gravity-driven fluid flow that developed in response to tectonic uplift.

ACKNOWLEDGEMENTS

First, I would like to thank my advisor J. Fred Read, who suggested this project to me, assisted in all stages of the work, and provided financial support. Dr. A. K. Sinha allowed use his lab for preparation of ICP analyses and acted as a committee member. Dr.'s J. R. Craig, L. Glover III, and J. D. Rimstidt acted as committee members, and generously shared their expertise.

New Jersey Zinc Corporation and Austinville Limestone Company donated drill core for the study. T. Gathright of the Virginia Division of Mineral Resources assisted in obtaining copies of mine maps showing drill core locations. ICP analyses were conducted at the Soil Testing and Plant Analysis Laboratory at Virginia Tech under direction of and . Stable isotope analysis of carbonates was conducted at Stable Isotope Laboratory, University of Miami, Rosenstiel School of Marine and Atmospheric Sciences, under the direction of . $^{87}Sr/^{86}Sr$ analyses were conducted by Chempet Research Corporation, under the direction of and . Thanks are extended to and for graciously conducting ^{18}O analyses of quartz and to for invaluable assistance in interpreting fluid inclusion data. kindly helped with microprobe analyses. Thanks are especially extended to fellow students , , who were the source of many interesting ideas and discussions. Many graduate students, including , , , , and also shared their expertise, and helped me refine my interpretations. Drafting was done by and assisted with photography. , , , and helped with core logging and sample preparation.

Financial support provided by Grant EAR 87-07737 from the National Science Foundation to J.F. Read, and grants from Texaco, Chevron, Appalachian Basin Industrial Associates, Geological Society of America, and a Grant-in-Aid of Research from the Scientific Research Society of Sigma Xi.

TABLE OF CONTENTS

CARBONATE RAMP TO RIMMED SHELF EVOLUTION: LOWER TO MIDDLE CAMBRIAN CONTINENTAL MARGIN, VIRGINIA APPALACHIANS 1

Abstract 2

Introduction 3

Geologic and Stratigraphic Setting 10

Platform to Basin Sequence 19

Lithofacies and Depositional Environments 24

Coastal and Peritidal Sequences 24

Cyclic Redbeds and Carbonates 24

Cyclic Peritidal Carbonates and Massive Dolomite 29

Organic Buildups 30

Carbonate Banks 30

Reefs and Back Reef Sands (Shelf Edge Facies) 31

Deeper Water Carbonates 33

Nodular Bedded Wackestone/Mudstone 33

Limeclast Sands (Foreslope Deposits) 35

Periplatform Breccia Deposits 36

Black Shaly Carbonates, Slope Breccias, and Shales 37

Carbonate Platform Evolution 39

Carbonate Ramp Phase 39

Drowning Phase and Initiation of Rimmed Shelf 45

Rimmed Shelf Phase..... 45
Comparison with Lower to Middle Cambrian Margins Elsewhere in North America..... 47
Conclusions..... 49

DOLOMITIZATION OF A CARBONATE PLATFORM DURING DEEP BURIAL: LOWER TO MIDDLE CAMBRIAN SHADY DOLOMITE, VIRGINIA APPALACHIANS..... 51
Abstract..... 52
Introduction..... 54
Methods..... 63
Marine Cements..... 65
Petrography and Geochemistry..... 65
Interpretation..... 66
Early Dissolution and Calcite Cementation..... 71
Description..... 71
Interpretation..... 72
Dolomite and Later Diagenetic Phases..... 75
Dolomite Distribution..... 75
Petrography..... 76
Replacement Dolomite (Zones 1, 2A)..... 76
Secondary Dissolution and Fracture Porosity..... 77
Pb-Zn Ore Deposition..... 82
Dolomite Cement (Zones 2B, 3, 4)..... 82

Authigenic Quartz..... 86
Late Calcite and Dedolomite..... 86
Geochemistry..... 87
Dolomite..... 87
Dolomite Stoichiometry..... 87
Dolomite $\delta^{18}O$ Composition..... 87
Dolomite $\delta^{13}C$ Composition..... 90
Dolomite Mn and Fe Contents..... 90
Dolomite Total Sr and $^{87}Sr/^{86}Sr$ Compositions..... 95
Authigenic Quartz..... 95
Late Calcite and Dedolomite..... 95
Fluid Inclusions..... 98
Primary Fluid Inclusions- Sphalerite..... 98
Primary Fluid Inclusions- Zone 2B Dolomite..... 98
Primary Fluid Inclusions- Late Calcite..... 98
Secondary Fluid Inclusions- Authigenic Quartz and Late Calcite..... 103
Geological and Petrographic Evidence of Timing of Paragenetic Sequence..... 108
Zone 1 Replacement Dolomite..... 108
Zone 2A Replacement Dolomite..... 108
Pb-Zn Ore Deposition..... 109
Zones 2B, 3, and 4 Dolomite Cements..... 110
Late Quartz and Calcite..... 110
Burial History and Diagenetic Temperatures..... 111

Burial History..... 111
Thermal History..... 113
Interpretation of Geochemistry..... 116
Significance of Dolomite Stoichiometry..... 116
Interpretation of $\delta^{18}O$ Composition..... 116
Interpretation of $\delta^{13}C$ Composition..... 121
Interpretation of Mn and Fe Contents..... 126
Interpretation of Total Sr and $^{87}Sr/^{86}Sr$ Compositions..... 131
Origin of Late Diagenetic Sequence..... 135
Zone 1 Replacement Dolomite..... 135
Zone 2A Replacement Dolomite..... 136
Burial Dissolution and Zn-Pb Mineralization..... 138
Zone 2B Dolomite Cement..... 140
Zones 3 and 4 Dolomite Cement..... 141
Authigenic Quartz..... 142
Late Calcite and Dedolomite..... 143
Regional Fluid Flow..... 144
Source of Mg^{2+}..... 146
Conclusions..... 149
REFERENCES..... 153
APPENDIX I..... 173
APPENDIX II..... 179
APPENDIX III..... 183
APPENDIX IV..... 185

APPENDIX V..... 189
VITA..... 191

LIST OF TABLES

TABLE 1. Trace Element and Isotope Geochemistry..... 68

LIST OF FIGURES

Figure 1. Geological map of Austinville region..... 5

Figure 2. Isopach map, palinspastic base..... 7

Figure 3. Regional stratigraphic cross-section..... 9

Figure 4. General stratigraphic section..... 12

Figure 5. General cross-section, Shady Dolomite and Rome Formation..... 15

Figure 6. Stratigraphic cross-section, across strike..... 18

Figure 7. Stratigraphic cross-section, across strike..... 21

Figure 8. Stratigraphic cross-section, along strike..... 23

Figure 9. Photographs of representative lithofacies..... 26

Figure 10. Relative sea level curve..... 41

Figure 11. Block diagrams summarizing evolution of platform margin..... 43

Figure 12. Regional balanced cross-section..... 58

Figure 13. Stratigraphic cross section showing dolomite distribution..... 60

Figure 14. Paragenetic sequence, Shady Dolomite..... 62

Figure 15. Stable isotope data..... 70

Figure 16. Photographs of dolomite types..... 74

Figure 17. Photographs of replacement dolomite fabrics..... 79

Figure 18. Photograph of zone 1 dolomite cores..... 81

Figure 19. Photographs of dissolution and dolomite cement fabrics..... 84

Figure 20. Zone 2A geochemistry versus crystal size..... 89

Figure 21. Mn and Fe chemistry..... 92

Figure 22. Mn versus Fe, zone 2A dolomite..... 94

Figure 23. $^{87}Sr/^{86}Sr$ data..... 97

Figure 24. Fluid inclusion data..... 100

Figure 25. Fluid inclusion pressure corrections..... 102

Figure 26. Quartz fluid inclusions, Th versus salinity..... 105

Figure 27. Photograph of 3-phase inclusions in quartz..... 107

Figure 28. $\delta^{18}O$ composition of dolomite and water versus temperature..... 120

Figure 29. Water-rock modelling of $\delta^{13}C$ composition..... 124

Figure 30. Sr versus Mn and Fe, zone 2A dolomites..... 129

CARBONATE RAMP TO RIMMED SHELF EVOLUTION: LOWER TO MIDDLE CAMBRIAN CONTINENTAL MARGIN, VIRGINIA APPALACHIANS

ABSTRACT

Drill cores through the Lower to Middle Cambrian Shady Dolomite carbonate platform (600 to 1200 m thick) in the Austinville, Virginia, region have provided critical platform margin facies relations not exposed in outcrop. The control provided by the closely-spaced drill cores has allowed detailed cross-sections to be constructed through the margin, which allow the evolution of the carbonate platform from a gently sloping, carbonate ramp, to a high relief, reef-rimmed shelf to be interpreted. The Shady Dolomite records the inception of carbonate sedimentation on the Lower Cambrian passive margin and forms the initial carbonate foundation for the overlying Cambrian-Ordovician carbonate shelf sequence.

Carbonate sedimentation was initiated on a submerged Lower Cambrian clastic shelf, resulting in deposition of a thick sequence (300 m) of deep ramp, nodular limestones. This facies shallows upward into a carbonate ramp fringed by low-relief, stromatactoid mudmound buildups (up to 30 m thick, and 3.5 km wide). Downslope these buildups pass into slope conglomerate and deep ramp carbonate facies; landward of the buildups, cyclic peritidal sequences developed. By latest Early Cambrian time, as the ramp increased in relief, skeletal algal bioherms and lime sands were established on the high energy margin to form a high relief (up to 500 to 700 m), rimmed shelf with thick (>600 m) off-platform deposits immediately seaward of the shelf edge. In the shelf interior, a major regression during Early to Middle Cambrian time resulted in development of a major unconformity and in deposition of redbeds. On the more rapidly subsiding outer platform, subsidence rates exceeded sea level fall rates, allowing continued upbuilding of the reefal rimmed shelf.

This rimmed shelf persisted for about 30 m.a. and influenced carbonate sedimentation throughout the Cambrian until it was destroyed by incipient collision during the Early Ordovician (Read, in press a).

INTRODUCTION

Cambrian and Ordovician carbonate rocks of the Appalachians accumulated on an extensive carbonate continental shelf which fringed eastern North America. Rodgers (1968) proposed that the platform margin was a high relief, shelf edge with an abrupt transition from shallow platform carbonate rocks to deep water, basinal facies. One of the proposed locations of this platform margin was near Austinville, Virginia (Figs. 1, 2, 3). Studies of the limited exposures of the Shady Dolomite in this region (Byrd, 1973; Pfeil, 1977; Pfeil and Read, 1980), documented an overall platform to basin transition, however, the poor exposures did not allow detailed reconstruction of the margin. Read and Pfeil (1983) reinterpreted the algal block bearing horizons, previously interpreted as shelf edge reefs (Pfeil and Read, 1980), as being allochthonous debris derived from a reefal rim that was not exposed in outcrop.

This high-relief, rimmed shelf along the Cambrian carbonate platform margin is evident elsewhere in the Appalachians (Rodgers, 1968), including western Newfoundland (James, 1981; James and Stevens, 1986), Pennsylvania (Gohn, 1976), and Maryland (Reinhardt, 1974; 1977; Demicco, 1985). However, in-place, Lower Paleozoic continental margin facies are not exposed in outcrop along eastern North America, and the nature of the shelf edge previously could only be inferred from the composition of allochthonous clasts in adjacent periplatform deposits. This study

Figure 1. Geological map of Austinville region (modified from Weinberg, 1971). Numbered dots refer to drill cores used in construction of cross sections (dashed lines). Numbers correspond to the following New Jersey Zinc Company drill cores: 1 = A679; 2 = A652; 3 = A92; 4 = A643; 5 = A616; 6 = A618; 7 = A623; 9 = A359; 10 = A241; 11 = A458; 12 = A682; 13 = A583; 14 = A591.

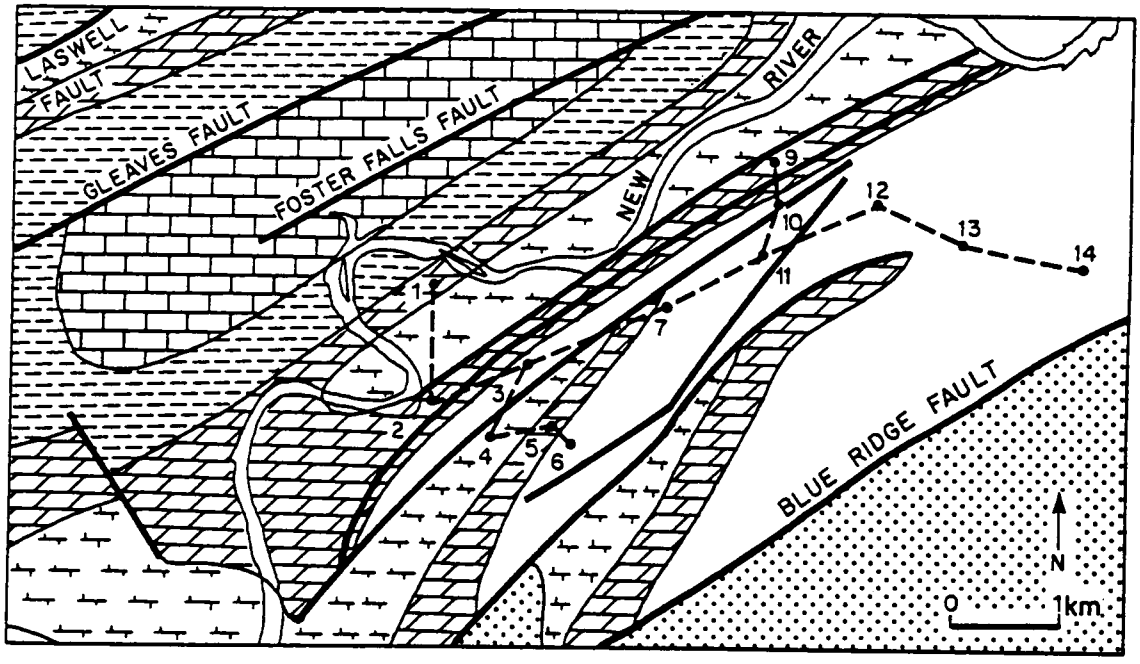
LASWELL FAULT
GLEAVES FAULT
FOSTER FALLS FAULT
NEW RIVER
BLUE RIDGE FAULT
1
2
3
4
5
6
7
9
10
11
12
13
14
N
0
1km

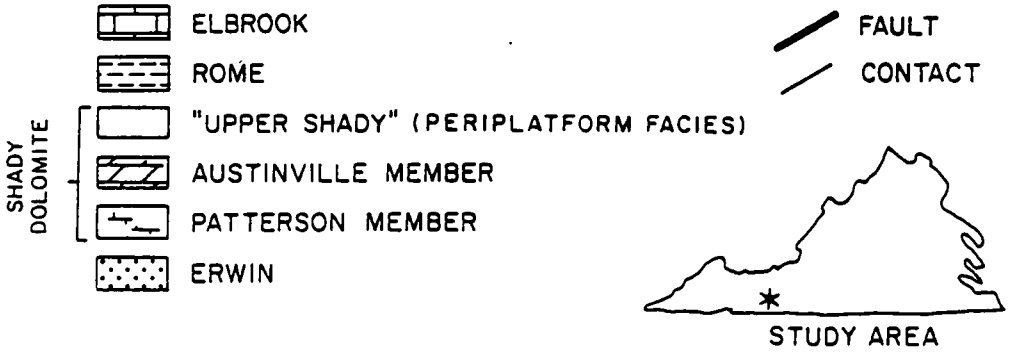
ELBROOK
ROME
"UPPER SHADY" (PERIPLATFORM FACIES)
AUSTINVILLE MEMBER
PATTERSON MEMBER
ERWIN
SHADY DOLOMITE
FAULT
CONTACT
STUDY AREA

Figure 2. Isopach map, palinspastic base showing regional thickness of Shady Dolomite and Rome Formation in the U.S. Appalachians; contours in meters. Heavy line at bottom of diagram is southeastern limit of carbonate shelf (after Read, in press a). Outline of the State of Virginia is dashed.

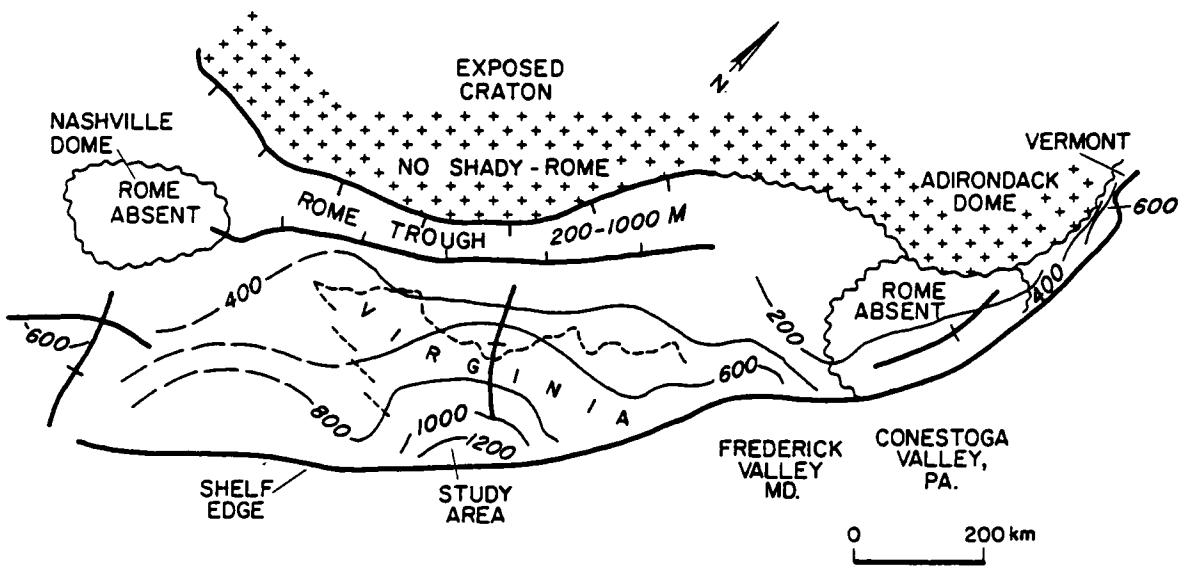
EXPOSED
CRATON
N
NASHVILLE
DOME
ROME
ABSENT
NO SHADY - ROME
ROME TROUGH
200-1000 M
VERMONT
ADIRONDACK
DOME
600
400
600
200
ROME
ABSENT
400
V I R G I N I A
600
800
1000
1200
SHELF
EDGE
STUDY
AREA
FREDERICK
VALLEY
MD.
CONESTOGA
VALLEY,
PA.
0
200 km

Figure 3. Regional stratigraphic cross-section (after Read, in press a), extending from the Rome Trough into the study area.

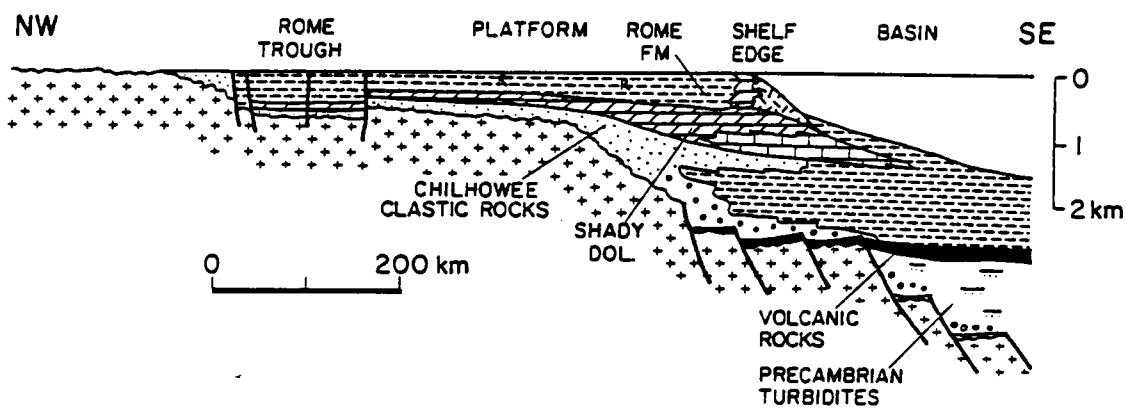
NW
ROME TROUGH
PLATFORM
ROME FM
SHELF EDGE
BASIN
SE
0
1
2 km
CHILHOWEE CLASTIC ROCKS
SHADY DOL
0
200 km
VOLCANIC ROCKS
PRECAMBRIAN TURBIDITES

documents the facies relations of the Lower to Middle Cambrian carbonate platform, based on 26 drill cores (9000 meters, total length) forming several transects through the critical platform margin transitions of the Shady Dolomite in the Austinville, Virginia region (Fig. 1). These cores have recovered the first known occurrence of in-place, shelf edge facies from the Cambrian continental margin of eastern North America. The control provided by closely-spaced cores allows detailed cross sections to be constructed, from which the evolution of the margin from a carbonate bank-dominated ramp to a reef-rimmed shelf can be interpreted.

The Shady Dolomite is of considerable interest because it represents the initial carbonate phase of the Cambrian continental shelf which developed on a basal clastic, fluvial to marine shelf system following Late Proterozoic rifting. Thus it may be a useful analog for initial phases of carbonate platforms which developed on other rifted margins such as the poorly explored, deeply buried Jurassic-Cretaceous carbonate shelf beneath the continental shelf of the eastern U.S.

GEOLOGIC AND STRATIGRAPHIC SETTING

Rifting of 1 b.y. old, North American Grenville basement rocks during the Late Precambrian resulted in initiation of an east-facing continental margin at approximately 690 m.a. (Wehr and Glover, 1985). A second rifting episode during the late Proterozoic to Early Cambrian affected the continental margin (Bond and others, 1984; Simpson and Eriksson, 1989; Patterson, 1987). Rb-Sr dating of volcanic rift basalts (Fig. 4) (Badger and Sinha, 1988) and fossils from rift-related clastic rocks (Simpson and Sundberg, 1987), suggest that this later rift event spanned the Precambrian-Early Cambrian

Figure 4. General stratigraphic section of Cambrian Chilhowee Group and Shady Dolomite/Rome sequence. Biostratigraphic ages for Chilhowee Group from Simpson and Sundberg (1987); biostratigraphic ages for Shady Dolomite from Willoughby (1977).

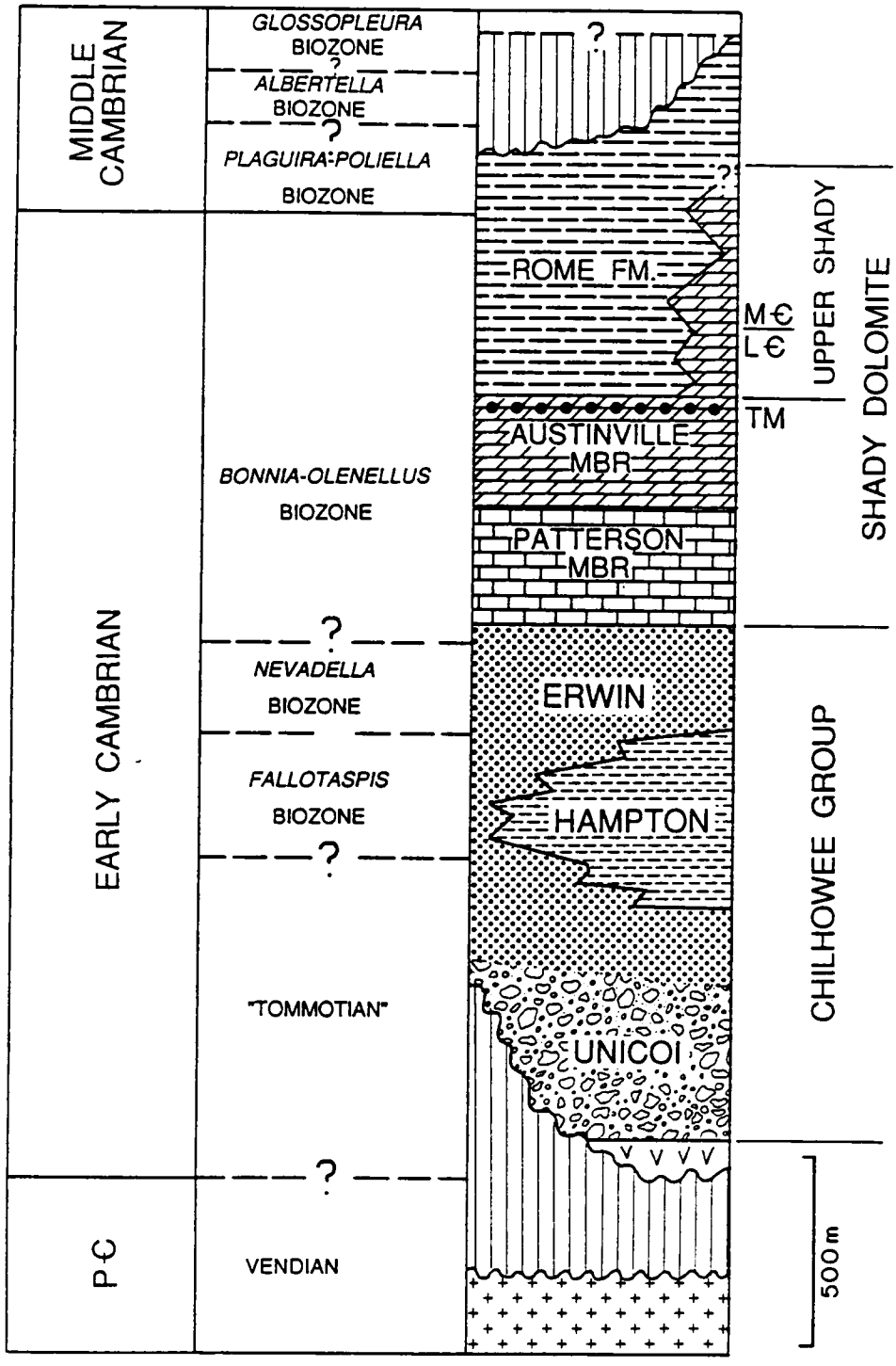
MIDDLE CAMBRIAN
EARLY CAMBRIAN
P-Є
GLOSSOPLEURA BIOZONE
ALBERTELLA BIOZONE
PLAGUIRA-POLIELLA BIOZONE
BONNIA-OLENELLUS BIOZONE
NEVADELLA BIOZONE
FALLOTASPIS BIOZONE
"TOMMOTIAN"
VENDIAN
ROME FM.
AUSTINVILLE MBR
PATTERSON MBR
ERWIN
HAMPTON
UNICOI
M-Є
L-Є
TM
UPPER SHADY
SHADY DOLOMITE
CHILHOWEE GROUP
500 m

boundary (≈570 m.a.) and may have continued into the early Early Cambrian period. Upper Proterozoic (?) to Lower Cambrian, Chilhowee Group clastic rocks (1200-1800 m) record a transition from rift and alluvial arkosic clastic sediments to marine shelf quartz arenites during the early Early Cambrian (Figs. 3, 4), reflecting the cessation of active rifting and the onset of passive margin development (Simpson and Eriksson, 1989). Sedimentation subsequently was controlled by thermotectonic subsidence (Bond and others, 1984) and eustatic sea level fluctuations rather than by active rifting (Simpson and Eriksson, 1989). Evolution of the Upper Proterozoic to Cambrian continental margin is discussed in Wehr and Glover (1985), Simpson (1987), Patterson (1987), Simpson and Eriksson (1989), and Read (in press a, b).

The Lower Cambrian Shady Dolomite (600 m) conformably overlies Chilhowee Group clastic rocks (Figs. 3, 4), recording the inception of carbonate sedimentation on the Lower Cambrian passive margin. Interior platform facies of the Shady Dolomite are overlain by cyclic red mudrocks and carbonate rocks of the Lower to Middle Cambrian Rome Formation (600-900 m), which pass southeast into the time equivalent, platform margin and periplatform facies (600 m) of the upper Shady Dolomite (Figs. 3, 4, 5), (Pfeil and Read, 1980). The Rome Formation is overlain by the Middle Cambrian Elbrook Dolomite (400-600 m) (Butts, 1940; Cooper and others, 1961).

The Shady Dolomite was thrust northwest over the Rome Formation along the Laswell fault and was overthrust along the Blue Ridge fault to the southeast by Cambrian and Precambrian metasedimentary and igneous rocks of the Blue Ridge (Fig. 1). Palinspastic reconstructions place the platform margin of the Shady Dolomite a minimum 100 kilometers southeast of its present location (Fig. 2). The critical platform margin transitions occur within the Laswell thrust sheet where the Shady Dolomite is cut by small

Figure 5. Generalized cross section of Shady Dolomite and Rome Formation in Austinville region. Vertical lines delimit extent of core control, dashed line indicates measured section from Pfeil and Read (1980). Q refers to quartzose lime sand unit (Taylor Marker).

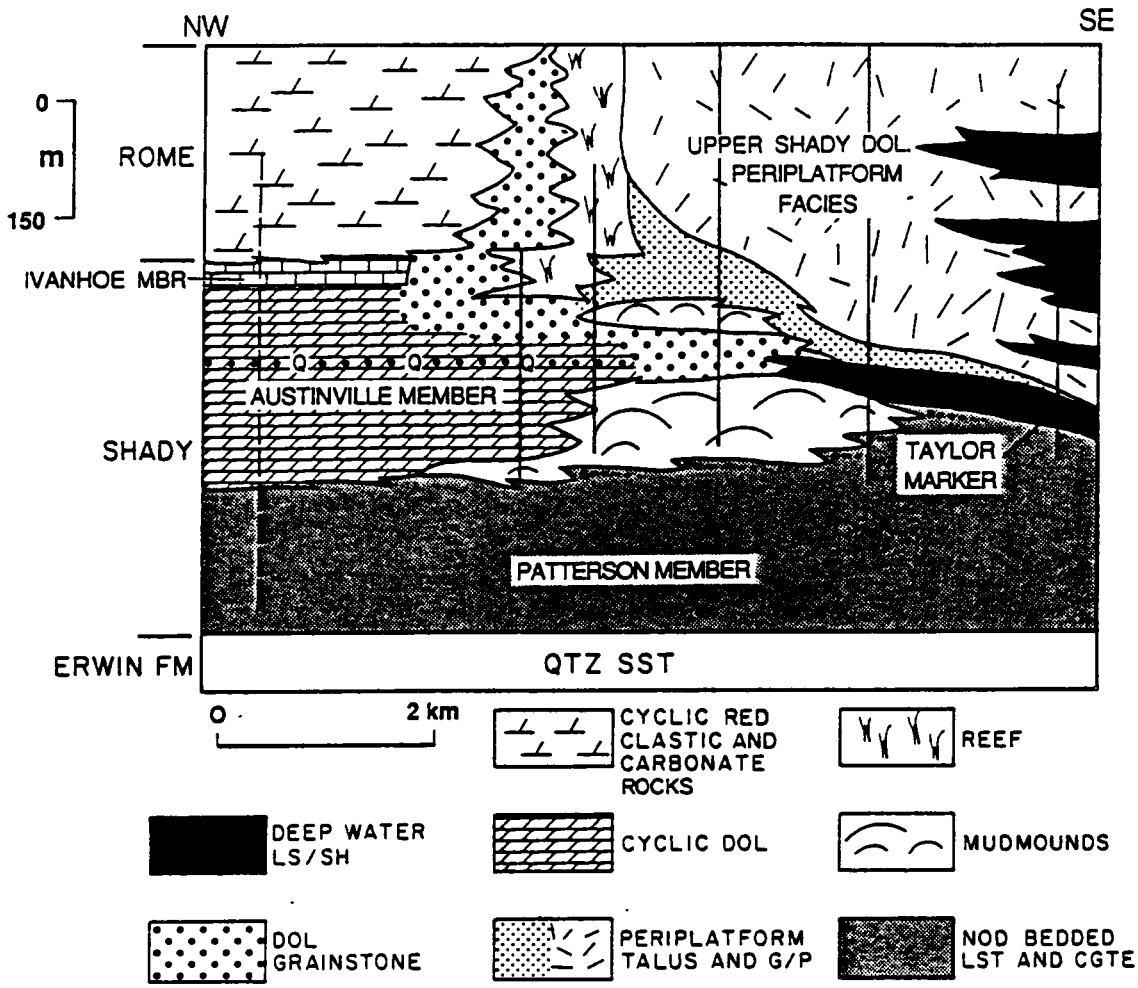
NW
SE
0
m
150
ROME
IVANHOE MBR
SHADY
ERWIN FM
UPPER SHADY DOL.
PERIPLATFORM
FACIES
AUSTINVILLE MEMBER
TAYLOR
MARKER
PATTERSON MEMBER
QTZ SST
0
2 km
CYCLIC RED
CLASTIC AND
CARBONATE
ROCKS
REEF
DEEP WATER
LS/SH
CYCLIC DOL
MUDMOUNDS
DOL
GRAINSTONE
PERIPLATFORM
TALUS AND G/P
NOD BEDDED
LST AND CGTE

scale reverse and thrust faults having less than a few hundred meters of horizontal displacement (Weinberg, 1971; Foley, 1980).

The *Bonnia-Olenellus* biozone extends from the underlying Erwin Formation (see Simpson and Sundberg, 1987, and references therein) to the upper Shady Dolomite (Fig. 4). *Salterella conulata* in the Patterson Member of the Lower Shady Dolomite (Byrd and others, 1973; Willoughby, 1977), confines the age of these deposits to the medial part of the *Bonnia-Olenellus* zone (Fritz and Yochelson, 1988). Archaeocyathids (Early Cambrian) are present in the Austinville Member (Butts, 1940; Willoughby, 1977; this study). The transition from Lower Cambrian trilobites of the *Bonnia-Olenellus* biozone to Middle Cambrian trilobites occurs within periplatform facies of the upper Shady Dolomite (Willoughby, 1977). However, the Middle Cambrian trilobite genera are not distinctive of a particular biostratigraphic zone, although they are no younger than *Glossopleura* zone (Willoughby, 1977). Much of the Rome Formation has been assigned a late Early Cambrian age (Willoughby, 1987; 1977 and references therein), although it locally extends into the Middle Cambrian (Willoughby, 1977). Therefore, based on the biostratigraphy (see above) and on stratigraphic reconstructions (Pfeil and Read, 1980; this study), platform margin facies and the lower portion of the periplatform sequence of the upper Shady Dolomite are time equivalent to the Rome Formation of the platform interior (Figs. 4, 6).

The lowermost trilobite zones of the Middle Cambrian are missing in interior platform, Rome beds, suggesting the presence of a regional unconformity (Hawke Bay event of Palmer and James, 1979) near the top of the Rome Formation (Fig. 4). It is not known if the lowermost trilobite zones of the Middle Cambrian also are missing in the periplatform sequence. However, no breaks in section or unconformities have been

Figure 6. Stratigraphic cross section, Shady Dolomite, Austinville region showing evolution of carbonate platform from ramp to rimmed shelf. Core locations correspond to geological map (Fig. 1), vertical lines indicate extent of core control. Stratigraphic sections physically correlated using top of Patterson Member (lower nodular limestone) and top of Taylor Marker (cycle VI; a widespread quartzose lime sand sheet that grades basinwards into quartz silt turbidites). Due to lack of internal biostratigraphic control, correlations are tentative. Roman numerals refer to large scale shallowing upward sequences recognized throughout study area. Nodular limestones of the lowermost Shady Dolomite shallow upward into and are interbedded with mudmound buildups. Mudmound buildups have a weak vertical stacking that define six shallowing upward sequences (cycles I through VI) recognized throughout study area. Top of cycle VI is a widespread quartzose sand sheet which grades seaward into quartz silt turbidites and shale (Taylor Marker). Subsequent sea level rise resulted in upbuilding of mudmounds and interbedded nodular limestones on the platform margin and restriction of carbonate influx to the outer ramp; which led to steepening of the platform margin and culminated in development of a high relief, rimmed shelf. Early-Middle Cambrian boundary occurs near the top of Rome Formation in interior platform locations (see text), approximate location of Early-Middle Cambrian boundary in off-platform sequence from Willoughby (1977).

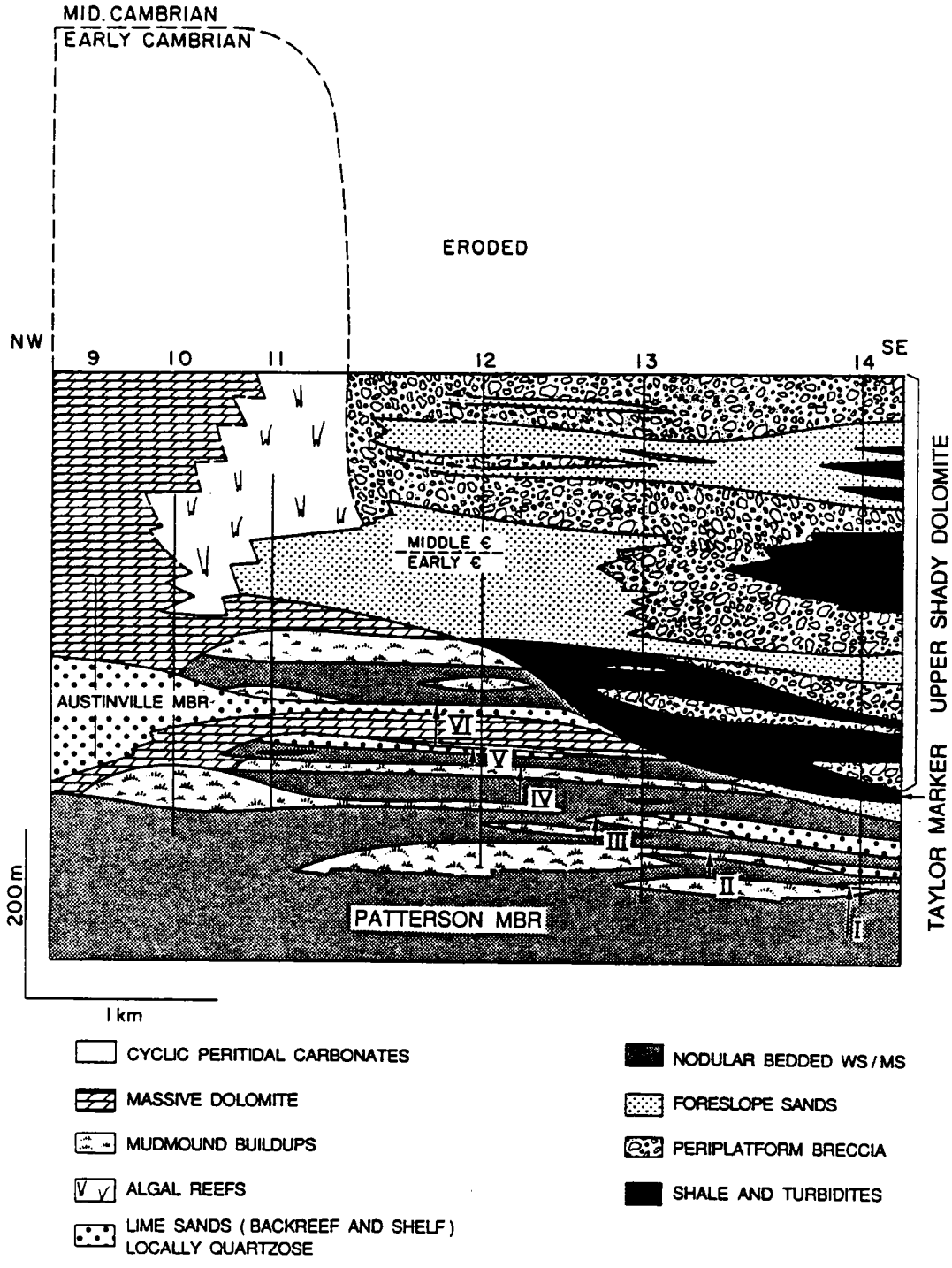
MID. CAMBRIAN
EARLY CAMBRIAN
ERODED
NW
SE
9
10
11
12
13
14
MIDDLE €
EARLY €
AUSTINVILLE MBR.
VI
V
IV
III
II
I
PATTERSON MBR
UPPER SHADY DOLOMITE
TAYLOR MARKER
200 m
1 km
CYCLIC PERITIDAL CARBONATES
MASSIVE DOLOMITE
MUDMOUND BUILDUPS
ALGAL REEFS
LIME SANDS (BACKREEF AND SHELF)
LOCALLY QUARTZOSE
NODULAR BEDDED WS / MS
FORESLOPE SANDS
PERIPLATFORM BRECCIA
SHALE AND TURBIDITES

observed in these deposits, and sedimentation may have been continuous, but condensed across the Early to Middle Cambrian boundaries.

Subsidence rates for the Lower Cambrian continental margin were estimated using the radiometric date for Catoctin basalts (570±36 m.y.; Badger and Sinha, 1988) from the lowermost Chilhowee Group (Simpson, 1987) and the location of the Lower to Middle Cambrian boundary within the upper Shady Dolomite. The estimated minimum subsidence rates from the thickness of the sequence (≈2000m) are 0.05 to 0.10 m/k.y.. However, poor internal time control limits the ability to assess the relative contribution to overall subsidence of active rifting/crustal attenuation versus later thermotectonic (passive margin) subsidence.

PLATFORM TO BASIN SEQUENCE

Fourteen representative cores forming two transects across depositional strike and one transect slightly oblique to depositional strike (Fig. 1) were logged in detail and cross sections were constructed (Figs. 5, 6, 7, 8). These cores all are located within the same thrust sheet; shortening within the transects is minimal (< few hundred meters), and was ignored in construction of the cross-sections. However, the carbonate sequence has been carried *en masse* over 100 kilometers from the east (Fig. 2).

The basal unit of the Shady Dolomite (Patterson Member) is a 300 m thick sequence of nodular bedded carbonate rocks (Fig. 5). This is overlain by 300 m thick Austinville member consisting of cyclic peritidal carbonate facies and massive dolomites which pass southeastward into outer ramp mudmound buildups that intertongue with carbonate conglomerate and nodular limestone (Fig. 5). Mudmound buildups are succeeded by

Figure 7. Stratigraphic cross section of ramp carbonates (across depositional strike) up to Taylor Marker time; stratigraphically higher sections lacking due to erosion. Nodular limestones of Patterson Member shallow upward and pass landward into mudmounds, which, in turn pass landward into massive dolomite and peritidal carbonates (Austinville Member). Six transgressive- regressive cycles are recognized. Top of cycle VI is quartzose lime sand sheet which fines basinwards into quartzose turbidites and shale.

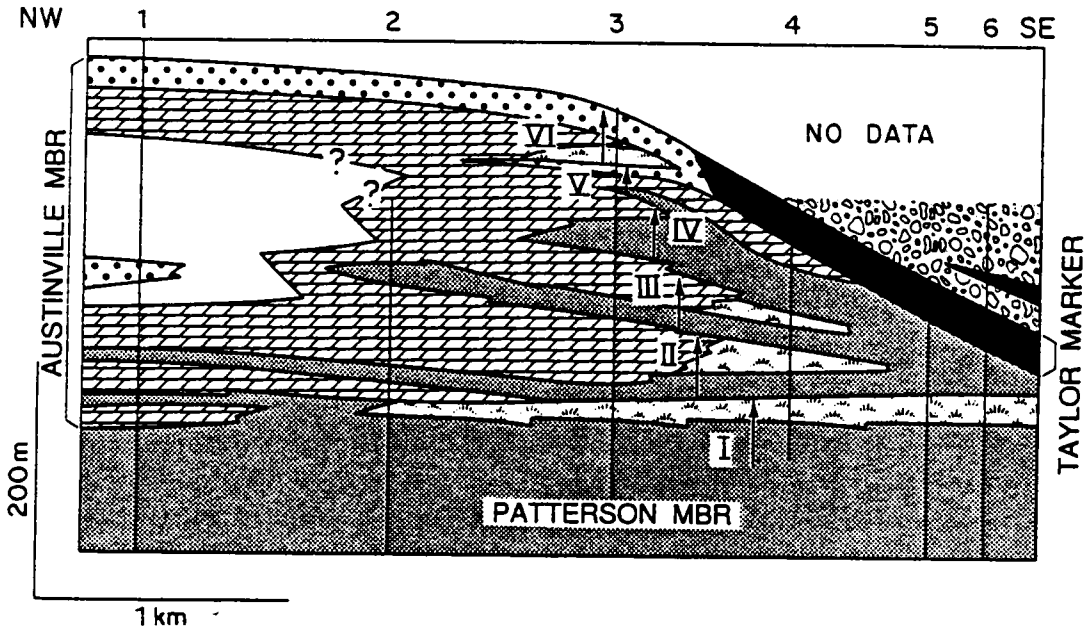
NW
1
2
3
4
5
6
SE
AUSTINVILLE MBR
NO DATA
VI
V
IV
III
II
I
TAYLOR MARKER
PATTERSON MBR
200 m
1 km
CYCLIC PERITIDAL CARBONATE ROCKS
MASSIVE DOLOMITE
MUDMOUND BUILDUPS
ALGAL REEFS
LIME SANDS (BACKREEF AND SHELF) LOCALLY QUARTZOSE
NODULAR BEDDED WS/MS
FORESLOPE SANDS
PERIPLATFORM BRECCIA
SHALE AND TURBIDITES

Figure 8. Stratigraphic cross section subparallel to depositional strike. Mudmound buildups are laterally continuous, some can be correlated over 3 km along depositional strike (eg., cycles II, III, and IV).

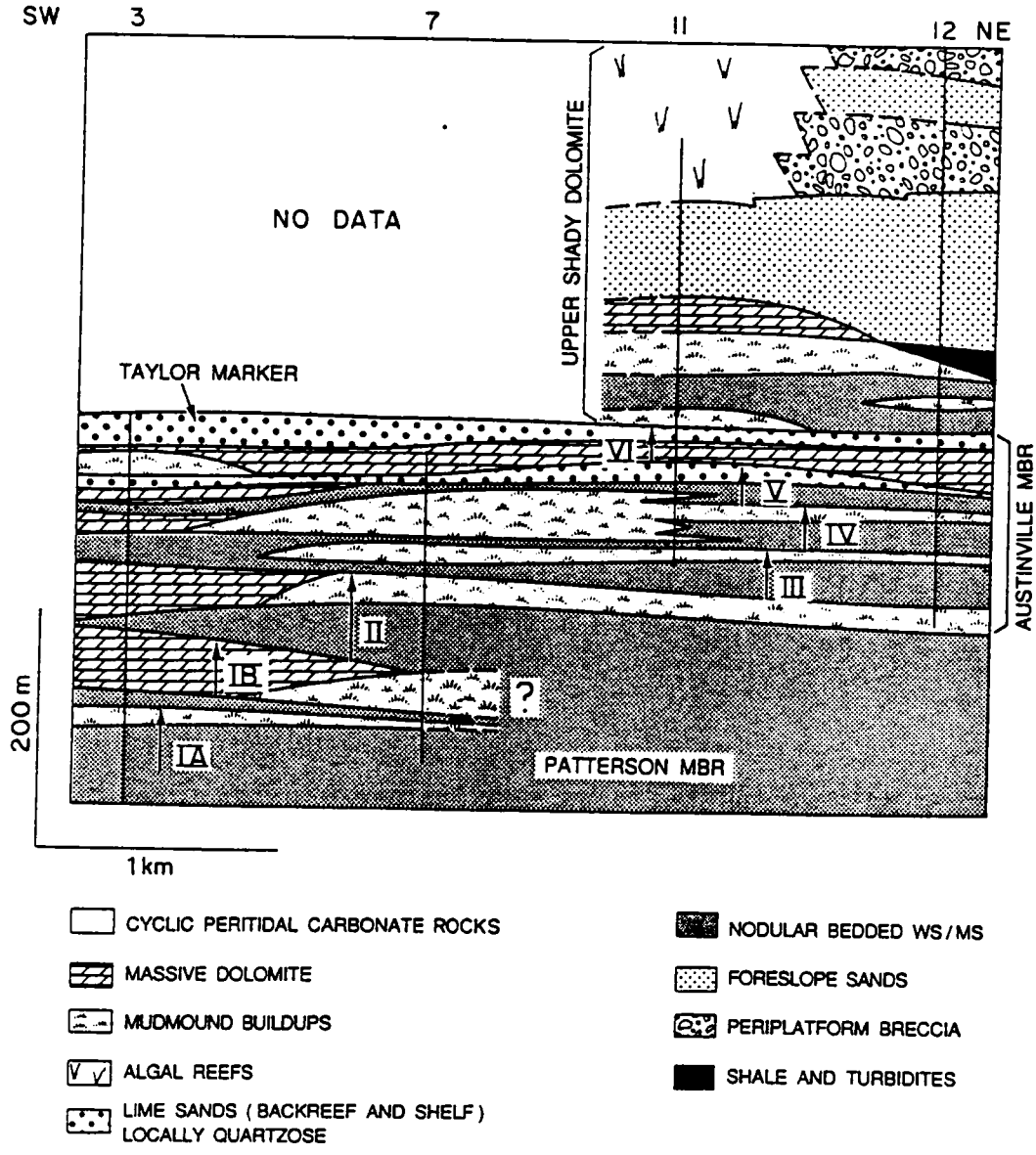
SW
3
7
11
12 NE
NO DATA
UPPER SHADY DOLOMITE
TAYLOR MARKER
VI
V
IV
III
II
IB
IA
?
PATTERSON MBR
AUSTINVILLE MBR
200 m
1 km
CYCLIC PERITIDAL CARBONATE ROCKS
MASSIVE DOLOMITE
MUDMOUND BUILDUPS
ALGAL REEFS
LIME SANDS (BACKREEF AND SHELF)
LOCALLY QUARTZOSE
NODULAR BEDDED WS/MS
FORESLOPE SANDS
PERIPLATFORM BRECCIA
SHALE AND TURBIDITES

skeletal algal reefs and interbedded lime sands. The reefs separate massively dolomitized carbonate rocks and redbeds of the Rome Formation from off-platform deposits of foreslope sands and periplatform breccias (upper Shady Dolomite, minimum 600 m thick) that fine basinward into black shaly limestones and shale (Fig. 5). Detailed descriptions of lithofacies in outcrop are given in Byrd (1973), Pfeil (1977), and Pfeil and Read (1980); reefal blocks occurring in periplatform talus deposits are described in detail by Read and Pfeil (1983) and Kobluk (1985), but these previous studies provide only a general outline of the facies relations because of the lack of subsurface data. The detailed facies relations and carbonate platform evolution, based on subsurface core control, are documented below.

LITHOFACIES AND DEPOSITIONAL ENVIRONMENTS

Coastal and Peritidal Sequences

Cyclic Redbeds and Carbonate Rocks. Redbeds and carbonate rocks of the Rome Formation extended eastward from the Rome Trough in central Kentucky and West Virginia to within a few kilometers of the shelf edge (Fig. 3). Rome redbeds were not included as part of this study because of limited outcrop and core availability, and considerable deformation. Dolomite and red mudrocks of the Rome Formation in the Austinville region consist of up to 10 m thick cycles of interbedded light gray dolomite and red shale (Fig. 9A) with local cryptalgal lamination, fenestrae, and mudcracks. They were deposited in a tidal flat to coastal plain setting as indicated by cyclic interbedding of shallow subtidal and tidal flat dolomite and clastic redbeds and the abundant mudcracks, cryptalgal laminations, and fenestral fabrics. Regional information on the Rome

Figure 9. Representative lithofacies, top of cores to right (arrow in upper left photo). A) Peritidal facies: top- laminated red mudrock and dolomite of Rome Formation; middle- cryptalgalaminites and pisolites from interior ramp facies of Shady Dolomite; bottom- fenestral and thrombolitic dolomite. B) Coarsely crystalline, massive dolomite. C) Microphotograph of massive dolomite. Primary grains (in this example, ooids) are only locally recognizable due to destruction of primary fabric by massive dolomitization. D) Stromatactoid wackestone/ mudstone facies from mudmound buildups. Stromatactoid cavities are floored by internal sediments and lined with fibrous marine cement, followed by saddle dolomite which precipitated in remaining void space during burial diagenesis. E) Algal boundstone with abundant marine cement-lined shelter voids. F) Microphotograph of dolomitized algal boundstone with numerous clusters of skeletal algae, *Epiphyton*.

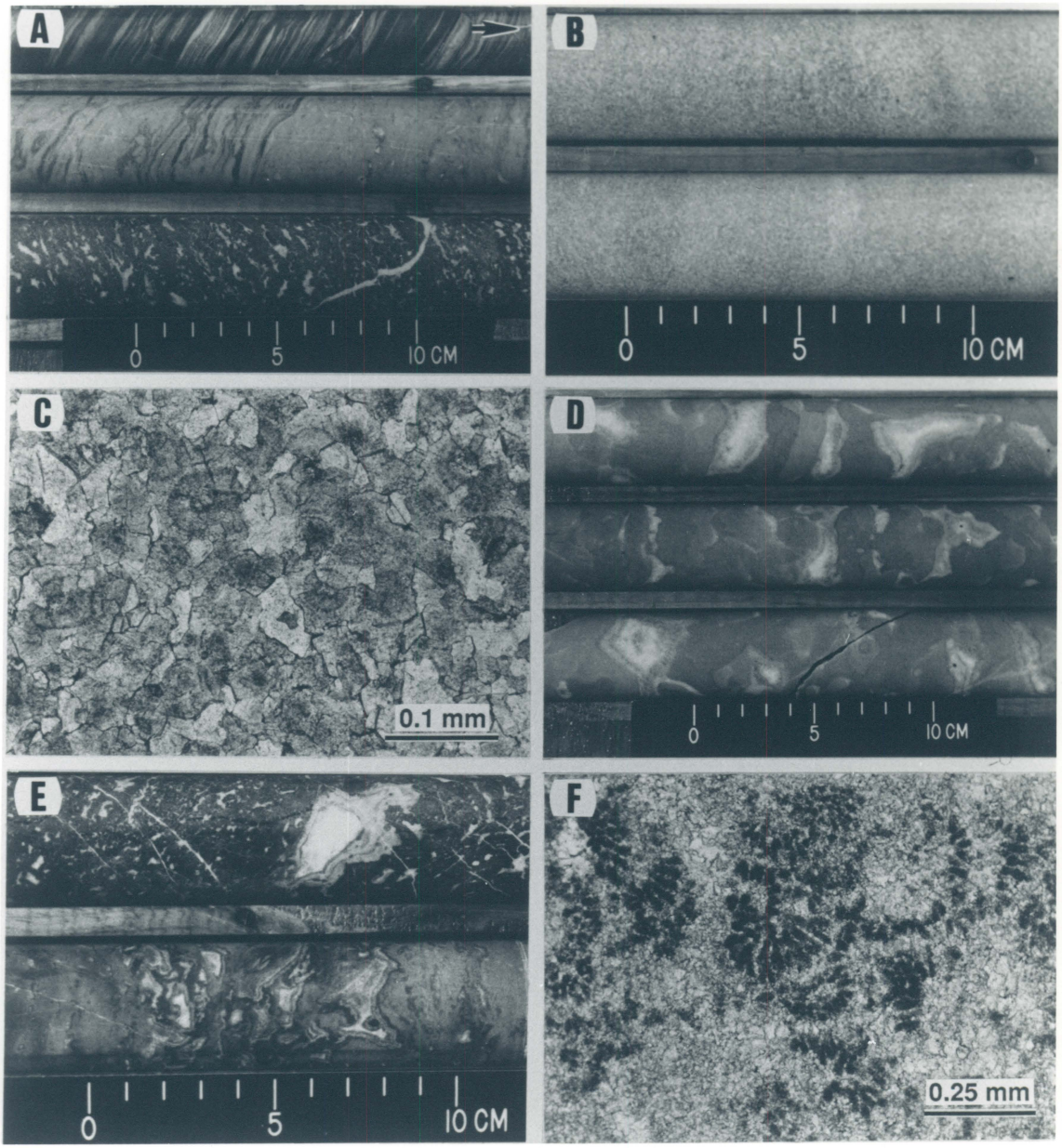
A
0
5
10 CM
B
0
5
10 CM
C
0.1 mm
D
0
5
10 CM
E
0
5
10 CM
F
0.25 mm

Figure 9 (continued). G) Deep ramp, nodular limestones. Light gray limestone layers have been plastically deformed into boudins and brittlely deformed into pseudobreccia fabrics encased in dark argillaceous dolomite. H) Limeclast sand with relict bedding. I) Polymictic breccia containing clasts of reefal limestone (R) and reworked clasts of foreslope and slope sediments (S) in deformed shale matrix. J) Marine-cemented periplatform breccia, clasts are rimmed by thick crusts of banded marine cement up to few cm thick. K) Carbonate turbidites and shale. L) Monomictic breccia containing platy clasts of reworked foreslope and slope sediments.

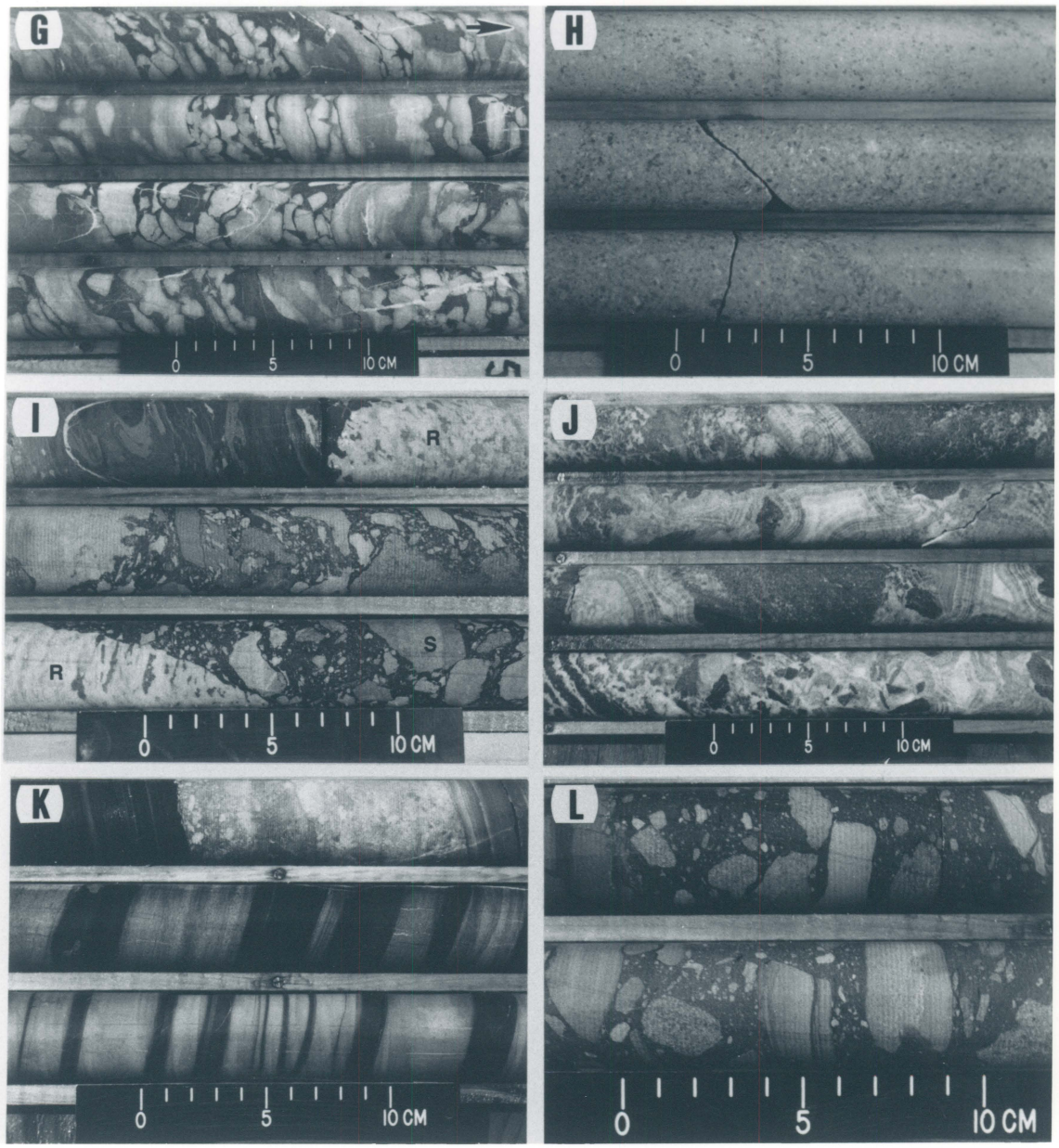
G
0
5
10 CM
H
0
5
10 CM
I
R
S
R
0
5
10 CM
J
0
5
10 CM
K
0
5
10 CM
L
0
5
10 CM

Formation is available in Sammon (1975) and Read (in press, a).

Cyclic Peritidal Carbonate Rocks and Massive Dolomite. Cyclic peritidal carbonate rocks and massive dolomites of the Austinville Member are landward of organic buildups and nodular bedded carbonate rocks (Figs. 5, 7). Peritidal carbonate rocks are arranged in cyclic, upward shoaling sequences (1 to 10 m thick), with basal pelletal/intraclastic/skeletal grainstones passing upwards into thinly layered lime mudstone, fenestral carbonates and local thrombolites capped by stromatolites and cryptalgal laminites (Fig. 9A). Basal coarse-grained units of cycles formed in a high energy, subtidal setting during a relative sea level rise. Later, as the platform aggraded and tidal flats prograded seaward, subtidal units were progressively overlain by shallow subtidal to intertidal lime mudstone, fenestral carbonates, and intertidal cryptalgal laminites.

Replacement by coarsely crystalline dolomite generally obscures or obliterates primary fabrics and sedimentary structures in the massive dolomites, making recognition of the precursor lithology difficult (Fig. 9B). Relict ooids, pellets, and ghost grainstone fabrics are locally evident (Fig. 9C). The geographic position of massive dolomites, and relict grainstone fabrics suggest that these dolomites were originally back-reef and shelf margin sands and possibly, lagoonal facies.

Peritidal and massive dolomites of the Austinville Member in platform interior locations are conformably overlain by the ≈40 m thick Ivanhoe Member (Fig. 5) consisting of fenestral and cryptalgal laminated limestone with minor dolomites and gray mudcracked shales, this member is conformably overlain by the Rome Formation (Pfeil, 1977; Pfeil and Read, 1980). This sequence may record a slight rise in sea level.

Organic Buildups

Carbonate Banks. Carbonate mudmounds or banks consist of light to brownish grey lime mudstone/ wackestone with interbedded dark gray, nodular limestone and shale. Mudmound complexes occur in a few km wide zone. They pass landward into massively dolomitized lagoonal carbonate facies and lime sands and interfinger downslope with nodular bedded limestone, slope carbonate conglomerate and argillaceous lime muds (Figs. 6, 7). Buildups are biostromal, individual mounds are between 1 and 30 meters thick and many are laterally extensive; individual mounds can be traced over 3.5 km along depositional strike (Fig. 8) and 2.5 km across strike (Fig. 6). Estimated depositional slopes on buildup flanks, based on the cross- sections, range from less than 0.5^{o} to locally up to 5^{o}. Flanking slope carbonate conglomerates also attest to development of significant syn-depositional relief on the buildups. The buildups form parts of shallowing-upward sequences (40-60 m thick) of deep ramp, nodular bedded carbonate rocks and shales that pass upward into slope carbonate conglomerate and mudmound buildups locally capped by shoal water massive dolomite and quartz sand-rich, limeclast grainstones.

Wackestone/mudstone bank facies lack bedding and commonly are intensively burrowed. Locally abundant stromatactoid cavities are floored with internal sediments and lined with fibrous to bladed marine cement (Fig. 9D). Scattered Archaeocyathids are present and appear locally to have constructed rigid framestones. Ooid/skeletal grainstone and packstone layers with local trilobites, *Salterella*, and echinoderms locally are interbedded with mudstone/wackestone core facies.

Mudmound buildups formed broad banks on the outer ramp. Restriction to a few kilometer wide zone suggests that they were localized over a preexisting slope break on

the underlying clastic ramp (see discussion under 'Carbonate Platform Evolution'). A subtidal setting below fair-weather wave base is indicated by the abundant lime mud, paucity of current-formed structures, whole unabraded fossils, and interbedded deep ramp nodular limestone and shale. Mudmound buildups of the Lower Cambrian sequence were relatively low in relief and were flanked by conglomerates and breccias of resedimented deep ramp nodular limestones which lack shallow water clasts. Synsedimentary cementation and development of hardgrounds contributed to the stabilization of the buildups. Stromatactoid cavities in the buildups may have resulted from decay of soft bodied organisms, erosion of lime mud between marine cemented crusts (Bathurst, 1982), and resedimentation by circulating marine waters. As the banks grew, internal erosion and resedimentation was succeeded by precipitation of marine cement in void spaces (Bathurst, 1982; Wallace, 1987).

The mudmound buildups developed on deep ramp carbonate facies, as these shallowed due to sediment upbuilding and/or relative sea level fall. During relative sea level rise, the mounds were buried beneath dark, shaly nodular limestone. Based on the estimated subsidence or accumulation rates (0.05-0.10 m/k.y., see above), the cyclic bank sequences reflect 0.5 to 1 m.y. (fourth order) relative sea level fluctuations.

Reefs and Back Reef Sands (Shelf Edge Facies). The cores have recovered in-place shelf margin skeletal algal reefs and lime sands not exposed in outcrop elsewhere in the Appalachians. The reef had a NE-SW trend and was approximately 0.5 to 1 km wide (Fig. 6). The cores are restricted to the basal 100 meters of reef, however a minimum thickness of 600 meters of reef (dashed profile in Fig. 6 is indicated by the thickness of off-platform deposits seaward of the shelf edge and by the thickness of

Rome redbeds on the adjacent platform. The shelf edge reefs and lime sands pass downslope into foreslope sands and periplatform talus which rapidly fine basinward into turbidites and shales (Fig. 6). The cored samples of the algal reefs are dolomitized. The best preserved reef fabrics are in allochthonous limestone blocks in periplatform talus, these have been described in detail by Read and Pfeil (1983) and Kobluk (1985). Although in-place reefs have been replaced by finely crystalline dolomite, primary growth fabrics remain well preserved. The reefs are boundstones with interstitial marine cements which also line shelter voids (Fig. 9E) and encrust algal framestone. Algal reefs were chiefly constructed by the skeletal algae *Epiphyton* (Fig. 9F) with locally abundant *Girvanella* and minor *Renalcis*. Shelter voids are floored by internal sediments to form geopetal structures that indicate the reefs are in place. Lime sands are well-sorted, coarse-grained, and contain rounded limeclasts and highly abraded and micritized skeletal grains.

Establishment of framebuilding calcareous algae by late Early Cambrian to early Middle Cambrian time permitted development of a high relief, rimmed shelf at the platform margin above the underlying low relief, bank complexes. The shelf margin was dominated by actively upbuilding skeletal algal reefs as indicated by the abundant algal-derived talus and debris flows in the adjacent off-platform settings. A high energy, shallow water setting for the shelf edge is indicated by the algal framestones, associated coarse lime sands with abraded and rounded grains, and by the probable photosynthetic nature of the reef-constructing algae. Although the precise facies relationships of the shallow water, carbonate platform with the flanking deeper water periplatform carbonate rocks cannot be directly determined, the shelf margin attained considerable relief, as evidenced by the abrupt shift from shallow water, shelf margin reefs and lime sands to

deep water, periplatform facies within a 1km wide zone (Fig. 6). The association of shallow water-derived breccias with deep water shaly carbonate rocks and shale also attests to a juxtaposition of high energy, shelf margin facies with deeper water, off-shelf facies.

A high relief platform margin is also indicated by the biostratigraphy. Most, if not all, of the Rome Formation (600 to 900 meters thick- Butts, 1940) is assigned a late Early Cambrian age, with the Early-Middle Cambrian boundary occurring either immediately above, or within the uppermost part of the Rome Formation (Fig. 4), (Willoughby, 1987; Willoughby, 1977 and references therein). Reconstructions of the margin using the known 600 to 900 m thickness of the Rome Formation on the platform, which, on the basis of the biostratigraphic data (Willoughby, 1977), is equivalent to about 200 m of offshelf facies between the top of the Taylor Marker (top of cycle VI) and the base of the Middle Cambrian (dashed profile in Fig. 6), suggests that the rimmed shelf had up to 500 to 700 meters relief above the proximal periplatform deposits in the study area. Total relief of the margin above the basin floor may have exceeded 1.5 km, assuming sediment starving of the distal, basinward locations. It further implies that much of the periplatform talus in the upper part of cores is Middle Cambrian Elbrook equivalent (Willoughby, pers. comm., 1987).

Deeper Water Carbonate Rocks

Nodular Bedded Wackestone/Mudstone. The basal unit of the Shady Dolomite, the Patterson Member, is a 300 m thick sequence of nodular bedded carbonate rocks (Figs. 6, 7). This lithofacies consists of wavy, 1-4 cm thick, alternating layers and nodules of light gray, lime mudstone or dolomite and dark gray to black, styolitized

seams of argillaceous dolomite; the facies has abundant boudinage structures and pseudobreccia fabrics (Fig. 9G). Limestone layers consist of lime mud with rare pellets, ooids, trilobites, *Salterella*, and echinoderms. Locally, where this facies passes landward or upward into mudmound buildups, there are interbedded slope conglomerates in a dark gray, shaly matrix.

This lithofacies formed on a gently sloping carbonate ramp following drowning of the Chilhowee clastic shelf and records the inception of carbonate sedimentation on the Lower Cambrian passive margin. A low energy, subtidal setting is indicated by the abundant lime mud and fine-grained argillaceous material, the scarcity of current-formed structures, and the open marine biota. Evenly layered facies lack burrows, suggesting that they formed in lower oxygenated waters than the more burrowed, nodular facies. The nodular fabrics probably reflect selective early cementation of lime mud layers at shallow burial depths (eg., Mullins and others, 1980), which formed rigid nodules around which the unlithified argillaceous layers deformed plastically during later compaction and pressure solution (Stoakes, 1980). Interbedded slope carbonate conglomerates formed from downslope movement of nodular limestone and failure of oversteepened slopes, especially adjacent to mudmound buildups.

The rhythmic interbedding of lime mud and shale may reflect short term (10^3 yr.) climatic fluctuations. During arid periods, shale influx into the basin would have decreased, so that relatively clean carbonate was deposited. During humid times, fine clastic influx into the deep ramp gave rise to argillaceous layers. The interbedded lime mud and shale may also reflect small scale fluctuations in sea level affecting the relative input of terrigenous material against a background of continuous carbonate sedimentation (Stoakes, 1980). Alternatively, rhythmically interbedded limestone and shale couplets

have also been attributed to secondary unmixing of $CaCO_3$ in argillaceous limestone (Hallam, 1986) or to bedding enhancement (Bathurst, 1987) during diagenesis and compaction.

Limeclast Sands (Foreslope Deposits). Thick limeclast sand deposits (up to 150 m thick) occur seaward of the shelf edge (Fig. 6). Limeclast grainstone/packstone units are light to dark gray, horizontally stratified (few cm thick layers) to massive (Fig. 9H). Thinly bedded units (5-10 cm thick) commonly are graded, particularly in more seaward locations.

Limeclasts are coarse sand- to granule-sized, subangular to rounded grains of micritic carbonate. Sorting is generally poor, interstitial lime mud and "floating" breccia clasts are common. Other grain types include ooids, quartz sand, pellets, and abraded skeletal fragments (calcareous algae, trilobites, and echinoderms), commonly with micritized rims. Larger clasts include algal boundstone, skeletal grainstone, pelletal packstone, reworked limeclast packstone, and black argillaceous limestone.

The periplatform limeclast sands accumulated in a foreslope setting as evidenced by their location (seaward of shelf edge reefs, landward of more distal, deep water carbonate rocks) and by their association with periplatform talus, turbidites, and shale. The foreslope sands differ from shelf edge lime sands in that their constituent grains are more rounded, they contain interstitial mud matrix, and they are interbedded with periplatform talus and shaly carbonate rocks (Pfeil and Read, 1980). Downslope transport of limeclast sands was by gravity flows, as indicated by the commonly observed massive bedding, horizontal stratification, abundant lime mud, poor sorting, and "floating" breccia clasts (Pfeil and Read, 1980). Limeclast sands were derived from the high energy platform

margin as evidenced by the abraded, rounded, and micritized grains and associated shallow-water ooids, skeletal grains, and algal boundstone clasts. Calcified algae may have been the source of many of the micritic limeclasts with subsequent micritization and diagenesis obliterating much of the primary fabric (Coniglio and James, 1985).

Periplatform Breccia Deposits. Thick accumulations (up to 200 m thick) of allochthonous periplatform breccias occur immediately seaward of the shelf edge (Fig. 6). Breccias are interbedded with limeclast sands, thinly bedded argillaceous carbonate rocks and shales. They pass landward into limeclast sands and shelf edge bioherms and grade downslope into turbidites, shale, and slope carbonate breccias lacking platform-derived clasts. Breccias are in small channel-form deposits (up to several meters thick and 10 or more meters wide) (Pfeil, 1977) to sheet-like deposits extending over 2 km along depositional strike and 3 km across strike (Fig. 6).

Periplatform breccias are generally unsorted and nongraded, and include clast-supported, sand-supported, and mud-supported fabrics. The breccias are polymictic and contain gravel- to boulder-sized clasts of marine-cemented algal boundstone (up to 20 m in diameter), ooid grainstone, limeclast grainstone/packstone, and reworked clasts of foreslope limeclast sands and black argillaceous limestone and turbidites. Disoriented geopetal fabrics demonstrate that the algal blocks are allochthonous and were transported downslope from the shelf edge (Read and Pfeil, 1983). Interstitial sediments include limeclast sand, black argillaceous carbonate, and shale (Fig. 9I). Clast-supported breccias lacking fine-grained matrix material are locally cemented with isopachous marine cement in locations immediately adjacent to the shelf edge (Fig. 9J). Marine cement consists of thick isopachous crusts (up to several cm thick) of fibrous, inclusion-rich

calcite. Marine cementation contributed to stabilization of the breccia bodies, making them more resistant to erosion by wave action and downslope movement.

Polymictic breccias are periplatform talus that accumulated in a lower foreslope to toe of slope setting as evidenced by the admixture of shallow water clasts with slope clasts and associated argillaceous carbonate and black shale which become increasingly dominant seaward. Algal clasts and other shallow water detritus were transported downslope by debris flows, which may have been initiated by oversteepening and slumping of unstable slopes or perhaps by seismic activity during Rome Trough rifting. Deposition on a steep, unstable slope is indicated by the abundant slump features, synsedimentary deformation, and pull-apart structures in the interbedded shaly carbonate rock (see below).

Black Shaly Carbonate Rocks, Slope Breccias, and Shales. Shaly carbonate rock and shales are interbedded with foreslope sands and breccias adjacent to the platform margin and become more abundant basinwards (Fig. 6). Shaly carbonates are black, thinly bedded, millimeter to 10 cm thick layers of limestone, argillaceous carbonate, and laminated black shale. The limestone layers include lime mudstone and nongraded to graded pelletal/limeclast packstone layers which fine up into lime mudstone or shale. There also are some coarse turbidite layers (centimeter- to decimeter-thick), of pelletal packstone and quartz silt which grade upward into argillaceous carbonate and shale (Fig. 9K). Pull-aparts of limestone layers with argillaceous laminations deformed around soft or brittle limestone boudins locally are well developed. Shaly limestones locally contain channel-form units of monomictic breccia (≈0.5 m thick, several meters wide; Pfeil, 1977), containing platy clasts of reworked dark gray to black, thinly bedded

slope limestone in a matrix of highly deformed, dark shaly limestone (Fig. 9L). Ripple laminations and wavy bedding are common locally.

Black argillaceous carbonate rocks and shales were deposited off the shelf in poorly oxygenated, relatively deep water, below storm-wave base, as evidenced by the abundant lime mud and fine argillaceous material, the dark gray to black color, the paucity of bioturbation structures, and the fine, even lamination. Lower to Middle Cambrian deep water carbonate sediments were derived entirely form the shallow platform, because calcareous plankton, a major sediment contributor to modern deep water carbonate deposits (McIlreath and James, 1984), did not evolve until the Mesozoic era. Therefore, away from the shelf edge, influx of shallow water derived periplatform carbonate diminished and increasingly more shaly carbonate accumulated. Deposition was by suspension settling of mud washed off the shallow shelf and by turbidity currents. Pull-apart structures formed from downslope creep of the slope deposits, with the more rigid limestone layers being fragmented into platy clasts. Monomictic breccias of reworked slope sediments were deposited following failure of oversteepened slopes or by erosion of slope beds by sediment-gravity flows. Black shales formed in more distal locations, where influx of shelf-derived carbonate debris was less important or during times when carbonate influx from the shelf was decreased. Rhythmic interbedding of limestone layers and black shale may reflect episodic transport of shelf edge and foreslope sediments into downslope locations due to storm or tectonic activity or they may record periodic climatic and/or sea level fluctuations affecting the relative contributions of shelf-produced carbonate and terrigenous mud.

CARBONATE PLATFORM EVOLUTION

Lack of internal biostratigraphic control within the *Bonnia-Olenellus* biozone limits correlation of relative sea level curves from the study area with those elsewhere. Thus, it is not possible to distinguish between eustatic from tectonic signals and the Shady-Rome relative sea level curves (Fig. 10) are only of local use.

Carbonate Ramp Phase

The transition from Early Cambrian clastic shelf to carbonate platform sedimentation may reflect a number of factors: the migration of North America toward the equator during this time (Bond and others, 1984); global warming after Late Precambrian glaciation (Read, in press b); a semi-arid climate limiting clastic influx from the craton (Read, in press b); and/or a decrease in clastic sediment supply during sea level rise (Fig. 10) combined with erosion of cratonic highlands. In the upper Erwin Formation, a deepening upward sequence is recognized (Simpson, 1987), which culminated in drowning of the clastic shelf. A 300 meter thick sequence of nodular-bedded, deep ramp carbonate facies of the lower Shady Dolomite was deposited above the Erwin clastic sediments on a gently sloping ramp (Fig. 11A), recording inception of carbonate sedimentation of the Lower Cambrian passive margin.

Nodular-bedded, deep ramp carbonate facies shoal upward into mudmound buildups and slope carbonate conglomerate. These buildups formed banks in a few kilometer wide zone on the outer ramp, and were surrounded by nodular limestone facies, which passed landward into massive dolomite and peritidal carbonate rocks (Fig. 11A). These mudmound buildups lacked rigid frameworks and were restricted to a low energy setting

Figure 10. Relative sea level curve for the Shady Dolomite in the Austinville region. Dotted line is overall eustatic sea level rise documented for all continents through the Cambrian. In the Shady/Rome sequence, two large-scale transgressive- regressive sequences are recognized ('A' and 'B') the earlier ('A') resulted in drowning of the Erwin clastic shelf and development of a carbonate ramp which culminated in deposition of a widespread quartzose sand sheet at the top of the Austinville Member. The second large scale transgressive-regressive sequence ('B') led to initiation of the reefal rimmed shelf of the upper Shady Dolomite and culminated in deposition of regressive red beds and unconformity development in interior platform locations (Hawke Bay-Rome event) while greater subsidence rates on the outer platform resulted in continued deposition of carbonates of the upper Shady. Superimposed on large scale transgressive-regressive sequence ('A') are smaller scale shallowing upward sequences, indicated by Roman numerals, corresponding to those of mud mound sequences identified in cross sections (Figs. 6, 7, 8).

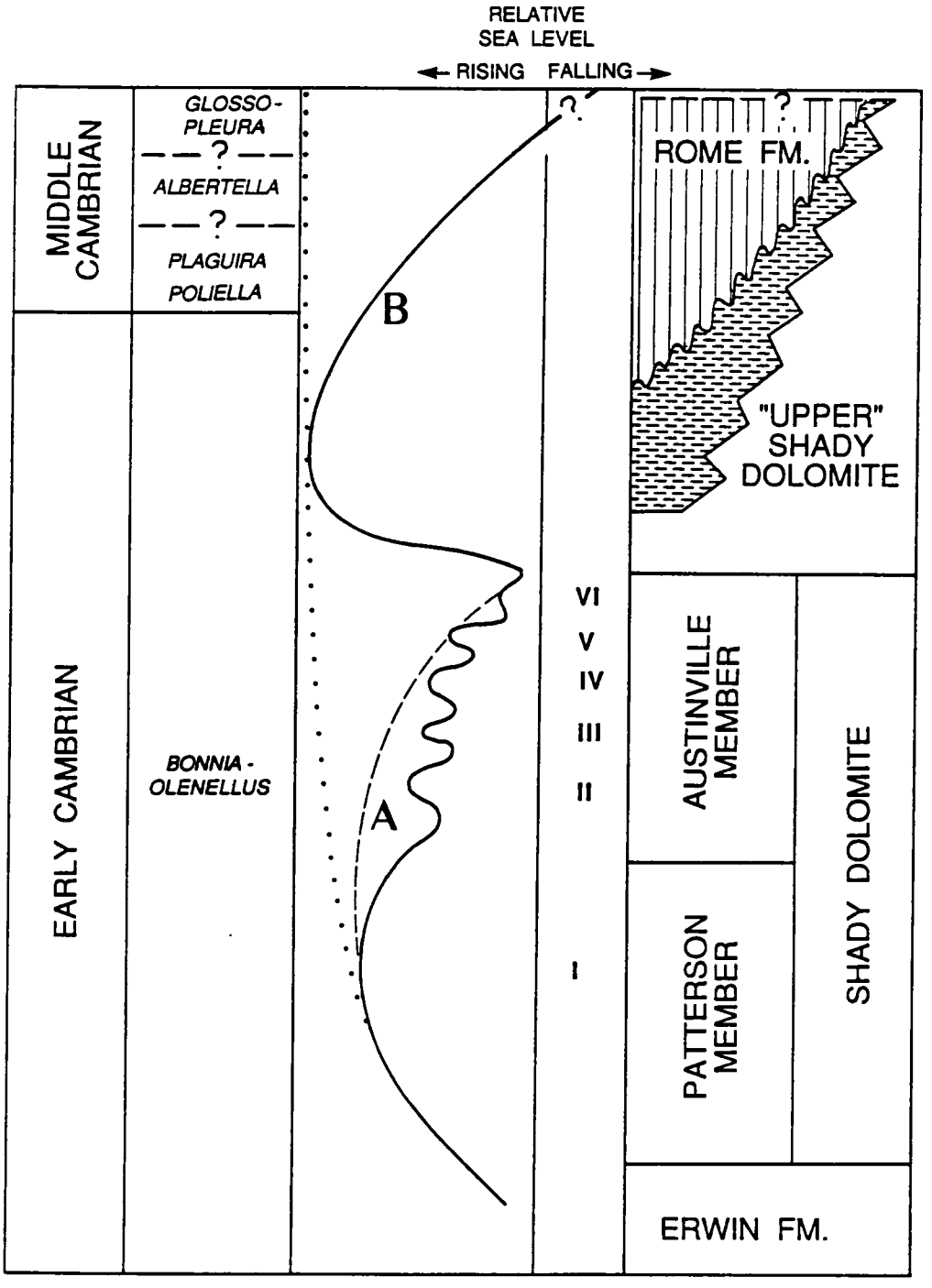
RELATIVE
SEA LEVEL
RISING
FALLING
MIDDLE CAMBRIAN
EARLY CAMBRIAN
GLOSSO-PLEURA
ALBERTELLA
PLAGUIRA
POLIELLA
BONNIA - OLENELLUS
B
A
VI
V
IV
III
II
I
ROME FM.
"UPPER" SHADY DOLOMITE
AUSTINVILLE MEMBER
PATTERSON MEMBER
SHADY DOLOMITE
ERWIN FM.

Figure 11. Block diagrams summarizing evolution of Lower to Middle Cambrian carbonate platform, lithologic symbols same as those used in Figure 4. Lower heavy lines in figures 11B, 11C, and 11D indicate topography of subjacent depositional surface (from previous block diagram).

A) Drowning of Chilhowee clastic shelf (lower dotted unit) resulted in deposition of a thick sequence of nodular limestones, which were succeeded by a carbonate ramp fringed by mud banks which passed downslope into nodular limestones and breccia.

B) During a major fall in relative sea level (not illustrated), a widespread quartzose lime sand sheet was deposited over previous ramp facies. Subsequent rise in relative sea level resulted in establishment of mudmound buildups and interbedded nodular limestones which grade downslope into shale.

C) During continued sea level rise, mud mounds were succeeded by skeletal algal reefs, which resulted in initiation of a rimmed shelf morphology. Immediately seaward of the shelf edge reefs were thick deposits of foreslope sands which pass downslope into shale and periplatform breccia deposits.

D) A major regression during the Middle Cambrian resulted in transport of clastics to the outer platform. Subsidence rates on the platform margin exceeded the rate of sea level fall, and led to development of a high relief reefal rim, which aggraded and prograded seaward. Immediately seaward of the shelf edge, thick deposits of periplatform talus accumulated, fining basinward into turbidites and shale.

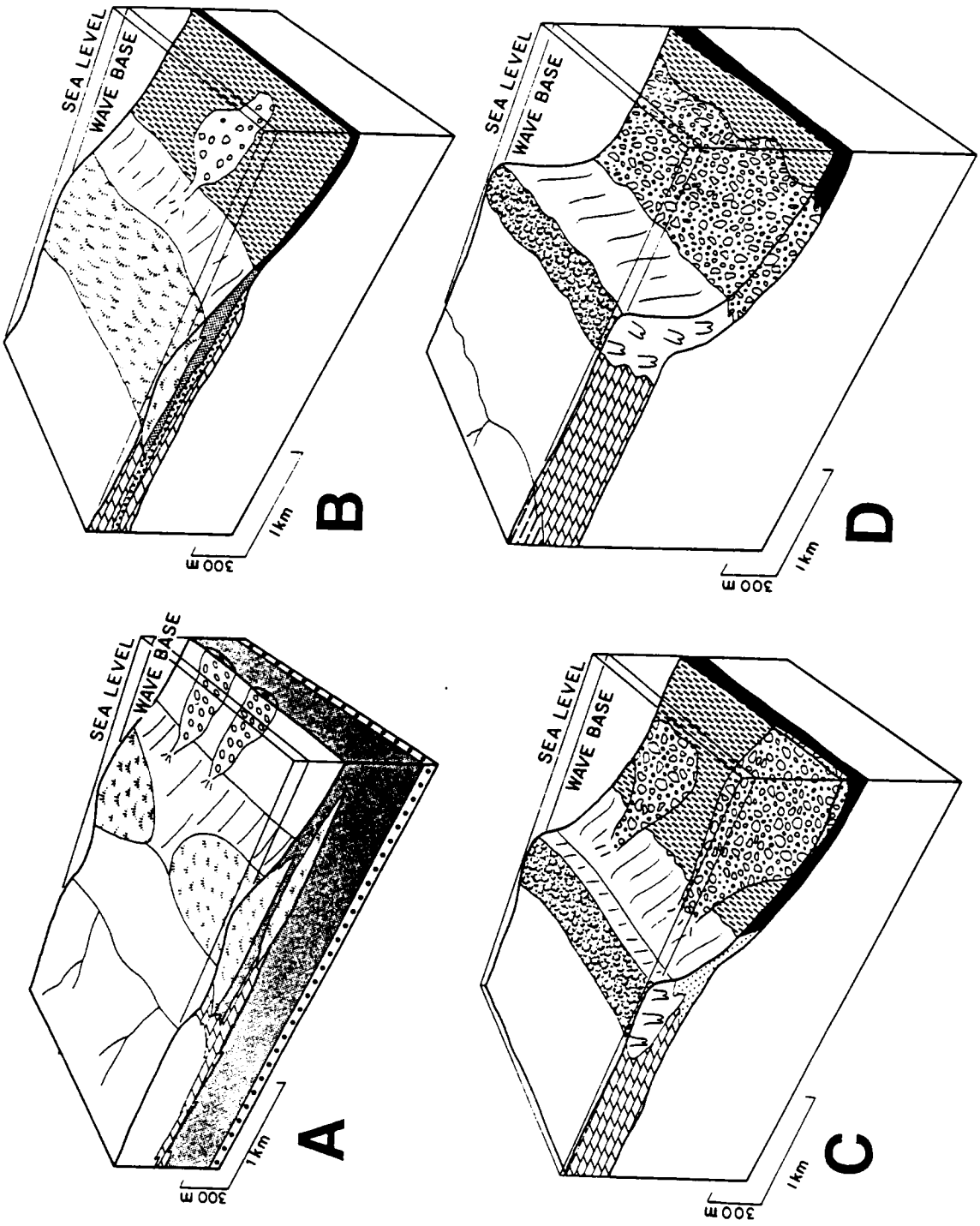
SEA LEVEL
WAVE BASE
300 m
1 km
A
B
C
D

below fair weather wave base on a low relief, gently sloping carbonate ramp. Mudmound buildups and later algal reefs were confined to a relatively narrow (few km wide) zone near the transition from shallow to deep shelf sedimentation in the underlying Erwin Formation (Simpson, 1987), suggesting that the antecedent clastic shelf topography may have influenced the location of organic buildups.

The mudmound buildups of the Shady Dolomite consist of 40 to 60 meter thick, cyclic sequences with basal deep ramp carbonate rocks that shoal upward into mudmound buildups and/or shoal water lagoonal facies and lime sands. The mudmounds have a weak vertical stacking. Six shallowing-upward cycles are recognized from the ramp stage of the Shady Dolomite carbonate platform (Figs. 6, 7, 8). Based on the estimated average subsidence rates for the Shady Dolomite (0.05-0.10 m/k.y., see above), these cycles represent relative sea level fluctuations (Fig. 10) on the order of 0.5 to 1.0 m.y. (fourth order).

Three quartzose lime sand sheets blanket the outer ramp. Influx of quartz sand reflect exposure of the interior platform source region. This could be due to sea level lowering in which case the quartzose sands would be low stand deposits. Alternatively, they may reflect incipient tectonic uplift in the Rome Trough area, which underwent considerable tectonic activity during Rome deposition (Read, in press a; b). The quartzose lime sands are overlain by argillaceous limestone deposited in a low energy, subtidal setting, indicating submergence during rising sea level, which resulted in reestablishment of mudmound buildups on the outer ramp along with interbedded deep ramp carbonate facies (Fig. 11B).

Based on the reconstructed margin, initial slopes on the ramp were <10 m/km (<0.5^{o}). Throughout the ramp stage, the slopes increased due to differential upbuilding

of the ramp relative to the basin, which was sediment starved.

Drowning Phase and Initiation of Rimmed Shelf

Slopes on the ramp immediately prior to major burial beneath deep water shale were 60-70 m/km (3 to 4°), assuming that the shale blanketed the slope, rather than interfingering. Black shales and algal block-bearing breccias onlapped the outer ramp slope during drowning (Fig. 6), perhaps associated with long term relative sea level rise (rising portion of curve 'B' in Fig. 10). These breccias were derived from the reef updip, and correlate at least to the updip lowest occurrence of reefal rim. This reconstruction suggests water depths were at least 200 m (Fig. 6). Synchronous with drowning, the reefal rim was initiated at the landward margin of the mudmounds of the earlier ramp, resulting in a few kms of backstepping.

This drowning event may be indicated on the platform interior by the Ivanhoe Member (Pfeil and Read, 1980), a peritidal limestone overlying massive dolomites of the Austinville Member and overlain by red mudrocks and dolomites of the Rome Formation. If the Ivanhoe Limestone and the black shales do not correlate, then the Ivanhoe may represent another flooding event prior to Rome redbed deposition.

Rimmed Shelf Phase

As the shelf rim continued to build up, thick deposits of foreslope sand accumulated immediately to seaward (Fig. 11C). These foreslope sands may reflect rising sea levels submerging the shelf at this time, favoring production of uncemented shelf edge sands (Droxler and Schlager, 1985). Limited cementation of these sands may indicate that the shelf margin was still relatively low in relief at this time. Cores 10 and 11 (Fig. 6)

indicate that the reef initially prograded over the foreslope sands. Biostratigraphic data suggest that the foreslope sands and their down- slope breccia equivalents are the condensed off-platform equivalent of the Rome-age rimmed shelf (Fig. 6).

The reefal rim continued to build upward, while basinal sections were starved of sediment, producing a high-relief, rimmed margin (Fig. 11D). The major development of this high relief margin appears to have been during a time of regional regression on the craton and inner shelf (falling portion of curve 'B' in Fig. 10) (Hawke Bay event, Palmer and James, 1979). This was marked by widespread deposition of terrigenous red beds in a coastal plain to tidal flat setting on the platform interior. A major disconformity, recognized on the basis of the biostratigraphy, occurs in the upper Lower Cambrian to lower Middle Cambrian sequence in the Appalachians and elsewhere bordering Iapetus (Palmer and James, 1979; Palmer, 1981). Core control through the shelf rim is limited to the lowermost part (Fig. 6) and it cannot be ascertained whether shelf edge facies became emergent during Rome regression. However, the thick accumulations of algal debris in the periplatform deposits implies that the shelf margin continued to be dominated by upward-growing algal reefs. This suggests that subsidence rates on the outer platform exceeded any sea level fall during Rome time, thus producing the accommodation space for platform upbuilding.

The thick periplatform breccias above the foreslope sands (Fig. 6) may be due to localization and outgrowth of shelf-edge reefs and subsequent oversteepening during stable or slowly rising sea level, or they may reflect increased seismic activity during rifting of the upper Lower to lower Middle Cambrian Rome Trough (Read, in press a). The biostratigraphic data suggest that most of these breccias postdate the Rome-age rimmed margin, and are of Middle Cambrian Elbrook age (Fig 6) (Willoughby, pers.

comm., 1987).

Tectonic versus eustatic influence on the relative sea level fall during Rome deposition is difficult to assess. The Rome or Hawke Bay regressive event in the Appalachians is correlative with transgression in the western part of North America (Palmer and James, 1979), and it cannot be determined with certainty whether this regressive event in the Appalachians reflects a eustatic lowering of sea level or tectonic controls. Tectonic uplift of the platform interior due to thermal arching during Rome Trough rifting may have occurred in the late Early to Middle Cambrian. Uplift of the platform interior and associated igneous activity also occurred in eastern Canada at this time (James and others, in press and references therein).

COMPARISON WITH LOWER TO MIDDLE CAMBRIAN MARGINS ELSEWHERE IN NORTH AMERICA

The Shady Dolomite platform initially was ramp-like, and dominated by downslope mudmound buildups. Initial ramp-like margins also characterize Lower to Middle Cambrian carbonate sequence in the Canadian Appalachians (James and others, in press) and in the southern Canadian Rockies (Aitken, 1971; Aitken and McIlreath, 1984). Lack of periplatform breccias low in the offshelf sequences in the Maryland-Pennsylvania-Vermont Appalachians also indicate that the initial margins were gently sloping ramps (Gohn, 1976; Reinhardt, 1974; 1977).

The carbonate ramp of the lower Shady Dolomite was subsequently drowned during a relative rise in sea level, prior to rimmed shelf development. A similar drowning of the carbonate platform is also recognized in the Vermont sequence where the deep water

Parker Slate overlies Dunham platform carbonate facies (Read, in press a; Gregory and Mehrtens, 1982). Whether this drowning event is younger than in the Shady Dolomite sequence is not clear. However the distribution of the Parker Slate suggests that deepening of the Dunham shelf was confined to an embayment of the Dunham-Monkton shelf edge, perhaps related to normal faulting.

The low relief carbonate ramp of the lower Shady Dolomite was succeeded by algal reefs which constructed a high-relief, rimmed shelf flanked by thick accumulations of periplatform facies. Development of a high-relief rimmed shelf above earlier ramp facies in the late Early to Middle Cambrian period also typifies the margin in the southern Canadian Rockies (Cathedral escarpment- McIlreath, 1977; Aitken and McIlreath, 1984), Canadian Appalachians (James and others, in press), and the U.S. Appalachians (Gohn, 1976; Reinhardt, 1974; 1977; this paper). This reflects preferential sedimentation on the platform margin relative to the sediment starved basin. Maximum relief on the margin (up to 1500 m) likely occurred in the central Appalachians of Maryland-Pennsylvania-Virginia (Read, in press b).

Major development of the Shady Dolomite rimmed shelf occurred during widespread deposition of terrigenous clastic rocks and unconformity development associated with regional regression (Hawke Bay-Rome event), which is recognized throughout the Appalachians (Palmer and James, 1979). This implies that subsidence rates on the outer platform exceeded relative sea level fall rates, thus providing the accommodation space for continued reefal upbuilding. The Cathedral escarpment of the southern Canadian Rockies developed during the time spanned by unconformity development in the shelf interior of the Appalachians, indicating higher relative subsidence rates in western Canada.

The carbonate platform margin was localized in the Appalachians above the existing

shelf-slope transition, possibly above the Late Proterozoic hinge zone (Read, in press a; b). The location of the Middle Cambrian carbonate platform margin in the southern Canadian Rockies was similarly influenced by the Kicking Horse Rim, a topographic high which developed in this region by the Early Cambrian (Aitken, 1971).

CONCLUSIONS

The Lower to Middle Cambrian Shady Dolomite records the evolution of a Cambrian carbonate platform that developed over approximately 15 m.y. above a rift to marine shelf clastic sequence. Long term subsidence rates were 0.05 to 0.10 m/k.y. Relative sea level rise submerged the clastic ramp and resulted in deposition of a thick sequence of deep ramp nodular carbonate rocks. These shoal upward into a carbonate ramp fringed by mudmound buildups, which was accompanied by progressive steepening of the ramp margin. Relative sea level rise caused drowning of the outer ramp beneath black shale. This was accompanied by backstepping, and development of an algal reefal rim (500 to 700 m, minimum relief) flanked by periplatform talus. Late Early Cambrian to early Middle Cambrian regression, possibly associated with Rome Trough rifting, caused widespread deposition of red beds on the shelf interior while the more rapidly subsiding outer platform was not exposed, but continued to increase in relief by upbuilding of the shelf margin above the adjacent basin. This rimmed shelf persisted for the remainder of the Cambrian until it was destroyed by Early and Middle Ordovician incipient collision.

Carbonate ramp to rimmed shelf transitions occur in Cambro-Ordovician rocks elsewhere in North America, but few can be studied in the detail provided by the drill cores through the Shady Dolomite platform margin. Furthermore, the detailed core

coverage makes this one of the best cored Paleozoic shelf margins anywhere in the world, and perhaps provides an analog for poorly drilled, deeply buried Mesozoic margins that developed above Triassic-Jurassic rift and shelf clastic facies along the eastern U.S.

DOLOMITIZATION OF A CARBONATE PLATFORM DURING DEEP BURIAL: LOWER TO MIDDLE CAMBRIAN SHADY DOLOMITE, VIRGINIA APPALACHIANS

ABSTRACT

The Lower to Middle Cambrian Shady Dolomite carbonate platform records several episodes of replacement dolomitization and dolomite cementation during late burial. Although much of the sequence is dolomitized, remnant limestones record a prior history of meteoric dissolution and calcite cementation. The first dolomite generation, zone 1, occurs as rare relict, corroded cores, which were replaced and overgrown by zone 2A dolomite, the dominant replacement phase. Zone 2A dolomites are burial, because they postdate calcite cement, are associated with fractures and stylolites, form anhedral mosaics indicative of elevated precipitation temperatures, and in part, are contemporary with hydrocarbon migration. Following replacement dolomitization, the sequence was subjected to dissolution, coeval with late fracturing and brecciation. Brecciated host dolomite fragments are locally encrusted by pyrite, sphalerite, and galena. Zone 2B dolomite is the dominant dolomite cement, and precipitated after major fracturing and ore deposition. A second episode of fracturing, brecciation, and minor dissolution affected zone 2A and 2B dolomites, followed by zone 3 and 4 dolomite cementation, minor sphalerite, authigenic quartz, and late calcite and dedolomite.

Stable isotope compositions of marine calcite cements are tightly clustered ($\delta^{18}O$ = -7.5 to -6.1 ‰ PDB; $\delta^{13}C$ = +0.2 to +0.8 ‰ PDB). Zone 1 dolomite cannot be directly sampled but it apparently has similar geochemistry as zone 2A dolomite. The depleted ^{18}O and enriched ^{13}C compositions of zone 2A dolomite ($\delta^{18}O$ = -10.2 to -7.0; $\delta^{13}C$ = +1.0 to +1.6) relative to marine cements reflect precipitation at elevated temperatures from fluids in equilibrium with the host limestone. Zone 2B dolomite cement ($\delta^{18}O$ = -10.3 to -7.4; $\delta^{13}C$ = +0.4 to +1.1) has similar $\delta^{18}O$ as zone 2A

dolomite, indicating precipitation from fluids with similar temperatures and $\delta^{18}O$ composition as zone 2A dolomitizing fluids. Zones 3 and 4 dolomite cements ($\delta^{18}O$ = -13.8 to -11.3; $\delta^{13}C$ = -0.7 to +0.9) are more depleted in ^{18}O than previous zones, reflecting increased temperatures.

The dolomites are all stoichiometric. Mn and Fe contents in zone 2A replacement dolomite (Mn = 100 to 1200 ppm; Fe = 300 to 6000 ppm) exhibit a well-defined, linear covariation, interpreted to reflect primarily a pH control. Mn and Fe are highest in more coarsely crystalline dolomite, which may indicate precipitation under more acidic conditions immediately prior to burial dissolution. Zone 2B dolomite cement has relatively low Mn and Fe contents (Mn = 100 to 300 ppm; Fe = 240 to 1300 ppm), suggesting less acidic conditions following major dissolution, which is compatible with dolomite cementation. Zone 3 dolomite (Mn = 230 to 340 ppm; Fe = 0 to 800 ppm) has the lowest Fe/Mn ratios, reflecting pyrite precipitation whereas zone 4 dolomite cement has enriched Mn up to 1400 ppm and Fe up to 9000 ppm, indicating that the late fluids were enriched in Mn and Fe.

Zone 2A replacement dolomite and zone 2B dolomite cement have similar low Sr contents (25 to 65 ppm); $^{87}Sr/^{86}Sr$ ratios (0.70900 to 0.70971) coincide with marine calcite cement (0.70869 to 0.70975), indicating that Sr derived from limestone dissolution dominated the fluid Sr chemistry during replacement dolomitization and early dolomite cementation. Sr contents in zones 3 and zone 4 dolomite cements are 60 to120 ppm, and $^{87}Sr/^{86}Sr$ ratios (0.71025 to 0.71445) are higher, recording the influx of radiogenic Sr-enriched brines during late stage dolomite cementation. Late calcite and dedolomite ($^{87}Sr/^{86}Sr$ = 0.70963 to 0.71234) are similarly enriched in radiogenic Sr.

Primary fluid inclusions in zone 2B dolomite, and sphalerite, which immediately

predates the dolomite, suggest that the dolomite precipitated from hot (100 to 175°C), saline (23-26 wt.% NaCl equiv.) fluids. Later, halite-bearing inclusions in quartz and calcite indicate hotter (175 to 225°C), more saline (30 to 33 wt.% NaCl equiv.) fluids. These temperatures are compatible with estimated maximum burial depths in excess of 5 kilimeters.

The replacement dolomites, Pb-Zn ore minerals, dolomite cements, and late quartz and calcite formed coeval with late Paleozoic deformation. The burial signature of the replacement dolomites reflects that imparted during burial dolomitization of limestone, rather than diagenetic overprinting of an abundant near-surface metastable dolomite precursor, because some petrographic or geochemical evidence of an abundant dolomite precursor should have been preserved, other than the rare, relict zone 1 cores that are geochemically similar to the burial dolomite.

Burial dolomitization of limestone requires importation of large quantities of Mg^{2+}. However, the $^{87}Sr/^{86}Sr$ ratios of the replacement dolomite are identical to marine carbonate, indicating that the Mg^{2+} was not from basinal shales, but may have been derived from pressure solution of the structurally lower Knox Dolomite that was being overthrust in the late Paleozoic. Regional, deeply penetrating fluid flow that developed in response to tectonic uplift may have transported this Mg^{2+} via fault and fracture conduits to the Shady Dolomite platform margin to dolomitize the sequence during late burial.

INTRODUCTION

Dolomitized carbonate platform margins bordering large basins are economically important because they may become significant hydrocarbon reservoirs and hosts for

Zn-Pb deposits. Dolomitization processes that may affect such carbonate platforms include: reflux of evaporatively concentrated sea water on exposed tidal flats (Patterson and Kinsman, 1982); dolomitization by normal sea water in a subtidal setting (Behrens and Land, 1972); dolomitization of outer platform facies by convective circulation of sea water (Aharon et al., 1987); dolomitization in a mixing zone of sea water/meteoric water (Ward and Halley, 1985); and dolomitization during deep burial (Mattes and Mountjoy, 1980). However, there have been few detailed studies of dolomites associated with such ancient platform margins.

Although most workers favor early dolomitization by sea water, modified sea water, or mixed sea water/meteoric water because of the availability of Mg^{2+} (cf. Land, 1985), some have proposed that dolomitization of platform margins may occur during deep burial (Mattes and Mountjoy, 1980). Geochemically, replacement dolomitization is favored at elevated burial temperatures, because fluids with lower Mg/Ca ratios are still potentially dolomitizing, reaction rates are greatly increased and kinetic inhibitors are decreased, and the considerable time that carbonate platforms reside in the burial regime allows sufficient time for dolomite replacement to proceed to completion (Mattes and Mountjoy, 1980; Zenger, 1983; Hardie, 1987). However, criticism of extensive dolomitization of limestone during burial has focussed on the Mg^{2+} source and delivery mechanism in the deep subsurface (Morrow, 1982; Land, 1985). Although petrographic, geochemical, and isotopic analysis of dolomites may indicate their timing and origin, the problem is compounded in many dolomitized sequences by replacement of earlier dolomite phases by successively later dolomite. This may overprint the original isotopic and trace element geochemistry of the early dolomite, and make it appear to be of burial origin (Land, 1985).

The Lower to Middle Cambrian Shady Dolomite (Pfeil and Read, 1980; Barnaby and Read, in press), which had been extensively cored for Zn-Pb exploration (Fig. 1), provided an excellent opportunity to study this problem. The study area is in the easternmost thrust sheet of the Valley and Ridge province of southwest Virginia (Fig. 12). Outer carbonate platform facies of the Shady Dolomite have been extensively dolomitized (Fig. 13), and a major goal of this study was to determine the relative timing and origin of the dolomites, in the context of the regional geologic history of the carbonate platform. Plane light and cathodoluminescent petrography were used to establish a paragenetic sequence of replacement dolomitization, dolomite cementation, and determine their relation to meteoric diagenesis, Pb-Zn ore deposition, and precipitation of late quartz and calcite (Fig. 14). Individual diagenetic generations were sampled for Ca, Mg, Fe, Mn, and Sr, stable isotopes ($^{18}0$, ^{13}C), and radiogenic isotopes ($^{87}Sr/^{86}Sr$) and fluid inclusions. The geochemistry of the various dolomite generations allowed the chemical and isotopic composition of the diagenetic fluids and their geochemical evolution to be evaluated. This, in conjunction with the regional geologic history, allowed constraints to be placed on likely dolomitization processes. The evidence suggests that the Shady Dolomite platform margin was dolomitized in a burial environment during regional, gravity-driven fluid flow that developed in response to tectonic uplift during Alleghanian deformation. It is emphasized that these conclusions apply only to the 5 km wide outer edge of the Shady Dolomite platform of the study area, which lacks significant tidal flats, and does not apply to the 400 km wide platform interior of the Shady Dolomite (Fig. 3), which may contain significant amounts of early dolomite.

Figure 12. Regional balanced cross-section (after Kulander and Dean, 1986; Bartholomew, 1987). Knox Group dolomites indicated by black, Shady Dolomite of study area shown by arrow (immediately west of Blue Ridge Fault). Structure of lowermost thrust sheet beneath Blue Ridge and Pulaski faults has been greatly simplified.

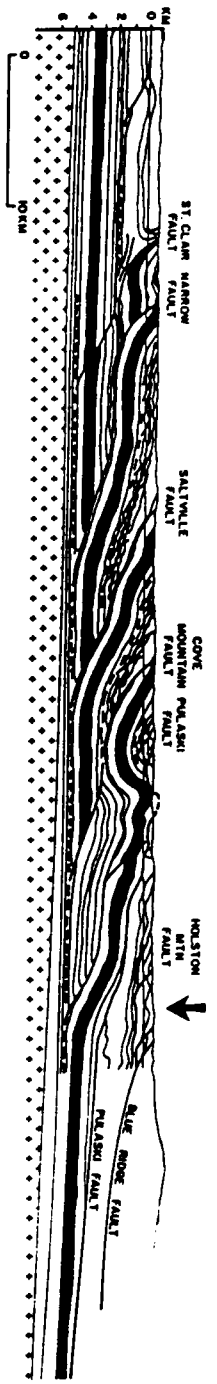
KM
0
2
4
6
0
10 KM
ST. CLAIR FAULT
NARROW FAULT
SALTVILLE FAULT
COVE MOUNTAIN FAULT
PULASKI FAULT
HOLSTON MTN FAULT
BLUE RIDGE FAULT
PULASKI FAULT

Figure 13. Top diagram is stratigraphic cross-section modified from figure 6. On lower diagram, dots indicate the locations of thin sections which were examined using plane light and cathodoluminescent petrography. Distribution of unreplaced limestones indicated by stipple pattern. Distribution of dolomite zones shown by vertical lines labelled 1, 2A, 2B, 3, and 4, indicating the presence or absence of each zone.

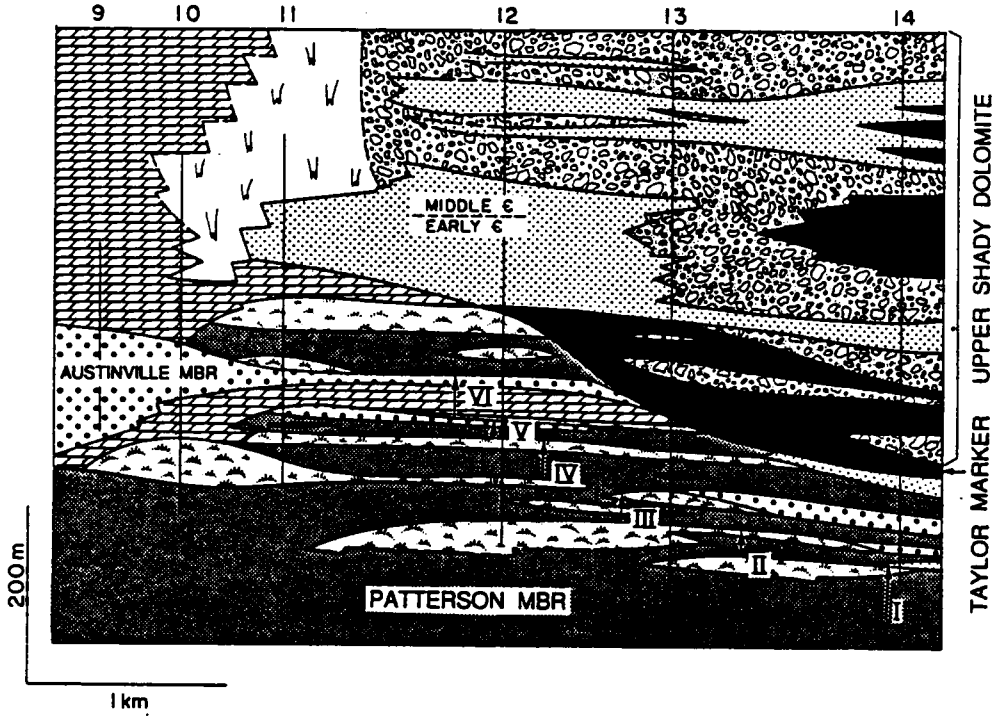
9
10
11
12
13
14
MIDDLE Є
EARLY Є
AUSTINVILLE MBR
VI
V
IV
III
II
I
PATTERSON MBR
TAYLOR MARKER
UPPER SHADY DOLOMITE
200 m
1 km

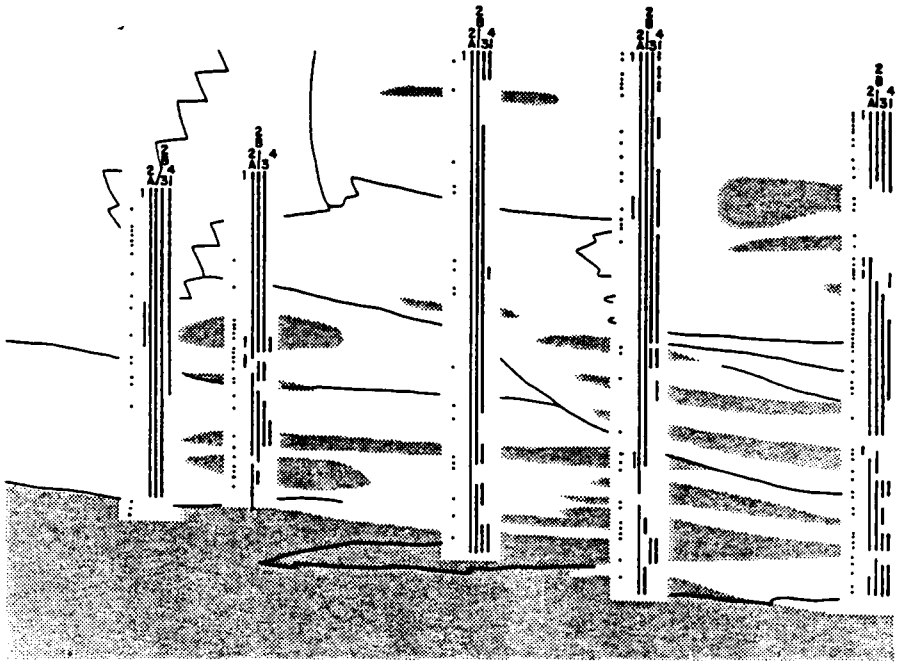

Figure 14. Paragenetic sequence, Shady Dolomite in Austinville region. Geologically younger events to the right.

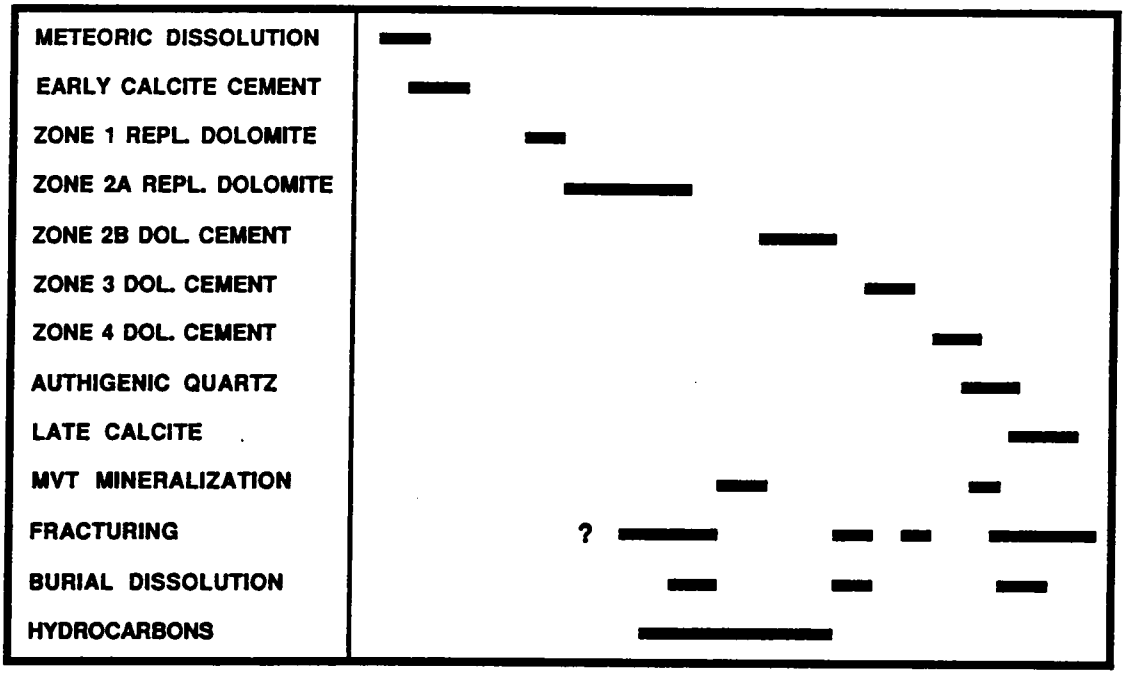
METEORIC DISSOLUTION
EARLY CALCITE CEMENT
ZONE 1 REPL. DOLOMITE
ZONE 2A REPL. DOLOMITE
ZONE 2B DOL. CEMENT
ZONE 3 DOL. CEMENT
ZONE 4 DOL. CEMENT
AUTHIGENIC QUARTZ
LATE CALCITE
MVT MINERALIZATION
FRACTURING
?
BURIAL DISSOLUTION
HYDROCARBONS

METHODS

Twenty six drill cores (9360 m total length) of the Early to Middle Cambrian Shady Dolomite in southwestern Virginia were logged (Fig. 1). The closely-spaced drill cores form several transects through the Shady Dolomite platform margin, and allowed detailed cross sections to be constructed (Figs. 6, 7, and 8), permitting the facies relations and evolution of the carbonate platform to be documented (Barnaby and Read, in press). Samples were taken from all lithologies, with emphasis on the replacement dolomites and dolomite cements. Over 450 uncovered thin sections were stained (Dickson, 1965) and examined using conventional petrographic techniques and cathodoluminescent petrography with a Technosyn Cold Cathode Luminescence Model 8200 Mk II (16 to 18 kV gun potential, 0.6 mA beam current, and ≈ 0.03 torr vacuum).

For elemental and isotopic analyses, ultrasonically cleaned, unstained rock chips were microsampled using a bench mounted milling machine equipped with dental drills under a binocular microscope. The samples were examined under cathodoluminescence before and after drilling, to ascertain that individual dolomite and calcite generations, based on cathodoluminescent petrography, were isolated for analysis. Following drilling, the samples were reground to the depth of maximum drill penetration, repolished, and examined under cathodoluminescence to ensure that the sample consisted solely of the desired diagenetic phase.

Major and trace element compositions (Ca, Mg, Fe, Mn, Sr) of individual dolomite and calcite generations, were determined by Inductively Coupled Plasma Spectroscopy (ICP). The analytical procedure is described in detail in the appendix. Between 0.0140 and 0.0160 grams of carbonate sample was dissolved in 10 ml of 0.2 N HCl for 4 hours,

under constant agitation. This weak acid was used to minimize contamination by leaching of clays or other admixed detrital or authigenic minerals. After dissolution, the samples were acidified by adding of 1 ml of 3.5 N HCl, to bring the acidity to 0.5 N, and the acidified sample was immediately centrifuged and decanted into polyethylene sample bottles with screw closures. The insoluble residue was filtered and weighed, and if significant (> 3%), deducted from the sample weight.

The aliquots were analysed using a Jarrell-Ash ICAP 9000 Simultaneous Spectrometer; Sr was analysed using a Jarrell-Ash Atomscan 2400 Sequential Spectrometer. Analytical accuracy, determined by analysis of blind solution standards, was generally within 3%, and never more than 6 % in error. Analytical precision, determined by replicate analyses of British Chemical Standard (BCS) No. 368 dolomite, are ($\pm$ 1σ): Ca = $\pm$3.6 %; Mg = $\pm$3.5 %; Fe = $\pm$9.5 %; Mn = $\pm$3.9 %, and Sr = $\pm$2.6 %.

Stable isotope analysis of carbonates was conducted at Stable Isotope Laboratory, University of Miami, Rosenstiel School of Marine and Atmospheric Sciences, under the direction of Peter Swart. The analytical procedure is outlined in Dawans and Swart (1988) except that no correction was applied for dolomite-phosphoric acid fractionation. A blind standard (NBS 19) was submitted as a check on the analytical accuracy, the result was in excellent agreement with the accepted value.

$^{87}Sr/^{86}Sr$ analyses were conducted by Chempet Research Corporation, under the direction of R. W. Hurst and T. E. Davis. Ultraclean methods were used to eliminate possible contamination. Calcites were digested in 5 ml of 5% ULTREX acetic acid; dolomites were digested in 5 ml of 10% ULTREX acetic acid; both were performed at room temperature. Reactions were complete after 5-10 minutes; beakers were examined for fine particulates using a stereo microscope; in all cases, no residue was observed. Sr

was separated using standard ion exchange techniques and analyzed on a 30 cm, 90° sector, thermal ionization mass spectrometer; isotopic fractionation was corrected using the accepted $^{87}Sr/^{86}Sr$ ratio of 0.11940. Analytical precision was better than ± 0.00004 (1σ). $^{87}Sr/^{86}Sr$ data are reported adjusted to a value of 0.71022 for NBS-987.

Fluid inclusion samples were selected and prepared using procedures according to Hollister et al. (1981). The samples were never heated above room temperature during preparation. Two- and three-phase inclusions were analyzed using a USGS-type gas-flow heating and freezing stage. The thermocouple used for temperature determinations was routinely calibrated to ensure accurate temperature readings.

MARINE CEMENTS

Petrography and Geochemistry

Marine cements are common in outer platform facies and form banded isopachous crusts up to several centimeters thick that line primary voids in banks and reefs, and encrust clasts in periplatform breccias (Fig. 9J). They predate and are interlayered with infiltrated internal marine sediments, are locally truncated by clast boundaries (Read and Pfeil, 1983), and predate early compaction and clear equant cements.

The marine cements consist of fibrous to bladed, turbid brown crystals with undulatory, radial-fibrous or radiaxial extinction. Fibrous cements contain one or more stacked layers of nestled elongate crystals or tightly packed, cone-shaped bundles of smaller subcrystals. Bladed marine cements consist of turbid, elongate crystals oriented normal to the substrate, with planar intercrystalline boundaries and rhombohedral crystal terminations. Under cathodoluminescence, the marine cements exhibit nonluminescent to

very dull orange-brown luminescence, although later overgrowths of brightly to dully luminescent cement (commonly finely subzoned) are locally developed.

The isotopic and geochemical composition of petrographically well-preserved Early Cambrian marine cements are given in Table 1 and figure 15. These data provide a baseline with which to assess the chemistry of later diagenetic phases.

Interpretation

The cements precipitated from marine water during and soon after sedimentation and are petrographically identical to Early Cambrian (James and Klappa, 1983), and Tertiary to Recent high-Mg marine cements (Schroeder, 1972; James et al., 1976; Kendall, 1977; James and Ginsburg, 1979; Saller, 1986; Aïssaoui, 1988).

The ^{18}O compositions are comparable to Early Cambrian marine cements in Labrador (James and Klappa, 1983) but are depleted in ^{18}O relative to Recent marine cements ($\delta^{18}O \approx$ -1.0 to +2.3: Shinn, 1969; Ginsburg et al., 1971; James and Ginsburg, 1979; González and Lohmann, 1985). This ^{18}O depletion may reflect different ^{18}O composition of seawater in the geologic past (eg., Perry, 1967; Perry and Tan, 1972; Perry et al., 1978; Brand and Veizer, 1981), although others (Muehlenbachs and Clayton, 1976; Gregory and Taylor, 1981; Muehlenbachs, 1986) suggest that the ^{18}O composition of seawater has remained essentially constant since the Archean. If the depleted ^{18}O values reflect precipitation from seawater of similar ^{18}O composition to that of today, but at higher temperatures (Knauth and Epstein, 1976), it implies that ocean temperatures were at least 25°C warmer in the Lower Cambrian, which appears to be unlikely. The ^{18}O compositions of the marine cements may also reflect alteration by ^{18}O depleted waters, although their narrow range of $\delta^{18}O$ values would require that the cements were

Table 1. Summary of geochemical and isotopic data for marine cement, host limestone, zone 2A replacement dolomite, zones 2B, 3, and 4 dolomite cement, and late calcite. N = number of analyses, avg. = average.

TABLE 1. SUMMARY OF TRACE ELEMENT AND ISOTOPE GEOCHEMISTRY

	PPM MG		PPM MN		PPM FE		PPM SR	
	RANGE	AVG. (N)	RANGE	AVG. (N)	RANGE	AVG. (N)	RANGE	AVG. (N)
MARINE CEMENT	2090 to 2700	2420 (5)	45 to 155	80 (5)	60 to 300	115 (5)	140 to 200	165 (5)
HOST LIMESTONE	1900 to 2920	2315 (5)	65 to 195	110 (5)	100 to 580	265 (5)	145 to 200	175 (5)
ZONE 2A REPL. DOL.	--	--	100 to 1200	420 (81)	400 to 6000	1920 (81)	25 to 65	40 (80)
ZONE 2B DOL. CEMENT	--	--	100 to 300	165 (13)	240 to 1300	650 (13)	30 to 45	40 (13)
ZONE 3 DOL. CEMENT	--	--	230 to 340	260 (9)	0 to 800	340 (9)	60 to 130	100 (9)
ZONE 4 DOL. CEMENT	--	--	740 to 1300	1030 (2)	4000 to 9300	6650 (2)	90 to 135	110 (2)
LATE CALCITE	1240 to 3260	2095 (9)	75 to 4805	2110 (9)	95 to 1470	665 (9)	90 to 510	190 (9)

	$\delta^{18}O$		$\delta^{13}C$		$^{87}Sr/^{86}Sr$
	RANGE	AVG. (N)	RANGE	AVG. (N)	RANGE (N)
MARINE CEMENT	-7.5 to -6.1	-6.9 (16)	+0.2 to +0.8	+0.5 (16)	0.70869 to 0.70975 (4)
HOST LIMESTONE	--	--	--	--	--
ZONE 2A REPL. DOL.	-10.2 to -7.0	-8.7 (36)	+1.0 to +1.6	+1.3 (36)	0.70900 to 0.70971 (6)
ZONE 2B DOL. CEMENT	-10.3 to -7.4	-8.7 (10)	+0.4 to +1.1	+0.8 (10)	0.70933 to 0.70966 (4)
ZONE 3 DOL. CEMENT	-13.8 to -13.0	-13.4 (10)	-0.7 to +0.6	-0.1 (10)	0.71033 to 0.71072 (2)
ZONE 4 DOL. CEMENT	-13.8 to -11.3	-13.0 (7)	+0.4 to +0.9	+0.7 (7)	0.71025 to 0.71445 (2)
LATE CALCITE	-16.6 to -6.6	-9.9 (25)	-4.7 to -0.1	-1.3 (25)	0.70963 to 0.71234 (4)

Figure 15. Stable isotope data, all expressed relative to PDB. Open squares = marine calcite cement; open circles = zone 2A replacement dolomite; filled circles = zone 2A replacement dolomite with zone 1 cores; open triangles = zone 2B dolomite cement; diamonds = zone 3 dolomite cement; filled squares = zone 4 dolomite cement; filled triangles = late calcite cement. Estimated marine dolomite based on marine cement stable isotope values, using $\Delta^{18}O_{dol\text{-}calcite}$ = +2 to +4 ‰ (Land, 1980; McKenzie, 1981).

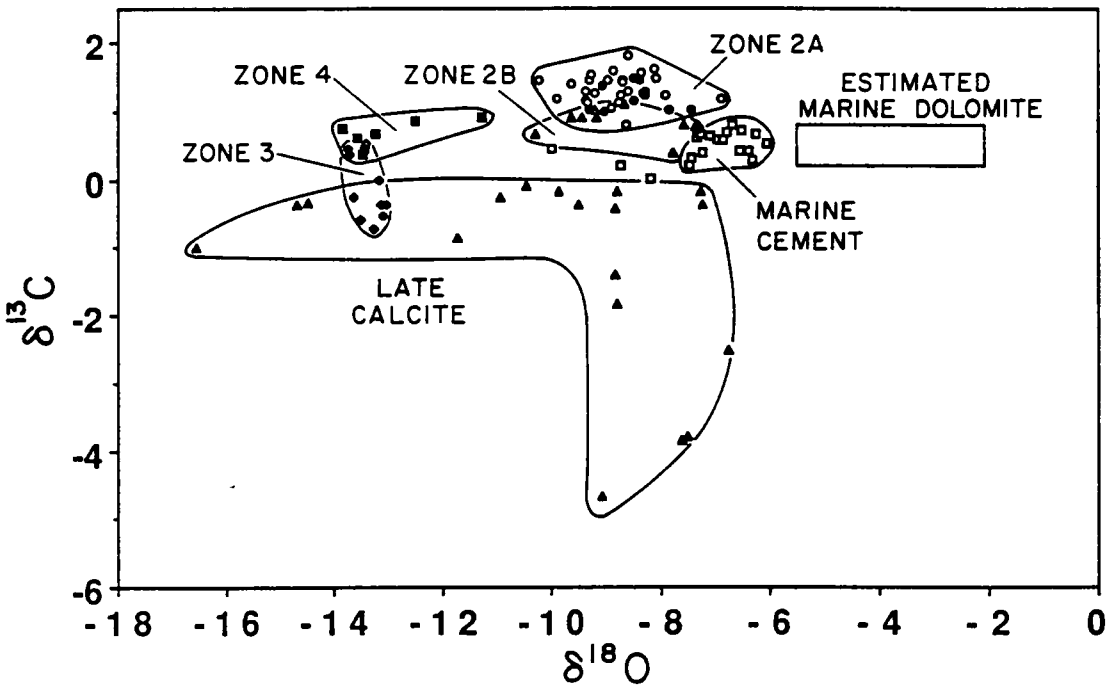
ZONE 4
ZONE 2B
ZONE 2A
ESTIMATED
MARINE DOLOMITE
ZONE 3
MARINE
CEMENT
LATE
CALCITE
2
0
-2
-4
-6
δ13C
-18
-16
-14
-12
-10
-8
-6
-4
-2
0
δ18O

completely reequilibrated to the $\delta^{18}O$ composition of the diagenetic fluid. In any case, the $\delta^{18}O$ values of the marine cement are a *minimum* estimate of their original ^{18}O composition, and these values provide a *minimum* estimate of the magnitude of isotopic depletion of later diagenetic phases.

The $\delta^{13}C$ composition of the marine cements is considered representative of the host limestone, because it was not likely to have been depleted during meteoric diagenesis since ther are no Cambrian land plants. Furthermore, the initial $\delta^{13}C$ composition of a calcite is difficult to alter by meteoric waters, because the dissolved bicarbonate concentration in these waters is low relative to that in the calcite.

The Mn and Fe contents of the marine cements (less than 150 and 300 ppm, respectively) are compatible with precipitation from oxygenated marine waters. The low Mg contents (< 2700 ppm), the paucity of microdolomite (c.f., Lohmann and Meyers; 1977), and the low Sr contents (< 200 ppm) indicate that the marine cements and host limestone underwent mineralogic stabilization in meteoric fresh waters during which Mg and Sr was expelled.

The $^{87}Sr/^{86}Sr$ ratios yielded from the marine cements (Table 1) coincide with those reported by Veizer and Compston (1974) for Lower Cambrian marine carbonates (0.70877 to 0.70975, corrected to 0.70800 for E & A standard).

EARLY DISSOLUTION AND CALCITE CEMENTATION

Description

Remnant limestones in the Shady Dolomite record an early episode of dissolution and clear calcite cementation. Leaching was largely confined to echinoderms in interior

platform carbonates. Cavities may be floored by crystal silt followed by drusy to equant, pink-staining, calcite cement which predates significant compaction and fracturing. In downslope talus blocks, there are locally two generations of geopetal lime silt that differ in orientation and predate the calcite cement (Read and Pfeil, 1983). The calcite cements (Fig. 16A) are nonluminescent to brightly luminescent to dully luminescent (this study; also Read and Pfeil, 1983). Because later dolomitization has obliterated most of the record of early calcite cementation, obscuring the regional CL cement stratigraphy (cf. Meyers, 1978), the early calcite cements were not included in the study other than to constrain the relative timing of the dolomite paragenesis.

Interpretation

Selective dissolution of unstable carbonate grains (largely high Mg-calcite echinoderms) is restricted to interior platform locations, indicating that the diagenetic fluids were undersaturated with respect to Mg-calcite in the updip portions of a paleoaquifer system and that the fluids increasingly equilibrated with the host carbonate as they flowed downdip. The calcite cements postdate marine cementation, grain dissolution, and emplacement of crystal silt but predate compaction, fracturing, and dolomite replacement. Thus they formed at relatively shallow burial depths.

The low Fe content of the early cements ($< \approx$1000 ppm Fe, Nelson and Read, in press) indicated by their pink stain (Dickson, 1965) reflects precipitation from relatively oxidizing waters which contained little Fe^{2+}. The nonluminescent calcite cement formed from oxidizing meteoric groundwaters in the updip portion of an aquifer near the recharge region (Frank et al., 1982; Barnaby and Rimstidt, 1989). The later bright and dully luminescent calcite cements formed under more reducing conditions in the downdip part

Figure 16. Photographs of dolomite types. In all microphotographs, scale bar = 0.5 mm. A) Cathodoluminescent microphotograph of early calcite cement with nonluminescent, brightly luminescent, and dully luminescent zones which are postdated by dark orange-red luminescent zone 2A replacement dolomite. B) Polished slab stained with alizarin red S, calcite stains red, dolomite is unstained; dolomite is associated with late fractures, and forms replacement halos adjacent to fractures. C) and D) Paired plane light and cathodoluminescent microphotographs. Limeclast grainstone replaced by dark orange-red luminescent zone 2A dolomite was fractured, followed by precipitation of zone 2B dolomite cement with identical dark orange-red luminescence as zone 2A dolomite. Zone 2B dolomite cement was followed by bright orange luminescent zone 3 dolomite cement (extreme right of 'D'). E) Cathodoluminescent microphotograph showing dark orange-red zone 2B dolomite cement which was fractured and overgrown by bright orange zone 3 dolomite cement, followed by a final void fill of dull orange-red zone 4 dolomite cement. F) Cathodoluminescent microphotograph showing relict dark orange-red zone 2B saddle dolomite cement spears that are overgrown and replaced (dedolomitized) by bright orange-yellow luminescent calcite.

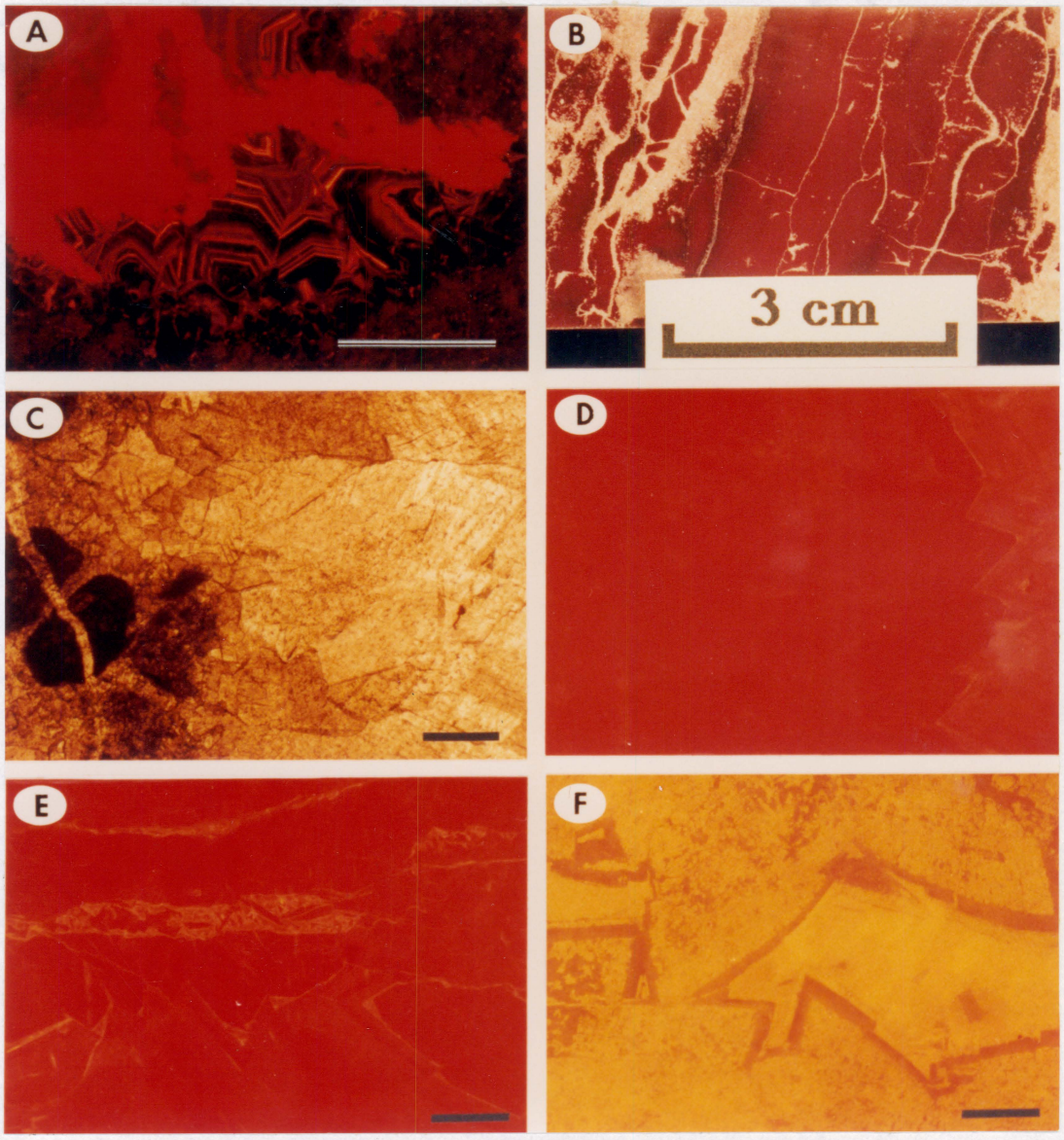
A
B
3 cm
C
D
E
F

of the aquifer away from the recharge region or during burial. The groundwaters from which the early calcite cements precipitated may have been recharged when the Shady Dolomite platform was subjected to subaerial exposure during intraformational sea level lowstands (Barnaby and Read, in press), or they may reflect aquifer recharge during development of the Rome unconformity following Shady Dolomite deposition.

Clear calcite cements in periplatform talus reefal blocks appear to have precipitated after downslope transport of the blocks, as indicated by the geopetal structures which were deposited both before and after rotation and downslope transport of algal blocks (Read and Pfeil, 1983). There is no indication that the off-platform, deep water carbonates were subaerially exposed during sea level lowstands (Barnaby and Read, in press), thus, the cementing fluids must have been derived from the exposed platform interior, either during low stands during deposition of the Shady-Rome sequence, or during Rome unconformity time. Given sufficient hydraulic head, meteoric ground waters in a confined coastal aquifer may extend far seaward of the shoreline (Collins and Gelhar, 1971; Frind, 1982), and these meteoric fluids may have flowed downdip to the off-platform Shady Dolomite sequence via permeable periplatform breccia and grainstone beds that are interbedded with impermeable shale and shaly carbonate.

DOLOMITE AND LATER DIAGENETIC PHASES

Dolomite Distribution

Most of the Shady Dolomite has been dolomitized. Relict limestones generally are interbedded with deeper water shale and shaly carbonates (Fig. 13), but also include peritidal limestones (Ivanhoe member) interbedded with minor shale beds and overlain by

red mudrocks and shale of the Rome Formation (Pfeil and Read, 1980). Dolomite replacement fronts generally are conformable with bedding, although some are discordant (Pfeil, 1977; this study). In partially dolomitized limestones, the replacement dolomite commonly is associated with tectonic fractures and stylolites of burial origin, and replacement dolomitization is most extensive adjacent to the fractures and stylolites, forming a replacement halo that extends out into the unreplaced host limestone.

Petrography

Based on plane light and cathodoluminescent petrography, four major generations of dolomite replacement and cementation have been defined which can be recognized throughout the region (Fig. 13). The cathodoluminescent dolomite stratigraphy provided the framework for determining the paragenetic sequence, and subsequent geochemical and isotopic sampling.

Replacement Dolomite (Zones 1, 2A). Replacement dolomite postdates marine cement and early meteoric calcite (Fig. 16A). Dolomite occurs as a selective replacement of lime mud and grains; a nonselective replacement along dolomitization fronts in limestone; and along fractures and stylolitic seams; more commonly, the dolomite completely replaces the precursor limestone.

Where the limestone host is partially replaced by dolomite, the more finely crystalline carbonate components (lime mud, algal filaments, ooids, limeclasts) generally are selectively dolomitized, whereas calcite cements (both marine and nonmarine) and calcitic skeletal grains are unreplaced. The dolomite may be disseminated throughout the limestone host, or associated with veins, fractures and stylolites (Fig. 16B). The

replacement dolomite is finely to coarsely crystalline, and composed of generally anhedral crystals. Completely dolomitized lithologies are composed of anhedral dolomite mosaics with little intercrystalline porosity. The dolomite crystals have nonplanar and curved, irregular and serrated boundaries (xenotopic dolomite), are turbid brown, inclusion-rich, and commonly have undulatory extinction (saddle dolomite). Euhedral, turbid dolomite cores with limpid overgrowths are locally well-developed. Locally, bitumen occurs in intercrystalline porosity in dolomite mosaics.

Fine to medium crystalline dolomite preserves the original fabric (Fig. 17A) and generally replaces fine-grained limestones. Echinoderm grains and marine cements are pseudomorphically replaced, with the replacement dolomite in optical continuity with the original calcite. Coarsely crystalline dolomite tends to obliterate or obscure the primary rock fabric. It appears to be largely confined to coarse-grained lithologies, in which sedimentary grains are locally preserved as ghosts defined by more turbid, inclusion-rich regions (Fig. 17B).

Two generations of replacement dolomite are indicated by cathodoluminescent petrography. Nonluminescent (to very dull), relict zone 1 dolomite cores are the first recognized dolomite generation (Fig. 18). Zone 1 dolomite is relatively uncommon (<< 5% of the replacement dolomite), and was extensively replaced, corroded, and overgrown by dark orange-red to dark red luminescent zone 2A dolomite (Figs. 16C, 16D), which accounts for over 95% of the total replacement dolomite.

Secondary Dissolution and Fracture Porosity. Late dissolution postdates zone 2A replacement dolomitization and is largely confined to the dolomitized lithologies. Secondary porosity in dolomites is non-fabric selective, and formed vuggy porosity and

Figure 17. Microphotographs of zone 2A replacement dolomite fabrics (plane light) scale bar = 0.5 mm. A) Replacement by finely crystalline zone 2A dolomite promotes preservation of precursor limestone fabric, in this example of a dolomitized algal bioherm, the skeletal algae (*Epiphyton*) are clearly defined. B) Replacement by coarsely crystalline zone 2A dolomite tends to obliterate the primary depositional fabric, only in rare samples are precursor grains (in this example - ooids) preserved as relict ghosts.

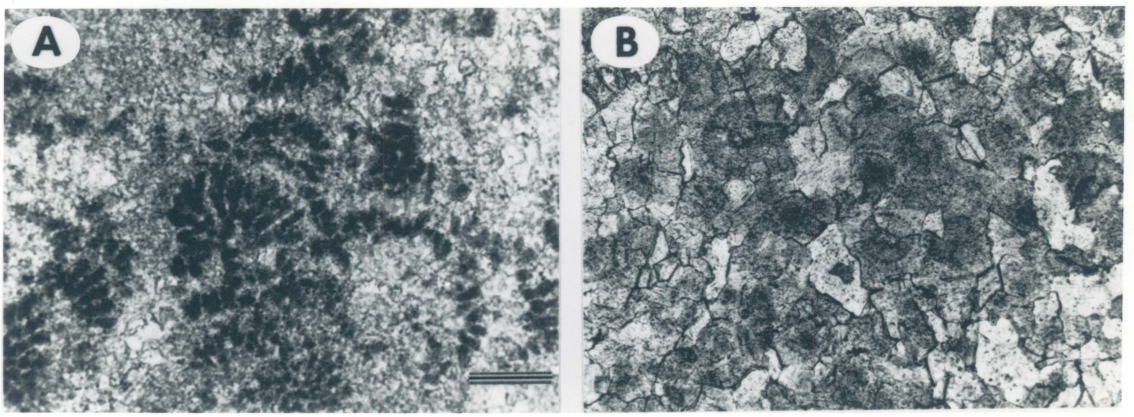
A
B

Figure 18. Cathodoluminescent microphotograph, scale bar = 25 μm. Nonluminescent zone 1 dolomite cores were overgrown, corroded, and replaced by a more brightly luminescent dolomite (zones 2A/2B), followed by an overgrowth of nonluminescent dolomite (correlative to the local nonluminescent overgrowths on zone 2B dolomite cement), and later brightly luminescent dolomite cement (zone 3) and a final dully luminescent dolomite cement (zone 4). Note that locally the zone 1 dolomite cores were preferentially replaced by zone 2A dolomite. See figure 16 for cathodoluminescent colors of zones 2A, 2B, 3, and 4 dolomite.

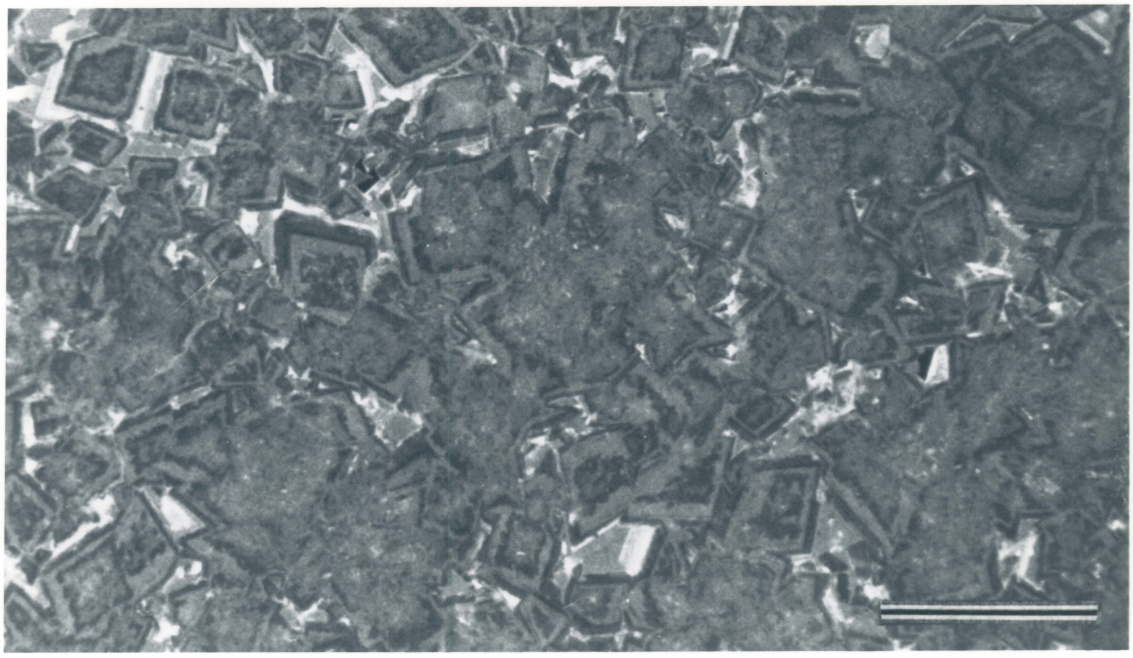

solution breccias. Preserved limestones were subjected to less late dissolution, which was chiefly fabric selective. Considerable secondary porosity and permeability also resulted from late fracturing and brecciation. Extensive fracturing formed breccias with angular brecciated clasts of host dolomite that locally float in a matrix of void-filling dolomite cement.

Pb-Zn Ore Deposition. Following replacement dolomitization, and development of fracture and dissolution porosity, the sequence was subjected to several episodes of Pb-Zn ore mineralization. Both replacement and void-filling ore depositional textures are recognized. The first episode of mineralization consists of pyrite, sphalerite, and galena, which encrust fractured and brecciated host replacement dolomite. These ore minerals were overgrown by dolomite cement, followed by minor amounts of void-filling sphalerite. The ore mineral paragenesis and textures are described in Foley (1980).

Dolomite Cement (Zones 2B, 3, 4). Dolomite cements occur in residual primary pore space and secondary dissolution and fracture porosity (Fig. 19A). They locally overgrow MVT ore minerals, but more commonly, the dolomite cement directly overgrows the host dolomite. Fracture and dissolution voids locally are floored by geopetal dolomite sediment (Fig. 19B). These geopetal structures generally are oriented correctly with respect to present-day up, regardless of the dip of the enclosing beds (Read and Pfeil, 1983; this study). Cement-supported rock fabrics, including zebra rock, are common (Fig. 19A) and locally the open-space filling dolomite cement is volumetrically more abundant than the fractured and brecciated host dolomite.

Sparry dolomite cements are white to light gray in hand specimen. Dolomite cements

Figure 19. Dissolution and dolomite cement fabrics. A) Zebra rock, consisting of brecciated and corroded remnants of host dolomite (dark gray) and open space-filling, white sparry dolomite cement. B) Microphotograph of zebra rock, scale bar = 0.5 mm. Stylotitized remnants of host dolomite (black) form framework of open void space, floored by dolomite silt, followed by coarsely crystalline dolomite cement.

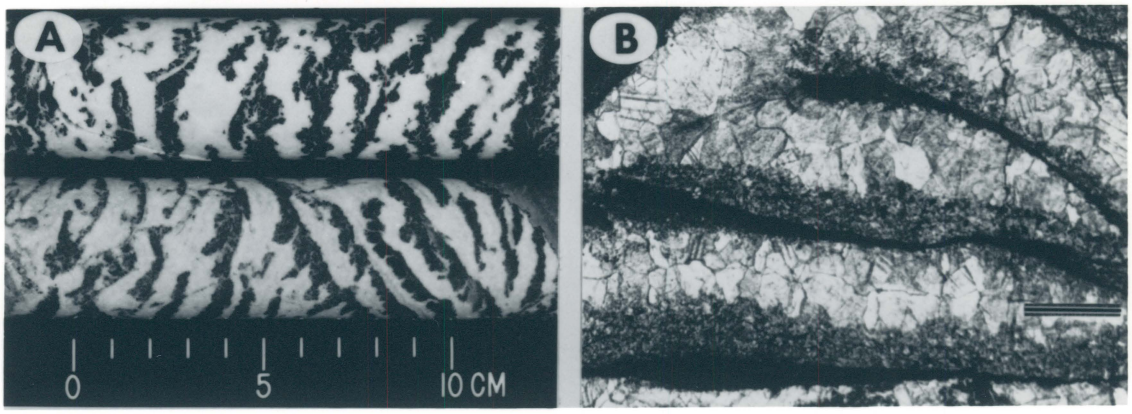
A
0
5
10 CM
B

with saddle (cf. Radke and Mathis, 1980) and nonsaddle morphologies and petrographic characteristics are common. Saddle dolomite cements consist of pore-lining, euhedral to subhedral spear-shaped crystals (few mm to several mm in length) of turbid brown, inclusion-rich dolomite with curved crystal faces and cleavage planes, and sweeping extinction under crossed polars. Dolomite cements also form anhedral mosaics of equant coarse to very coarse crystals. Euhedral, nonsaddle pore-lining dolomite cements with planar, rhombic terminations also are common. Both the saddle and nonsaddle dolomite cements commonly have clear overgrowths over more turbid cores. Locally, bitumen occludes remaining pore space.

Three major generations of dolomite cementation are recognized under cathodoluminescence. The first generation, zone 2B, has identical dark orange-red to dark red luminescence as zone 2A replacement dolomite (Fig. 16C, 16D). Zone 2B is volumetrically the major generation of dolomite cement, and may in part be coeval with zone 2A replacement dolomite. A thin rim of nonluminescent (to very dull) dolomite cement locally conformably overgrows zone 2B dolomite cement. Following zone 2B dolomite cementation, a second, less intensive, episode of fracturing, dissolution, and corrosion affected the sequence. Bright orange-red cathodoluminescent dolomite cement (zone 3) then precipitated as overgrowths on zone 2B dolomite cements, and heals fractures in the previous dolomite generations (Fig. 16E). Zone 3 dolomite is commonly associated with pyrite, which generally occurs as a thin, discontinuous rim that encrusted the dolomite substrate prior to precipitation of zone 3 dolomite cement. Zone 3 cement is locally subzoned with alternating fine growth zones of slightly brighter and more dully luminescent dolomite.

Dull, brownish orange-red dolomite cement (zone 4) conformably overgrows zone 3

dolomite and occurs as a final void-filling cement (Fig. 16E). Zone 4 dolomite also locally occurs in fractures which transect previous dolomite cement generations. Zone 4 dolomite was followed by precipitation of sphalerite, authigenic quartz, late calcite and dedolomite.

Authigenic Quartz. Precipitation of authigenic quartz largely followed dolomite cementation, although inclusions of zone 4 dolomite in quartz growth zones indicate that initial quartz precipitation was synchronous with the latest saddle dolomite cementation. Authigenic quartz was overgrown (commonly corrosionally) by late stage calcite cement.

Late Calcite and Dedolomite. Late stage calcite occurs as a cement in residual porosity and in fractures, overgrows corroded earlier replacement dolomite and dolomite cement, and replaced dolomite to form dedolomite (Fig. 16F). The calcite cement consists of coarse equant crystals with cleavage twins. Dedolomite is fabric selective, and is largely confined to the more turbid, inclusion-rich cores of zone 2A and 2B dolomite. Dedolomite fabrics are similar to those described in Frank (1981) and Budai et al. (1984). Dedolomite may occur as scattered patches in dolomite cores, or may nearly completely replace the dolomite, leaving only residual, limpid dolomite rims. Dedolomite also is developed along fractures and cleavage traces in dolomite. The dedolomite replacement calcite is in optical continuity with the dolomite.

The calcite and dedolomite stains pink to purple with Dickson's (1965) solution, the stained zonation is variable. They luminesce a homogeneous bright orange-yellow, followed by later dully luminescent calcite cement. The bright orange-yellow luminescent calcite exhibits no relation to the stain color. The last calcite generation consists of thin

veins of dully luminescent, blue-staining calcite.

GEOCHEMISTRY

Dolomite

Dolomite Stoichiometry. Based on ICP analyses, the zone 1 and zone 2A replacement dolomites, and zone 2B and zone 3 dolomite cements are all nearly stoichiometric (50 ± 1 mole % $CaCO_3$). Zone 4 dolomite cements exhibit a slight Ca enrichment, with up to 2 mole % excess $CaCO_3$.

Dolomite $\delta^{18}O$ Composition. The $\delta^{18}O$ values of zone 1 replacement dolomite could not be directly determined due to its pervasive replacement by zone 2A dolomite. However, samples of zone 2A dolomite with zone 1 cores (up to 20% of the sample volume, estimated visually) have comparable $\delta^{18}O$ compositions to samples of zone 2A dolomite that lack zone 1 cores (Fig. 15), suggesting that zone 1 and zone 2A replacement dolomites are isotopically similar. The ^{18}O compositions for all the zone 2A replacement dolomites are similar, despite differences in crystal size (Fig. 20), dolomite fabric, or lithology and depositional environment of the limestone precursor. They are depleted in ^{18}O relative to the marine calcite (Table 1, Fig. 15).

$\delta^{18}O$ values for zone 2B dolomite cement are identical to those of the zone 2A replacement dolomites (Table 1, Fig. 15). The late stage zones 3 and 4 dolomite cements are depleted in $\delta^{18}O$ by 3 to 4 ‰ relative to the earlier dolomite generations.

Figure 20. Zone 2A replacement dolomite, $\delta^{18}O$, $\delta^{13}C$, Fe, Mn, and total Sr versus crystal size. Fe and Mn contents are higher in the more coarsely crystalline dolomites, whereas $\delta^{18}O$, $\delta^{13}C$, and Sr remain essentially constant regardless of crystal size.

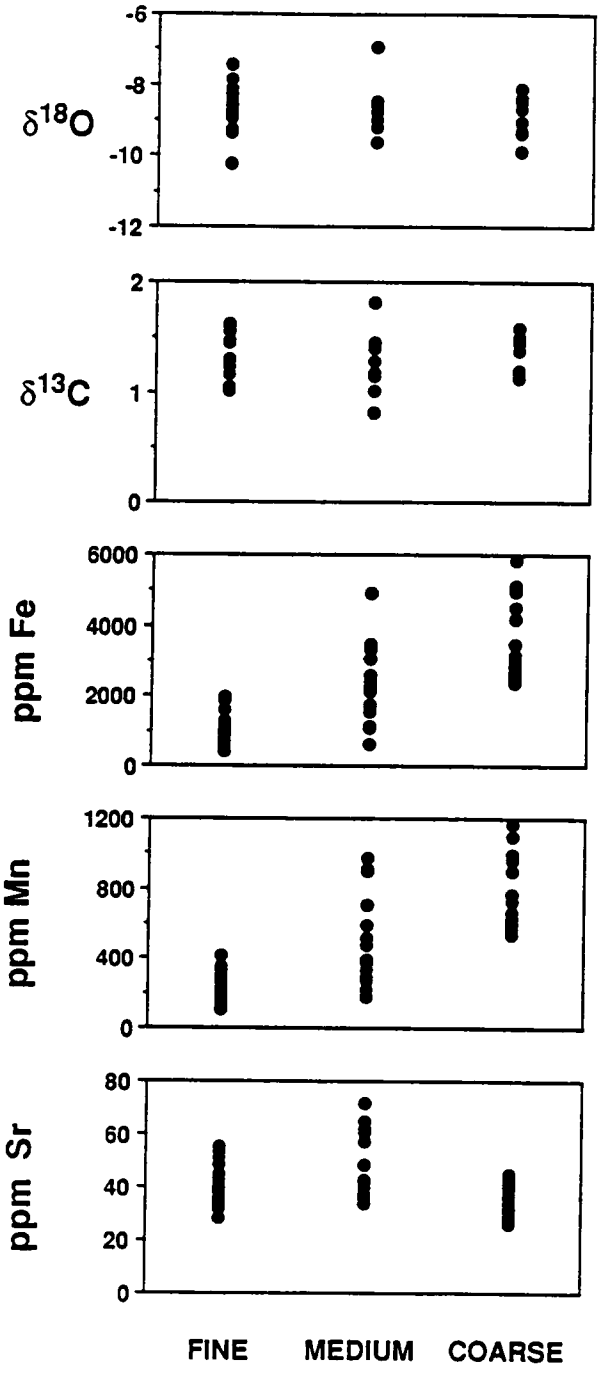
δ18O
-6
-8
-10
-12
δ13C
2
1
0
ppm Fe
6000
4000
2000
0
ppm Mn
1200
800
400
0
ppm Sr
80
60
40
20
0
FINE
MEDIUM
COARSE

Dolomite $\delta^{13}C$ Composition. The $\delta^{13}C$ composition of zone 1 replacement dolomite appears to be comparable to that of zone 2A replacement dolomite (Fig. 15). The ^{13}C compositions of the zone 2A replacement dolomites exhibit limited variation, and are independent of crystal size (Fig. 20), dolomite fabric, or the lithofacies of the limestone precursor. Zone 2A dolomite is enriched in ^{13}C relative to marine calcite (Table 1, Fig. 15).

The ^{13}C values for the zone 2B dolomite cements are depleted relative to the zone 2B replacement dolomites, but are similar to the marine cements (Table 1, Fig. 15). The $\delta^{13}C$ composition of zone 3 dolomite cement trends towards slightly depleted values, whereas $\delta^{13}C$ values of zone 4 dolomite cement are similar to marine carbonate and to zone 2B dolomite cement.

Dolomite Mn and Fe Contents. Samples of zone 2A replacement dolomite with zone 1 dolomite cores, and samples of zone 2A dolomite lacking such cores have similar Mn and Fe contents. The Mn and Fe compositions of zone 2A replacement dolomites (Table 1, Fig. 21) exhibit a statistically significant ($r^2 = 0.90$) positive covariation (Fig. 22), with Fe content averaging about five times greater than Mn content. Mn and Fe contents are higher in progressively more coarsely crystalline dolomite (Fig. 20).

Mn and Fe contents of zone 2B dolomite cements (Table 1) are similar to the more depleted values for the zone 2A replacement dolomites, and exhibit the same linear covariation (fig. 21). Zone 3 dolomite cement has the lowest Mn/Fe ratios of all the dolomites. Zone 4 dolomite cement is the most enriched in Mn and Fe.

Figure 21. Mn and Fe chemistry of marine cements, dolomite zones, and late calcite. Dotted squares = marine calcite cement; solid circles = zone 2A replacement dolomite; open circles = zone 2B dolomite cement; open squares = zone 3 dolomite cement; triangles = zone 4 dolomite cement; diamonds = late calcite cement.

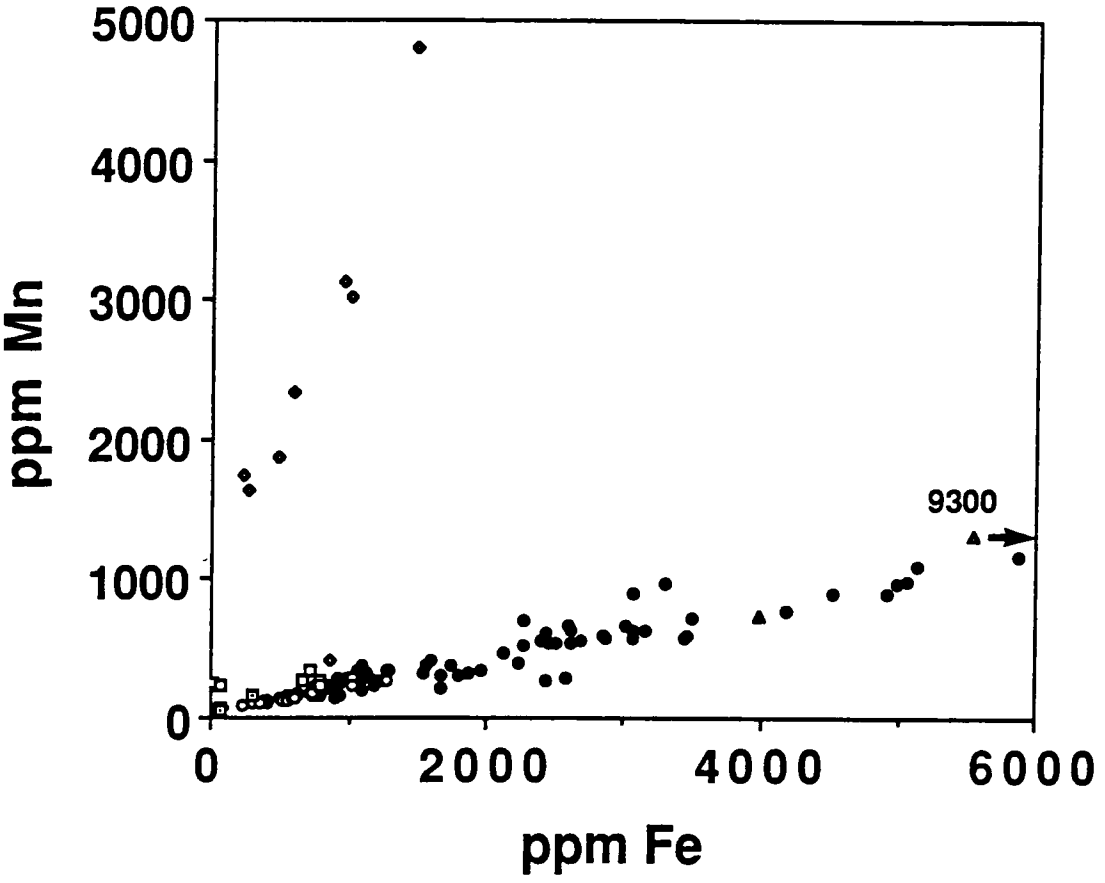
5000
4000
3000
2000
1000
0
ppm Mn
9300
0
2000
4000
6000
ppm Fe

Figure 22. Mn vs Fe plot of zone 2A replacement dolomite. Plot exhibits a statistically significant, positive covariation. The open circles represent dolomitized argillaceous deeper water dolomite samples. They exhibit the greatest deviation from the linear relationship, which likely reflects variable leaching of Mn and Fe from admixed detrital phases; if these detrital-rich samples were excluded from the data set, the correlation coefficient would be even greater.

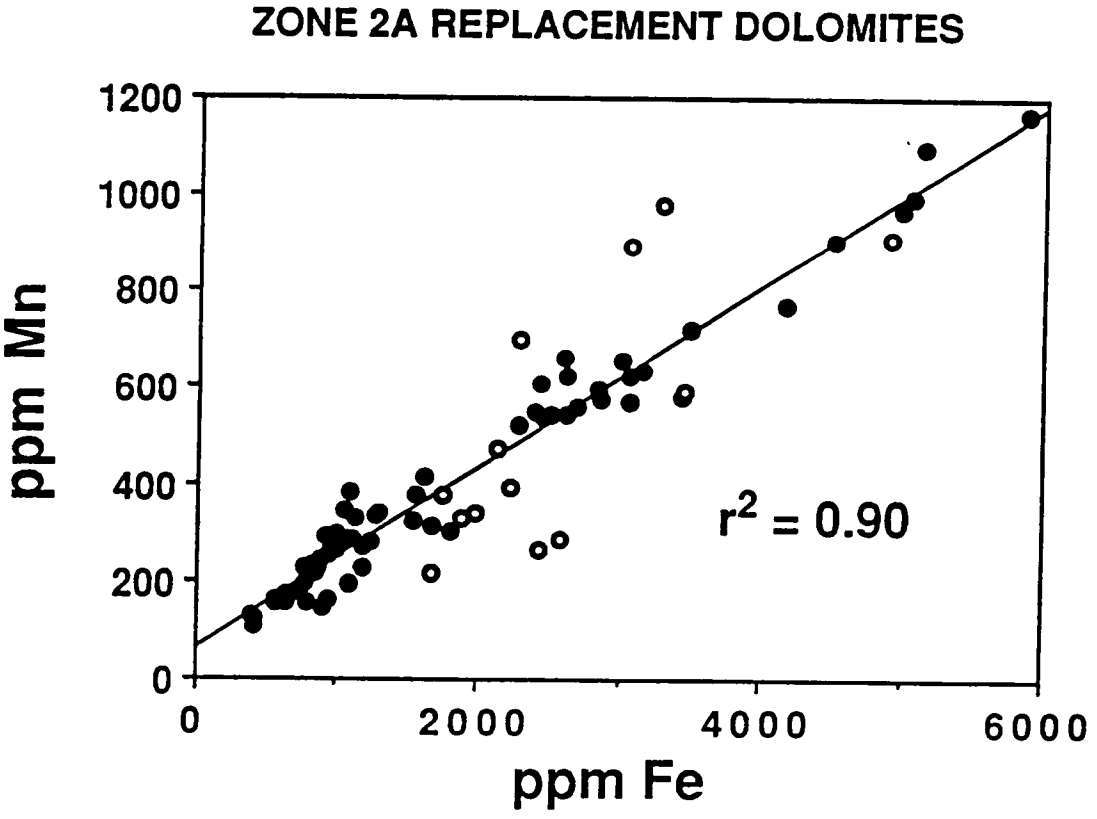
ZONE 2A REPLACEMENT DOLOMITES
ppm Mn
1200
1000
800
600
400
200
0
0
2000
4000
6000
ppm Fe
r2 = 0.90

Dolomite Total Sr and $^{87}Sr/^{86}Sr$ Compositions. Zone 1 replacement dolomite apparently has similar total Sr contents as the zone 2A replacement dolomites, which are uniformly low in Sr (Table 1), independent of the crystal size (Fig. 20), dolomite fabric, or precursor lithology. Zone 2B dolomite cement has similarly low total Sr contents. $^{87}Sr/^{86}Sr$ ratios for zone 2A replacement dolomites and zone 2B dolomite cement are identical to those of the marine cements (Table 1, Fig. 23). Zones 3 and 4 dolomite cement are enriched in total Sr, and have higher $^{87}Sr/^{86}Sr$ ratios than previous dolomite generations and marine cements.

Authigenic Quartz

Two quartz samples yielded similar $\delta^{18}O$ values ($\delta^{18}O$ = +20.2 ‰ SMOW).

Late Calcite and Dedolomite

The $\delta^{18}O$ and $\delta^{13}C$ values (Table 1, Fig. 15) are variable, and no systematic variation with respect to the stained zonation is evident. No consistent isotopic trend was defined from successive sampling into the center of voids. In addition, there is no apparent geographic or stratigraphic relationship of the stable isotope composition of the late calcites.

Mg contents display limited variation (Table 1). Mn/Fe ratios are higher than for the dolomites (Fig. 21). Total Sr contents also are higher than for the earlier dolomites, and the late calcites are enriched in radiogenic Sr (Fig. 23).

Figure 23. $^{87}Sr/^{86}Sr$ data for marine calcite cement, zone 2A replacement dolomite, zones 2B, 3, and 4 dolomite cement and late calcite cement.

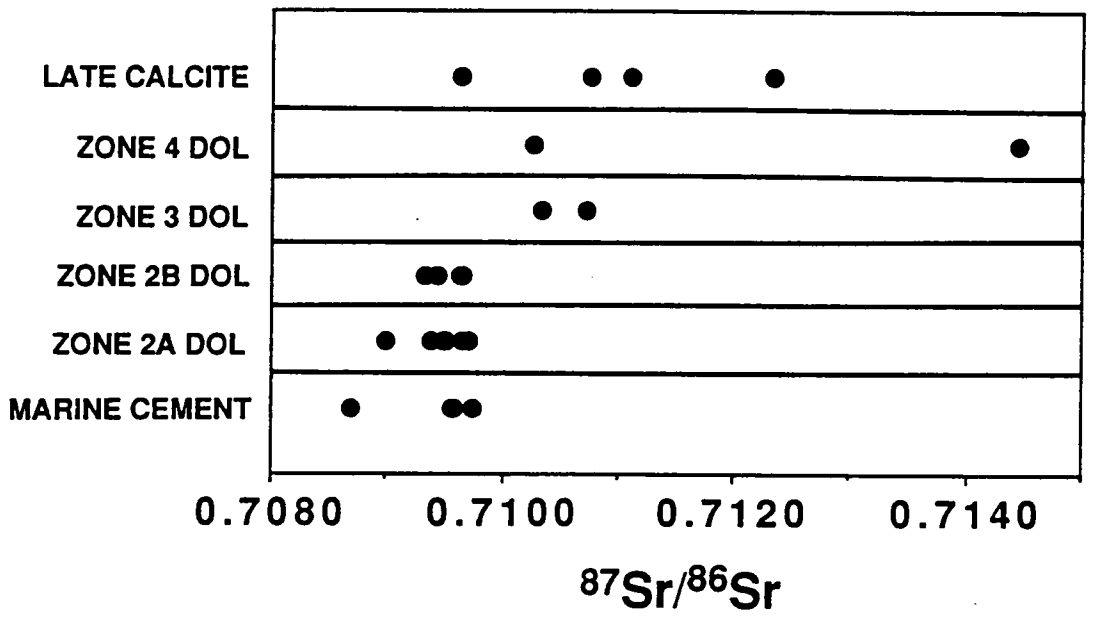
LATE CALCITE
ZONE 4 DOL
ZONE 3 DOL
ZONE 2B DOL
ZONE 2A DOL
MARINE CEMENT
0.7080
0.7100
0.7120
0.7140
87Sr/86Sr

FLUID INCLUSIONS

Primary Fluid Inclusions - Sphalerite

Primary, 2-phase fluid inclusions in sphalerite homogenize at 100 to 160°C (Foley, 1980). No freezing data is available for the sphalerite inclusions, which precludes estimating the inclusion salinities or applying pressure corrections to the homogenization temperatures.

Primary Fluid Inclusions - Zone 2B Dolomite

Primary 2-phase fluid (liquid + vapor) inclusions in zone 2B dolomite cement are confined to the turbid, inclusion-rich dolomite cores, which are overgrown by limpid zone 2B dolomite cement lacking primary inclusions. Homogenization temperatures are 120 to 150°C (Fig. 24A). Tm ice (-23.1 to -21.5°C) is lower than the binary eutectic of the NaCl-H_2O system (-20.8°C), indicating the presence of Ca^{2+} and/or Mg^{2+}. If hydrohalite were present above Tm (temperature of melting) ice, it was not detected due to the small inclusion size (< 5 μm). Estimated salinities, based on Tm ice and lack of halite daughter minerals, are 23.3 to 26.3 weight percent NaCl equivalent. The intersection of the inclusion isochores with hydrostatic geothermal gradients define minimum pressures of 400 to 750 bars and pressure-corrected temperatures of 150 to 225°C (Fig. 25A).

Primary Fluid Inclusions - Late Calcite

Late calcite contains primary (?) 2-phase fluid inclusions which do not occur along obvious microfractures or cleavage traces and cannot be positively attributed to a

Figure 24. Fluid inclusion data: N = number of samples; 1^{o} = primary inclusions; 2^{o} = secondary inclusions; Th = temperature of homogenization, 2-phase inclusions; Th L-V (L) temperature of vapor bubble homogenization, 3-phase inclusions; Tm NaCl = temperature of melting of halite daughter crystals (= temperature of total homogenization), 3-phase inclusions. C, C' and E, E' are Th L-V (L) and Tm NaCl, respectively, for the same fluid inclusions. A) Primary inclusions, zone 2B dolomite. Tm ice (-23.1 to -21.5°C) indicates the presence of $Ca^{2+} \pm Mg^{2+}$, estimated salinities are 23.3 to 26.3 wt. % NaCl equiv. (see text). B) Secondary inclusions, authigenic quartz. Tm ice (-14.5 to -20.8°C) and Tm hydrohalite (-20.0 to 0.0°C), indicate inclusion salinities of18.2 to 22.9 wt. % and 23.3 to 26.3 wt. % NaCl equivalent, respectively (see text). C) Secondary 3-phase fluid inclusions in quartz, temperature of vapor bubble homogenization. C') Same 3-phase inclusions, temperature of total homogenization by halite dissolution (Tm NaCl). Tm NaCl indicates salinities were 30.5 to 33.1 wt. % NaCl equivalent. D) Primary inclusions, late calcite. Estimated salinities are 23.3 to 26.3 wt. % NaCl equivalent, based on freezing measurements (see text). E) Secondary 3-phase inclusions in calcite are cogenetic with 3-phase inclusions in authigenic quartz. The higher vapor bubble homogenization temperatures likely reflect inclusion stretching. E') Same inclusions, temperatures of halite dissolution (Tm NaCl), correspond to inclusion salinities of 30.7 to 32.4 wt. % NaCl equivalent.

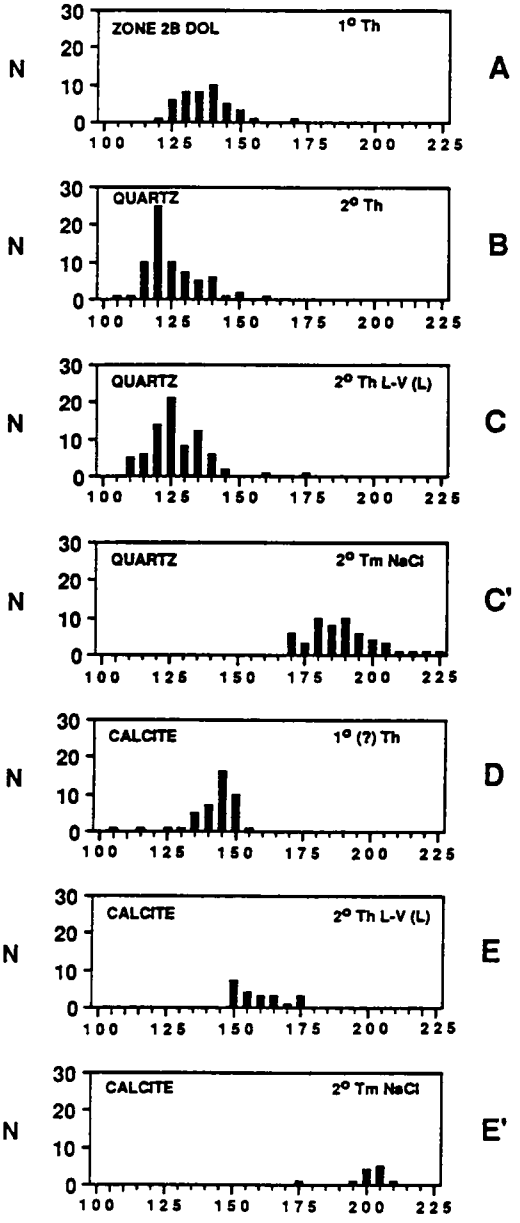
ZONE 2B DOL
1° Th
A
QUARTZ
2° Th
B
QUARTZ
2° Th L-V (L)
C
QUARTZ
2° Tm NaCl
C'
CALCITE
1° (?) Th
D
CALCITE
2° Th L-V (L)
E
CALCITE
2° Tm NaCl
E'
N
30
20
10
0
100
125
150
175
200
225
T °C

Figure 25. P-T diagrams of part of system NaCl-H_2O. H = halite, L = liquid; v = vapor. Isochores plotted from data of Potter and Brown (1977).

A) Primary 2-phase inclusions in zone 2B dolomite cement. Intersection of inclusion isochores with hydrostatic P-T gradients define pressure corrected temperatures of 150 to 225°C and minimum pressures of 400 to 750 bars.

B) Secondary 3-phase, halite-bearing inclusions in late quartz. Shaded region delimits minimum trapping pressures estimated from the intersections of the inclusion isochores with the liquidus curves corresponding to inclusion salinities (30.5 to 32 wt. % NaCl equiv.).

C) Actual P-T conditions of entrapment for halite-bearing inclusions may have been greater, and lie within the region defined by the two isochores projected to increasing P-T conditions, to a maximum burial temperature of 250°C. Estimated pressures range up to 1600 bars. P-T conditions (shaded region) generally exceed those defined by hydrostatic load, indicating that the fluids forming the inclusions were overpressured.

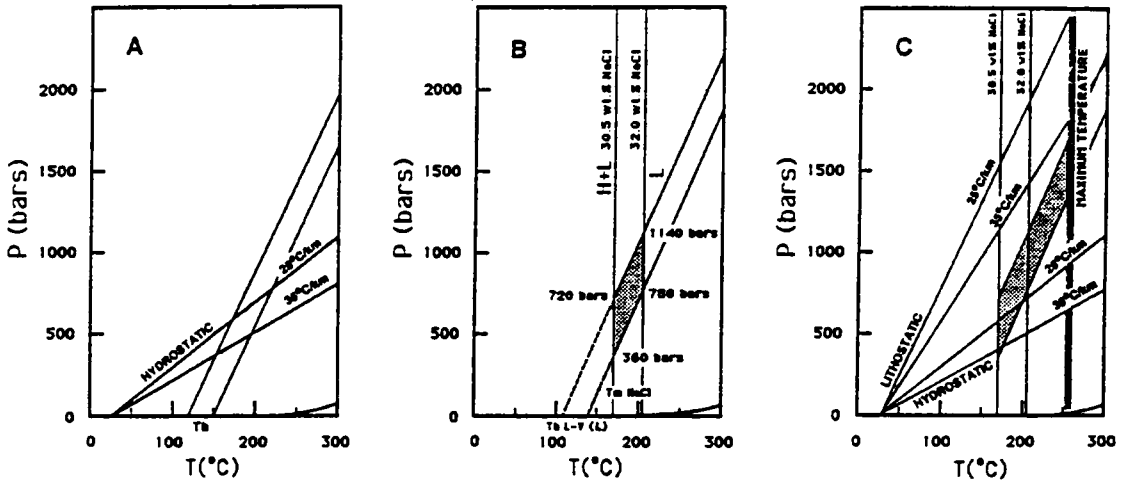
A
B
C
P (bars)
T(°C)
HYDROSTATIC
LITHOSTATIC
720 bars
786 bars
1140 bars
360 bars
MAXIMUM TEMPERATURE

secondary origin. Homogenization temperatures for these inclusions are 135 to 150°C (Fig. 24D). Tm ice (-24.2 to -23.4°C) is lower than the ternary eutectic of the NaCl-KCl-H_2O system (-22.9°C), indicating the presence of Ca^{2+} and/or Mg^{2+}. Estimated salinities, based on Tm ice and the lack of halite daughter minerals, range from 23.3 to 26.3 weight percent NaCl equivalent. Estimated minimum pressures are 430 to 770 bars, and minimum pressure-corrected temperatures are 165 to 225°C (hydrostatic pressure).

Secondary Fluid Inclusions - Authigenic Quartz and Late Calcite

Secondary 2-phase inclusions occur along healed microfractures in quartz, and homogenization temperatures are 115 and 140°C (Fig. 24B). Two types of inclusion behavior are evident upon freezing, in some inclusions Tm ice > Tm hydrohalite (Tm ice = -14.5 to -20.8°C), whereas in other inclusions, Tm ice < Tm hydrohalite (Tm hydrohalite = -20.0 to 0.0°C), yielding inclusion salinities of 18.2 to 22.9 wt. % and 23.3 to 26.3 wt. % NaCl equivalent, respectively (Fig. 26). In these latter inclusions, Tm ice is generally less than the ternary eutectic of the H_2O-NaCl-KCl system (-22.9°C), indicating the presence of $Ca^{2+} \pm Mg^{2+}$.

Three-phase (liquid + vapor + halite) fluid inclusions (Fig. 27) occur along microfractures in quartz and calcite. In the quartz inclusions, homogenization of the vapor bubble occurred at 110 to 145°C (Fig. 24C), vapor bubble homogenization occurred at 150 to 175°C for the calcite inclusions (Fig. 24E). Total homogenization by halite dissolution occurred at 170 to 225°C for the quartz and calcite inclusions (Figs. 24C', 24E'). Based on Tm NaCl, estimated salinities (Fig. 26) are 30.5 to 33.1 wt.% NaCl equivalent (Barnaby and Bodnar, 1988).

Figure 26. Secondary fluid inclusions from quartz, Th and Th L-V (L) for 2- and 3-phase inclusions, respectively, paired with estimated salinity. T °C = temperature of homogenization for 2-phase inclusions and temperature of vapor bubble homogenization for the 3-phase inclusions. Open circles = 2-phase inclusions with Tm ice > Tm hydrohalite, salinity estimated from Tm ice; filled circles = 2-phase inclusions with Tm ice < Tm hydrohalite, salinity estimated from Tm hydrohalite; open squares = 3-phase inclusions, salinity estimated from Tm halite daughter crystals.

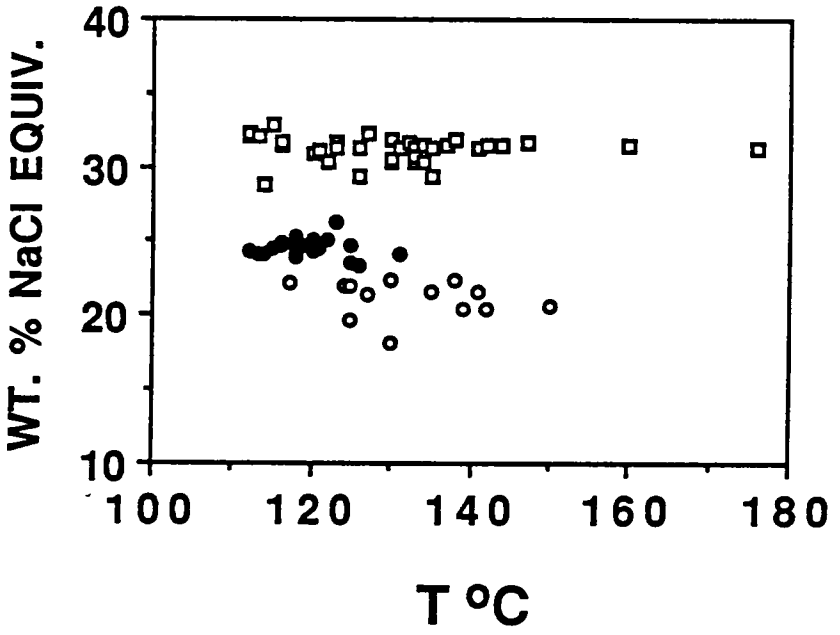
WT. % NaCl EQUIV.
40
30
20
10
100
120
140
160
180
T °C

Figure 27. Secondary 3-phase (halite + liquid + vapor) fluid inclusions in quartz, scale bar = 25 μm.

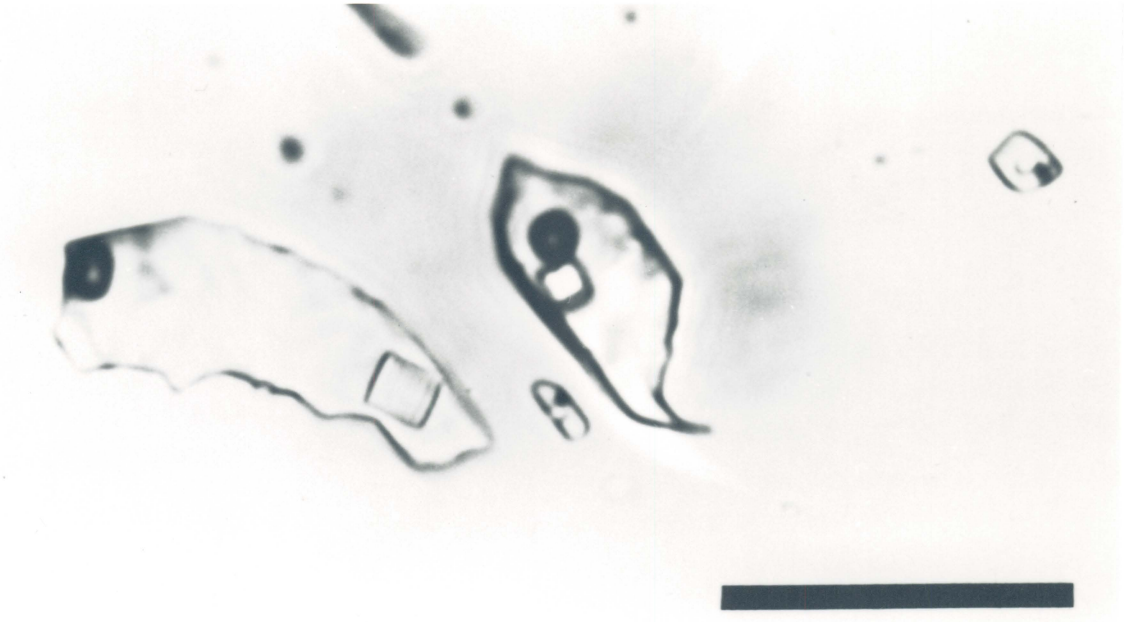

Homogenization temperatures for the 2-phase inclusions were similar to vapor bubble homogenization temperatures for the halite-bearing inclusions (Fig. 26). The separation between the estimated salinity ranges defined by the 2- and 3-phase inclusions reflects the difficulty of halite nucleation in slightly oversaturated solutions.

GEOLOGICAL AND PETROGRAPHIC EVIDENCE OF TIMING OF PARAGENETIC SEQUENCE

Zone 1 Replacement Dolomite

Zone 1 dolomite is rare (<< 5 % of the samples), which reflects either an initial scarcity of this dolomite type or pervasive replacement by later dolomite. Because zone 1 dolomite is typically present as relicts that were replaced and corroded by zone 2A dolomite, it must have been metastable. Due to its scarcity and poor development, the relative timing of zone 1 dolomite could not be determined, other than the observation that it predates zone 2A dolomite. Because it was overprinted by zone 2A dolomite, it was not possible to isolate zone 1 dolomite for geochemical and isotopic analysis, thus the geochemistry cannot be used to assess whether this dolomite is early or late. Evidence against a tidal flat origin for this dolomite is the lack of tidal flats along the outer platform of the Shady Dolomite in the study area. However a marine origin or mixing zone origin cannot be ruled out for this minor dolomite type.

Zone 2A Replacement Dolomite

Zone 2A replacement dolomite formed during late burial, because: 1) it postdates meteoric dissolution and calcite cements that formed during shallow to deep burial; 2) it

commonly is associated with tectonic fractures, veins, and stylolites of burial origin, and forms dolomite replacement halos extending out from these features into the host limestone; and 3) the anhedral mosaic (xenotopic) dolomite fabrics are indicative of elevated burial temperatures (> 50 to 100°C, Gregg and Sibley, 1984), and, 4) zone 2A replacement dolomite is coeval with hydrocarbon emplacement, as bitumen occurs in intercrystalline pore space in euhedral dolomite mosaics, where it arrested further dolomite overgrowth and coalescence. Hydrocarbon emplacement indicates temperatures in the oil window of approximately 60 to 150°C (Pusey, 1973).

The fabric preservation potential of zone 2A replacement dolomite was influenced by the grain size of the precursor limestone. Fine grained limestones were commonly replaced by finely crystalline, fabric preservative dolomite, because the precursor limestones had a high relative surface area, which provided numerous potential nucleation sites (Sibley, 1982; Bullen and Sibley, 1984; Sibley and Gregg, 1987). In contrast, the coarser grained limestones were replaced by coarsely crystalline dolomites that obscured or obliterated the original fabric, because the precursor limestone provided fewer nucleation sites (Sibley, 1982; Sibley and Gregg, 1987).

Pb-Zn Ore Deposition

Ore mineralization is late in that it was closely associated with tectonic faulting and fracturing; both pre- and post-ore deformation are recognized; and faults exerted an important influence on the ore body location (Weinberg, 1971). Ore minerals encrust fractured and brecciated host replacement dolomite, and occur in secondary dissolution porosity. The ore bodies were subjected to limited post-depositional deformation as attested by faulting (Weinberg, 1971), and curved cleavage traces in galena and

deformation twins in sphalerite (Foley, 1980; this study). The ore minerals formed at elevated temperatures (minimum 100 to 160°C) based on primary fluid inclusions in sphalerite (Foley, 1980).

Zones 2B, 3, and 4 Dolomite Cements

Dolomite cementation is late burial in that it postdates much tectonic fracturing, and late dissolution porosity. It also postdates Pb-Zn ore deposition, which formed at elevated temperatures. The dolomite cements are chiefly saddle dolomite, which forms at elevated temperatures (50 to 150°C, Gregg and Sibley, 1984; Radke and Mathis, 1980). Primary fluid inclusions in dolomite cement (Th = 120 to 150°C) also indicate burial temperatures.

Horizontal geopetal structures floored by geopetal dolomite silt in fracture- and dissolution-voids within steeply dipping beds indicate that the dolomite cements occluding the remaining void space postdate major folding. The fine dolomite silt may have formed by rapid nucleation and precipitation of silt-size dolomite crystals (Read and Pfiel, 1983), or it may consist of dolomite eroded from the void walls. The fractures and hydrothermal breccias in which much of the dolomite cement occurs result from hydraulic fracture processes and high pore fluid pressures (Phillips, 1972; Shearman et al., 1972; Roehl, 1981). Cement-supported rock fabrics and open fracture-filling dolomite cement attest to considerable open void space that was at least partially supported by overpressured fluids.

Late Quartz and Calcite

Late quartz and calcite underwent limited deformation after precipitation, as indicated by microfractures containing secondary fluid inclusions, and calcite deformation twins.

BURIAL HISTORY AND DIAGENETIC TEMPERATURES

Burial History

The Shady-Rome sequence in the study area underwent gradual burial to depths of about 3 kms during Middle Cambrian to Early Ordovician, based on stratigraphic thickness of the overlying Middle Cambrian to Early Ordovician section. This burial reflects continued passive margin sedimentation and subsidence. In the Middle Ordovician, the platform margin locally was uplifted and incorporated into the Taconic accretionary prism during arc-continental collision, indicated by reworked Cambrian and Early Ordovician detritus in later Ordovician foredeep conglomerates (Read, in press) a.

The post-Middle Ordovician burial history of the Shady Dolomite platform margin cannot be reconstructed based on stratigraphic thickness of the overlying Paleozoic section, because rocks younger than Ordovician have been eroded from the thrust sheet underlying the study area. The sequence underwent rapid burial during the Devonian when a thick wedge of clastic sediments was shed from tectonic uplands to the east. Maximum burial occurred during the Carboniferous-Permian when thick deposits of siliciclastics accumulated during deposition of Pennsylvanian-Permian fluvial-deltaic sequences. The sedimentary burial history constructed for the adjacent thrust sheet to the west (Mussman et al., 1988), indicates that the Shady Dolomite there attained maximum burial depths of 7 to 8 km by late Carboniferous time, coeval with major overthrusting.

In incompletely replaced limestones, zone 2A dolomite commonly is associated with tectonic fractures, and forms replacement halos adjacent to the fractures (Fig. 16B), indicating that tectonic fractures formed preferential conduits for the dolomitizing fluids and that zone 2A dolomitization postdates the onset of tectonic fracturing. Zone 2A

dolomite underwent additional fracturing, followed by MVT ore minerals, zones 2B, 3, and 4 replacement dolomite, and late quartz and calcite. Thus, the paragenetic sequence formed coeval with tectonic deformation.

Major thrust faulting and folding of the Paleozoic sedimentary rocks in the Valley and Ridge province of the central and southern Appalachians is associated with the Alleghanian orogeny, which occurred during the Late Carboniferous to Early Permian (Woodward, 1957; Hatcher and Odom, 1980, Van der Voo, 1979). The MVT ore minerals and later zones 2B, 3, and 4 dolomite cement formed during the waning stages of Alleghanian-age folding, faulting, and fracturing, because they were subjected to limited deformation following deposition, which also eliminates precipitation during earlier Taconic or Acadian tectonism. In folded beds, cavities that are floored by geopetal dolomite silt and occluded by zones 2B, 3, and 4 dolomite cement indicate that the cements were emplaced following major tectonic deformation. Finally, authigenic potassium feldspar genetically linked to MVT mineralization yield $^{40}Ar/^{39}Ar$ age dates (278 to 322 Ma) that coincide with proposed ages of Alleghanian deformation and overthrusting (Hearn et al., 1987, and references therein). Alleghanian-age MVT occurrences are found throughout the U.S. Appalachians, indicating that this event was of regional scale (Kaiser and Ohmoto, 1985).

Although the zone 2A replacement dolomites underwent considerable fracturing, it is unlikely that they formed during the previous Ordovician Taconic and/or Devonian Acadian orogens, because the zone 2A replacement dolomites are geochemically and isotopically similar to zone 2B dolomite cements, which imply precipitation at similar temperatures from similar fluids. The zone 2B dolomite cements postdate major late Paleozoic deformation (see above), and it is unlikely that the zone 2A replacement

dolomites, if they formed during earlier Taconic or Acadian tectonism, could record precipitation from fluids of similar temperature and geochemical and isotopic composition as the considerably later zone 2B dolomite cements. Thus the bulk of the replacement dolomites and dolomite cements are late Paleozoic in age.

Thermal History

Although maximum burial depths due to sedimentary overburden cannot be reconstructed for the Shady Dolomite outer platform, due to erosion of most of the overlying Paleozoic section, the burial history for the adjacent thrust sheet to the west indicates maximum burial depths of 7 to 8 km for the Shady Dolomite by the late Carboniferous (Mussman et al., 1988), which correspond to burial temperatures of 195 to 220°C, assuming a geothermal gradient of 25°C/km.

Although no conodont alteration index (CAI) data is reported from the easternmost thrust sheet of the Valley and Ridge province in the study area, extrapolation of the regional CAI isograds (Harris et al., 1978) indicates that the CAI index for Ordovician carbonates in the study area is probably greater than 4, indicating burial temperatures in excess of 185°C (Harris, 1979). Burial temperatures for Lower Cambrian carbonates would require an additional 50 to 75°C (at 25°C/km) to account for the overlying Middle Cambrian through Lower Ordovician section. Consequently, maximum diagenetic temperatures may have been 230°C or higher, assuming that the burial history was simple and not complicated by uplift during the Taconic orogeny.

Detrital K-feldspars yield $^{40}Ar/^{39}Ar$ ages that are older than the depositional age of the Shady Dolomite (Hearn et al., 1987). This implies that maximum diagenetic temperatures did not exceed ≈ 250°C, or else the accumulated, predepositional radiogenic

^{40}Ar in the detrital feldspars would have been lost (Hearn and Sutter, 1985).

The temperature and $\delta^{18}O$ composition of the zone 2A dolomitizing fluids likely were similar to those of the zone 2B dolomite, based on the similar ^{18}O and trace element composition of the two dolomite generations. Primary fluid inclusions in zone 2B dolomite (Th = 120 to 150°C) yield pressure corrected (hydrostatic overburden) temperatures of 150 to 225°C (Fig. 25A). These estimated temperatures are too high, because the ^{18}O depletion of zones 3 and 4 dolomite cements records an additional temperature increase of 40 to 60°C, which would place the maximum diagenetic temperatures above the 250° maximum constrained by the feldspar $^{40}Ar/^{39}Ar$ data. However, the dolomite inclusions may have been stretched by subsequent overheating during burial (cf. Bodnar and Bethke, 1984; Prezbindowski and Larese, 1987).

Estimated precipitation temperatures for the zone 2A replacement dolomite and the zone 2B dolomite cement are 100 to 175°C. This estimate is based on the homogenization temperatures for primary fluid inclusions in sphalerite (Th = 100 to 160°C) which precipitated after the zone 2A replacement dolomite but prior to zone 2B dolomite cement (Foley, 1980), and on the pressure-corrected (hydrostatic load) temperatures of the primary dolomite inclusions with low vapor bubble homogenization temperatures which were deemed less likely to have been stretched. Furthermore, hydrocarbon emplacement contemporaneous with zone 2A and 2B dolomite indicate temperatures of approximately 60 to 150°C. The intersection of the isochores from zone 2B fluid inclusions exhibiting the lower range of vapor bubble homogenization temperatures (120 to 125°C) with hydrostatic geothermal gradients, define minimum pressures of 400 to 600 bars (Fig. 25A). This corresponds to burial depths of 4 to 6 km (hydrostatic load). The fluid inclusion salinities (23.3 to 26.3 wt. % NaCl equiv.) are

compatible with precipitation from deep formation fluids, which typically have high concentrations of dissolved salts due to water-rock interaction at elevated temperatures.

Burial temperatures subsequently increased some 40 to 60°C, indicated by the ^{18}O depletion in zones 3 and 4 dolomite cement. Maximum diagenetic temperatures and pressures are indicated by secondary 3-phase fluid inclusions in late quartz and calcite (temperature of halite dissolution = 175 to 225°C). At these higher temperatures, the hydrocarbons were degraded to bitumen. The estimated salinities (30.5 to 33.1 wt.% NaCl equiv.) are typical of deep burial fluids. The possible P-T conditions of the late diagenetic fluids are delimited by the region within the inclusion isochores (Figs. 25B, 25C). Minimum trapping pressures of these 3-phase inclusions are defined by the intersection of the inclusion isochores with the liquidus curves corresponding to inclusion salinities, indicating minimum pressures of 360 to 1140 bars (Fig. 25B), actual pressures and temperatures may have been greater, and range up to 1600 bars, for the maximum possible temperature correction to 250°C (Fig. 25C). The range of pressures and temperatures thus obtained exceed those defined by hydrostatic load, indicating that the fluids were overpressured (Barnaby and Bodnar, 1988). This is consistent with petrographic evidence, including hydraulic fractures and cement-supported breccia fabrics, that indicate the former presence of overpressured fluids.

A minimum depth of formation calculated from the lowest temperature of halite dissolution (175°C) using a maximum likely geothermal gradient (30 to 35°C/km) is ≈ 5 km. In the active fold-and-thrust belt of Taiwan, hydrostatic pressured fluids persist to depths of 1.5 to 4 km, at greater depths, fluid pressures subsequently increase on the order of 170 bars/km (Suppe and Wittke, 1977). Using this analog, the maximum 1600 bars estimated pressure translates to burial depths on the order of 10 km. Therefore,

estimated burial depths were likely greater than 5 km but did not exceed 10 km. These estimated depths are consistent with burial depths for the Shady Dolomite estimated using sedimentary burial history (7 to 8 km, Mussman et al., 1988) and with estimated maximum burial temperatures based on $^{40}Ar/^{39}Ar$ data and 3-phase fluid inclusions.

INTERPRETATION OF GEOCHEMISTRY

Significance of Dolomite Stoichiometry

Because zone 1 dolomite cores are generally replaced by zone 2A dolomite, this suggests that they were initially a metastable, nonstoichiometric, Ca-rich dolomite phase (Land, 1980). The stoichiometry of zone 2A replacement dolomites most likely was imparted during dolomite precipitation, because their relatively narrow range of depleted $\delta^{18}O$ values and low Sr contents, and enriched $\delta^{13}C$ values exhibit no trend towards expected values for near-surface dolomites, and are thus incompatible with diagenetic overprinting of a metastable dolomite precursor. Zones 2B and 3 dolomite cements also are stoichiometric. The slight depletion in Mg in zone 4 dolomite cement reflects Fe substituting for the Mg sites in the dolomite (Kretz, 1982).

Interpretation of $\delta^{18}O$ Composition

The limited preservation of zone 1 dolomite prevents its isotopic composition from being defined with certainty. Since there is no difference between the $\delta^{18}O$ values of the rare samples of zone 2A dolomite with relict zone 1 cores and the $\delta^{18}O$ values of the zone 2A dolomite samples lacking such cores, both zone 1 and zone 2A dolomite may have had approximately similar ^{18}O compositions, or the ^{18}O composition of zone 1 dolomite may

have been reset during zone 2A replacement dolomitization.

The depleted $\delta^{18}O$ values of zone 2A replacement dolomite relative to marine calcite or to that estimated for a near-surface marine/hypersaline dolomite (Fig. 15) likely do not reflect neomorphic replacement of an early, metastable dolomite precursor (cf. Land, 1985). Zone 2A dolomites exhibit a tight clustering of $\delta^{18}O$ values, whereas diagenetic overprinting of a metastable marine/hypersaline dolomite precursor would likely preserve some memory of the enriched ^{18}O composition of the dolomite precursor (Land, 1980), and form a trend towards more pristine $\delta^{18}O$ values in less altered dolomites (cf. Land et al., 1975; Kupecz and Land, 1988; Graber and Lohmann, 1989; Montanez et al., 1988). The depleted ^{18}O composition of zone 2A dolomite also cannot reflect neomorphism of a ^{18}O depleted, mixing zone dolomite precursor, because the zone 2A replacement dolomites are consistently enriched in ^{13}C relative to marine carbonate, which likely reflects elevated precipitation temperatures (see below). Finally, the $\delta^{18}O$ composition of the zone 2A dolomites are independent of crystal size (Fig. 20); if neomorphic replacement and recrystallization of a metastable dolomite precursor had occurred, the more coarsely crystalline dolomites, which presumably record more extensive neomorphic alteration of an initial finely crystalline dolomite, should be more depleted in ^{18}O than finely crystalline dolomite (eg., Land et al., 1975).

Thus, the depleted ^{18}O composition of zone 2A replacement dolomites records that imparted during initial precipitation. Because the zone 2A replacement dolomites postdate meteoric dissolution and early calcite cementation, are penecontemporaneous with tectonic deformation, and form anhedral mosaics (xenotopic dolomite), the ^{18}O depletion primarily reflects precipitation at elevated temperatures. The elevated precipitation temperatures estimated for the zone 2A and 2B dolomites (100 to 175°C), based on

primary fluid inclusions, implies that the dolomitizing fluids were enriched in ^{18}O relative to marine fluids (0 to +8 °/oo SMOW, Fig. 28). This is compatible with ^{18}O compositions of present-day, warm, saline formation waters, which typically have $\delta^{18}O$ values greater than 0 °/oo SMOW, and range up to +8 °/oo SMOW or more (Clayton et al., 1966; Kharaka et al., 1973; 1977; 1980b; Dutton, 1987; Morton and Land, 1987; Land et al., 1988). This ^{18}O enrichment results from interaction of the formation water with ^{18}O -rich carbonates and silicate minerals of the enclosing sedimentary rocks at elevated burial temperatures (Clayton, et al., 1966; Hitchon and Friedman, 1969; Kharaka et al., 1973).

Zones 3 and 4 dolomite cement are depleted in ^{18}O relative to the earlier dolomites (Fig. 15). This shift towards more negative $\delta^{18}O$ values may reflect precipitation from fluids depleted in ^{18}O by ≈ 5 °/oo relative to the earlier dolomite generations, if they precipitated at similar temperatures (Fig. 28). However, if the $\delta^{18}O$ composition of the fluid remained the same (0 to +8 °/oo SMOW) from zones 2A and 2B dolomites to zones 3 and 4 dolomite, then the estimated temperature increase is 40 to 60°C, indicating precipitation temperatures of 150 to 235°C (Fig. 28). Given the range of temperatures, and the $\delta^{18}O$ values of authigenic quartz ($\delta^{18}O$ = +20.2 °/oo SMOW; n = 2), which precipitated coeval with and immediately following zone 4 dolomite cement, this indicates that the fluid compositions remained enriched in ^{18}O (0 to +8 °/oo) range, estimated using $\Delta^{18}O_{quartz\text{-}water}$ from Matsuhisa et al. (1979). Thus, the diagenetic waters remained enriched in ^{18}O throughout authigenic mineral precipitation. The highly variable $\delta^{18}O$ values for the late calcite reflect different precipitation temperatures and/or changes in the ^{18}O composition of the fluid, perhaps related to mixing and/or uplift.

Figure 28. $\delta^{18}O$ composition of water in equilibrium with dolomite as function of temperature, using $10^3 \ln \alpha = 3.2 \times 10^6/T^2 - 1.5$ (from Friedman and O'Neil, 1977). Marine = $\delta^{18}O$ composition of dolomite in equilibrium with Lower to Middle Cambrian seawater, estimated from marine calcite cement $\delta^{18}O$ values. Stippled region indicates estimated precipitation temperatures for zone 2A and 2B dolomite, based on primary fluid inclusions and other evidence. At these temperatures, the fluids would have been enriched in ^{18}O (0 to +8 ‰ SMOW).

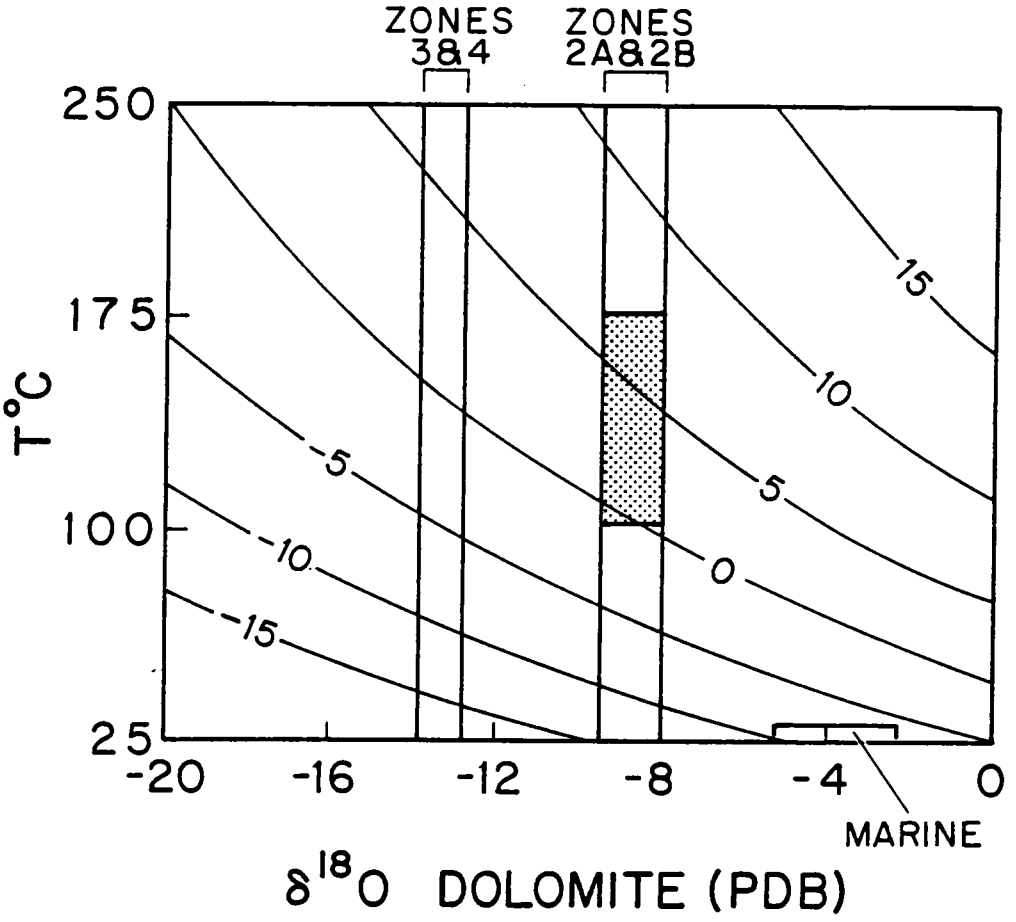
ZONES 3&4
ZONES 2A&2B
250
175
100
25
T°C
15
10
5
0
-5
-10
-15
-20
-16
-12
-8
-4
0
MARINE
δ18O DOLOMITE (PDB)

Interpretation of $\delta^{13}C$ Composition

The zone 1 and zone 2A replacement dolomites are consistently enriched in ^{13}C ($\approx$ +0.8 ‰) relative to the marine values and zone 2B dolomite cement (Table 1, Fig. 15). Most Cenozoic near-surface dolomites (other than those associated with organic rich sediments) typically have $\delta^{13}C$ compositions similar to those of coexisting marine carbonate (for example, Gross and Tracy, 1966; Supko, 1977; McKenzie, 1981; Saller, 1984; Aharon et al., 1987; Mitchell et al., 1987; Aïssaoui, 1988), suggesting that ^{13}C fractionation between calcite and dolomite is essentially zero at surface temperatures (McKenzie,1981). Thus, the ^{13}C composition of the zone 1 and 2A dolomites reflects ^{13}C enrichment during replacement dolomitization.

Diagenesis of organic matter can be eliminated as a source of ^{13}C enrichment for zone 2A dolomites. Dolomites associated with bacterial methanogenesis are confined to organic-rich sediments, and have extremely variable $\delta^{13}C$ compositions (-30 to +21 ‰ PDB, Murata et al., 1969; Deuser, 1970; Friedman and Murata, 1979; Kelts and McKenzie, 1984; Burns and Baker, 1987). The estimated precipitation temperatures of zone 2A replacement dolomites (100 to 175°C) are above the range of bacterial metabolism, and thus rule out bacterial methanogenesis. Thermal decarboxylation of acetic acid and other organic acids at temperatures > 80°C (eg., Carothers and Kharaka, 1978; 1980; Kharaka et al., 1986; Drummond and Palmer, 1986), also cannot account for the enriched zone 2A dolomite $\delta^{13}C$ values, because formation waters influenced by thermal decarboxylation are generally are not enriched in ^{13}C relative to marine carbonate (see fig. 7 in Carothers and Kharaka, 1980).

The narrow range of $\delta^{13}C$ values for the zone 1 and zone 2A replacement dolomites implies that the diagenetic waters were in carbon isotopic equilibrium with the host

limestone, and that the slight ^{13}C enrichment reflects ^{13}C fractionation between HCO_3^- (derived from limestone dissolution) and dolomite precipitated at elevated diagenetic temperatures. Using carbon isotope fractionation factors (Ohmoto and Rye, 1979) for the temperature range 100 to 175°C, a dolomite precipitating from such fluids would be enriched in ^{13}C by 1.0 to 1.6 °/oo relative to the host limestone, sufficient to account for the ^{13}C enrichment of the zone 2A replacement dolomites. Therefore, this mechanism of ^{13}C enrichment for the zone 2A dolomites further attests to burial dolomitization of limestone, rather than neomorphism of a metastable, near-surface dolomite with ^{13}C values similar to marine carbonate, because there would be no means of ^{13}C enrichment for the zone 2A dolomites if they reflected neomorphic overprinting.

Modelling the isotopic composition of the dolomites as a function of the water/rock ratio (Fig. 29) allows the ^{13}C composition of the carbonate species in the diagenetic water to be better defined. For example, at 125°C, using the average ^{13}C composition of the marine cements (+0.5 °/oo), and a HCO_3^- concentration of 0.10 molal (6100 ppm) in the diagenetic fluid, the model indicates that the zone 2A replacement dolomites cannot have precipitated from a fluid with $\delta^{13}C$ values of less than -1.5 °/oo PDB (Fig. 29A). By increasing the ^{13}C composition of the pore water to -1.0 °/oo PDB, the model defines ^{13}C values compatible with those of the dolomites (Fig. 29B). Further increasing the ^{13}C content of the pore water to +1.0 °/oo PDB (Fig. 29C) indicates that the diagenetic fluids would have imparted ^{13}C composition to the dolomites of up to +3.0 °/oo PDB or greater, which is inconsistent with the observed narrow range of ^{13}C variation for the replacement dolomites.

The estimated ^{13}C composition of the dolomitizing fluid, based on the model, is not greatly dependent on the assumed concentration of HCO_3^-; decreasing the concentration

Figure 29: Water-rock modelling of dolomite $\delta^{13}C$ composition using equations of Sverjensky (1981), at 125°C, $\delta^{18}O$ H_2O = + 2.5 °/oo SMOW. Filled circles = marine cement analyses; open circles = zone 2A replacement dolomite analyses, pluses = standard deviation of the data. The modelling utilized both an closed system approach (water/rock ratios up to 10^5) and open system conditions (water/rock ratios up to 10), which encompass the range of actual diagenetic conditions. For modelling purposes, the average $\delta^{13}C$ value and the most enriched $\delta^{18}O$ value of the marine cements (see Table 1) were used to define the stable isotope composition of the marine limestone precursor. Isotopic fractionation equations from Friedman and O'Neil (1977) and Ohmoto and Rye (1979) for ^{18}O and ^{13}C, respectively. In the temperature range of interest (100 to 175°C), the fractionation factors for ^{13}C are only slightly affected by temperature, and modelling the $\delta^{13}C$ composition of the zone 2A dolomites as a function of water/rock ratios within this temperature range yields similar values for the inferred $\delta^{13}C$ composition of the zone 2A dolomitizing fluid. A) If $\delta^{13}C$ of HCO_3^- in the fluid were only slightly depleted (-1.5 °/oo), the enriched $\delta^{13}C$ composition of the dolomites could not have been produced, even assuming the maximum likely HCO_3^- concentration in the fluid and high water/rock ratios. B) By increasing the $\delta^{13}C$ of HCO_3^- in the fluid to -1.0 °/oo, the modelling defines a narrow range of $\delta^{13}C$ values compatible with those yielded from the zone 2A dolomites. C) If the $\delta^{13}C$ composition of the fluid were somewhat enriched (+1.0 °/oo), the modelling predicts $\delta^{13}C$ values for the dolomites ranging up to +3 °/oo or more, unless all the dolomites record similar water/rock ratios. D) By decreasing the concentration of HCO_3^- in the fluid to 0.01 M, only a slight increase in the $\delta^{13}C$ composition of the HCO_3^- (to +0.5 °/oo) is required to account for the $\delta^{13}C$ composition of the dolomites.

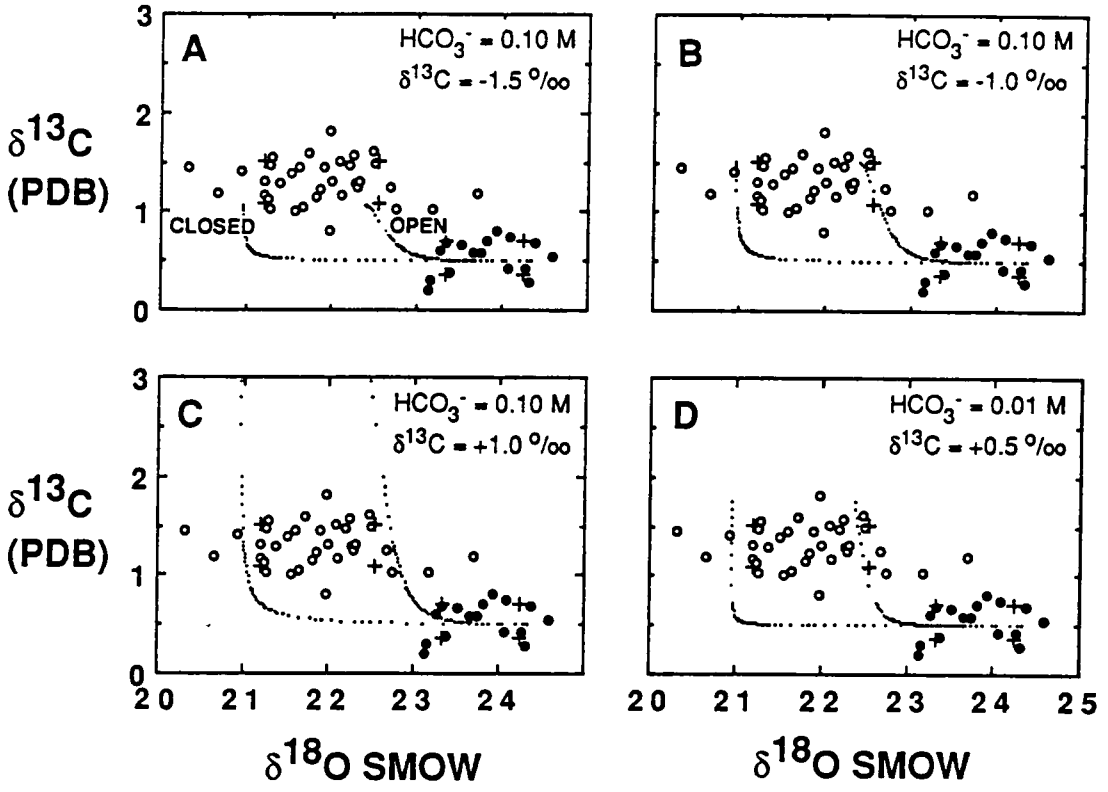
A
HCO_3^- = 0.10 M
$\delta^{13}C$ = -1.5 °/oo
CLOSED
OPEN
B
HCO_3^- = 0.10 M
$\delta^{13}C$ = -1.0 °/oo
C
HCO_3^- = 0.10 M
$\delta^{13}C$ = +1.0 °/oo
D
HCO_3^- = 0.01 M
$\delta^{13}C$ = +0.5 °/oo
$\delta^{13}C$ (PDB)
$\delta^{13}C$ (PDB)
0
1
2
3
20
21
22
23
24
25
$\delta^{18}O$ SMOW
$\delta^{18}O$ SMOW

of HCO_3^- to 0.01 molal (610 ppm) from 0.10 molal requires only a minor increase in the $\delta^{13}C$ composition of the fluid to account for the $\delta^{13}C$ values of the dolomites (Fig. 29D). The range of HCO_3^- concentrations (0.01 molal to 0.10 molal) considered in the modelling is compatible with the reported range of HCO_3^- concentrations in many oil field brines (Carothers and Kharaka, 1978; 1980). The estimated $\delta^{13}C$ of the diagenetic fluid also does not vary greatly with temperature changes between 100 to 175°C, therefore, given the likely HCO_3^- concentrations (0.01 to 0.10 molal), the model defines ^{13}C compositions between ≈ -1 to +1 ‰ PDB for the zone 1 and zone 2A dolomitizing fluid, compatible with HCO_3^- derived from host limestone dissolution.

The $\delta^{13}C$ values of zones 2B, 3, and 4 dolomite cement are slightly depleted relative to zone 2A replacement dolomite (Fig. 15). This indicates that the ^{13}C composition of the diagenetic water was no longer dominated by limestone dissolution, because there was little unreplaced limestone remaining by this time. The slight ^{13}C depletion of the dolomite cements relative to zone 2A replacement dolomite may reflect input of minor amounts of ^{13}C depleted CO_2 from organic diagenesis (< 5% organically-derived CO_2, assuming $\delta^{13}C$ values of the organics were ≤ -20 ‰) or importation of relatively ^{13}C depleted HCO_3^- from pressure solution of younger Cambrian and Ordovician carbonates (see Veizer et al., 1980) that were being overthrust at this time. Zone 3 dolomite cement is the most ^{13}C depleted of the dolomite generations, which likely reflects thermochemical $SO_4^=$ reduction, a process also indicated by the low Fe contents in zone 3 dolomite and by the associated pyrite, which would have depleted the fluid in Fe^{2+}.

The range of $\delta^{13}C$ values for the late calcites reflect varying contributions of ^{13}C enriched HCO_3^- derived from the host carbonate along with input of isotopically light organic carbon. The most ^{18}O depleted samples, implying higher temperature

precipitation, have $\delta^{13}C$ compositions in equilibrium with the host carbonate, compatible with water/rock interaction at elevated temperatures. The ^{13}C depleted calcites are more enriched in ^{18}O, which may reflect precipitation from cooler waters, which were less buffered by water-rock interaction with the host carbonate.

Interpretation of Mn and Fe Contents

Cathodoluminescent behavior in dolomite is controlled by the dolomite Fe/Mn ratios and by the concentration of Mn^{2+} and Fe^{2+}, which activate and inhibit dolomite cathodoluminescence, respectively (Pierson, 1981; Fairchild, 1983).

The Mn and Fe contents of *zone 1* dolomite appear to be similar to the zone 2A replacement dolomites and may record similar diagenetic environments, or diagenetic overprinting during zone 2A replacement dolomitization. Mn and Fe contents in *zone 2A* replacement dolomites have a statistically significant ($r^2 = 0.90$), positive covariation (Fig. 22). Fe greatly exceeds Mn (Fe/Mn $\approx$ 5) in the dolomite, indicating that the pore waters were enriched in Fe^{2+} relative to Mn^{2+}. This implies that sulfide activities, sulfate reduction and pyrite precipitation were insignificant during replacement dolomitization. Because Mn and Fe contents increase with crystal size, whereas Sr, ^{18}O, and ^{13}C remain essentially constant (Fig. 20), any explanation for the Mn and Fe contents must also account for the similar Sr and stable isotopic chemistry of the replacement dolomites.

The Mn and Fe covariation of the zone 2A dolomites cannot be attributed to precipitation rate or temperature effects on their distribution coefficients. Calcite distribution coefficients for Mn and Fe decrease with increasing precipitation rate and increasing temperature (Lorens, 1981; Dromgoole and Walters, 1987; Bodine et al., 1965) while those for Sr increase as temperature and precipitation rate increases (Kitano et

al., 1971; Lorens, 1981; Pingitore and Eastman, 1986; Stoessell et al., 1987). The distribution coefficients for dolomite should be similarly affected, following the reasoning of Kretz (1982). Thus, precipitation rate and temperature effects on the distribution coefficients for Mn and Fe are opposite to those of Sr. Mn and Fe contents do not inversely vary with respect to Sr for the zone 2A dolomite (Fig. 30), therefore, temperature- or precipitation rate-induced changes in the distribution coefficients for Mn and Fe cannot be the primary cause for the Mn and Fe variation. Furthermore, the zone 2A replacement dolomites all have similar ^{18}O compositions (Fig. 20), which implies essentially constant precipitation temperatures.

The Mn and Fe contents of the dolomites may reflect a redox control over the Eh- and pH-dependent solubility of Mn- and Fe-bearing minerals in a similar manner to those governing Mn and Fe contents of early calcite cements (Carpenter and Oglesby, 1976; Frank et al., 1982; Barnaby and Rimstidt, 1989). However, the Fe/Mn ratios of the zone 2A dolomites are considerably different than those expected for near-surface calcite cements (Barnaby and Rimstidt, 1989), and the Mn- and Fe-oxyhydroxides that govern the Mn^{2+} and Fe^{2+} chemistry of shallow meteoric waters are unstable in the diagenetic environments indicated for the dolomites. Thus, the Mn^{2+} and Fe^{2+} contents of the dolomitizing fluids apparently were governed by redox equilibria with Mn- and Fe-bearing minerals of unknown identity.

The higher Mn and Fe contents in the more coarsely crystalline dolomites (Fig. 20) likely record an increase in the Mn^{2+} and Fe^{2+} contents of the dolomitizing fluid during precipitation of the more coarsely crystalline zone 2A replacement dolomite. Because redox equilibria for the environments of dolomitization are poorly understood, it is unclear whether the Mn and Fe increase primarily reflects a decrease in Eh or pH. The

Figure 30. Zone 2A replacement dolomites, Sr versus Fe and Mn contents. No relationship of Sr contents with respect to the Fe and Mn chemistry is evident; which would be the case if the zone 2A dolomites were diagenetically overprinted, near-surface dolomites, as the less altered dolomites would contain high Sr and relatively low Fe and Mn, and the more extensively altered dolomites would contain low Sr and high Fe and Mn. The lack of correlation of Sr with Fe and Mn also eliminates distribution coefficients as a primary cause of the wide range of Fe and Mn contents (see text).

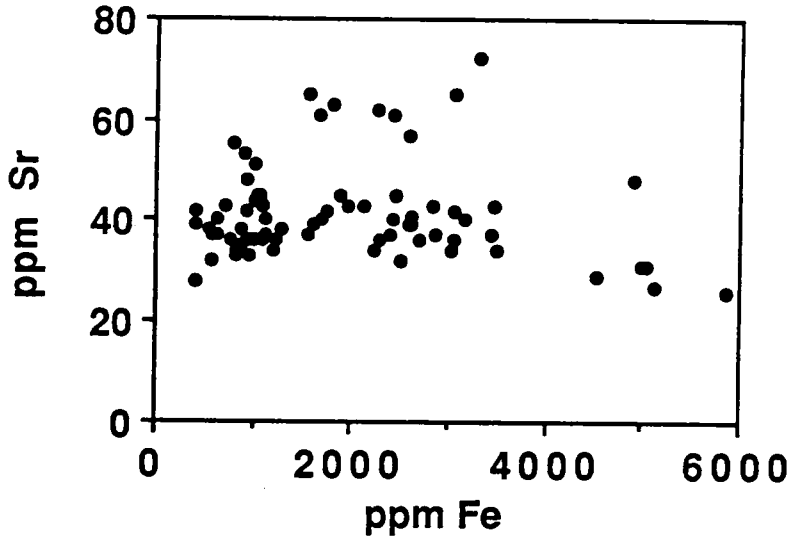
80
60
40
20
0
ppm Sr
0
2000
4000
6000
ppm Fe

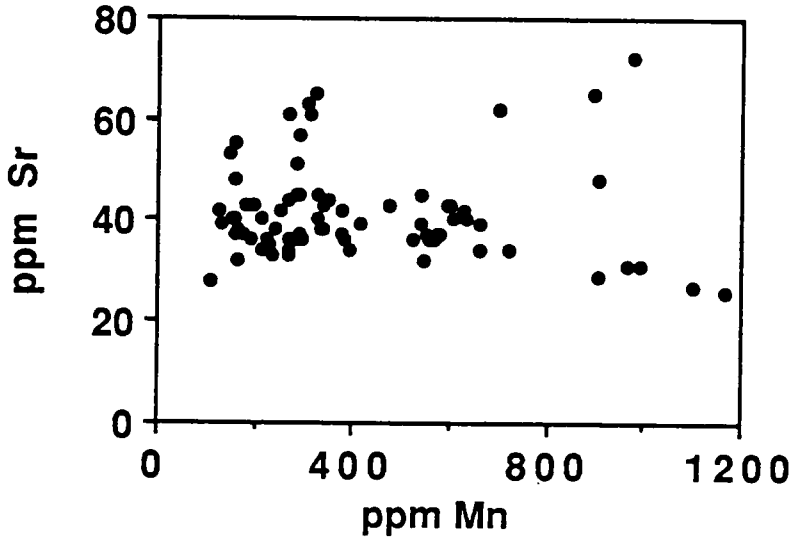
80
60
40
20
0
ppm Sr
0
400
800
1200
ppm Mn

pH may have been important because immediately following zone 2A replacement dolomitization, the sequence underwent a major episode of dissolution due to lower pH caused by influx of organic acids (Carothers and Kharaka, 1978; 1980) and/or acid produced by MVT ore deposition reactions (Anderson, 1983). More acidic conditions would have increased the solubility of Mn- and Fe-bearing minerals in the host rock, resulting in increasing Mn^{2+} and Fe^{2+} contents in the dolomitizing fluid, and hence, in the dolomite. Consideration of stability diagrams constructed for Mn- and Fe-oxyhydroxide phases using thermodynamic data (Naumov et. al., 1974; Barner and Scheuerman, 1978; Robie et al., 1978) for the estimated dolomitization temperatures (100 to 175°C) indicate that the equilibrium Mn^{2+} and Fe^{2+} content of a pore water will increase an order of magnitude for a decrease of 0.3 in the pH, and it is reasonable to assume that other Mn- and Fe-bearing mineral phases would manifest similar behavior. Thus the Mn and Fe increase with dolomite crystal size may reflect progressively more acidic conditions during replacement by more coarsely crystalline dolomite, immediately preceding the major episode of dissolution. However, Eh changes due to influx of organic matter cannot be ruled out.

Although *Zone 2B dolomite cement* has relatively low Mn and Fe contents (Table 1, Fig. 21) they have similar Mn/Fe ratios and display the same linear covariation as the zone 2A replacement dolomites, thus they have identical cathodoluminescence to the zone 2A dolomites. The lower Mn and Fe contents of zone 2B dolomites cannot reflect uptake of Fe and Mn by the preceding MVT mineralization, as this would only remove Fe^{2+} from solution by pyrite precipitation, and the Mn^{2+} contents of the solution would have been unaffected. Therefore, the same Mn and Fe covariation of zone 2B dolomite cement implies that the same Mn and Fe equilibria controls continued to dominate the solution

chemistry. Because zone 2B dolomite cements are depleted in Mn and Fe relative to the more coarsely crystalline zone 2A replacement dolomites, it may indicate a return to less acidic pH conditions following zone 2A dolomite precipitation and secondary porosity development, compatible with the dolomite cementation. However, an Eh control cannot be eliminated.

Zone 3 dolomite cement is depleted in Fe relative to Mn (Fig. 21) which accounts for its bright orange-red cathodoluminescence. The low Fe contents of zone 3 dolomite cement may reflect influx of organics and thermochemical sulfate reduction, which is supported by its ^{13}C depletion and by the associated pyrite. *Zone 4 dolomite cement* is enriched in Fe and Mn, and the Fe/Mn ratios are broadly similar to those of zone 2A and 2B dolomites, indicating low sulfide activities and a return to the Mn and Fe equilibria controls which dominated the earlier dolomite generations (zones 2A, 2B).

The higher Mn/Fe ratios of the late calcite cements compared to the dolomites (Fig. 21), indicate different Mn and Fe equilibria were governing the fluid chemistry, and may reflect uptake of Fe^{2+} by pyrite precipitation, which commonly is associated with the calcite.

Interpretation of Total Sr and $^{87}Sr/^{86}Sr$ Compositions

The zone 2A replacement dolomites are significantly depleted in total Sr (Table 1) relative to that expected for a dolomite precipitating from modern seawater (Sr = 500 to 800 ppm; Veizer, 1983; Behrens and Land, 1972; Land, 1980; Mitchell et al., 1987). It is unlikely that the low total Sr contents of the zone 2A dolomites reflect expulsion of Sr during neomorphism of a metastable dolomite precursor in fluids with low Sr contents (Behrens and Land, 1972; Bein and Land, 1983; Land et al., 1975), and/or by lower

distribution coefficients for Sr prevailing during neomorphic replacement (Bein and Land, 1983; Land, 1980). In such neomorphosed dolomites, a memory of the initial high Sr content is retained in some samples (Land et al., 1975; Bein and Land, 1983). If neomorphic replacement of a precursor early dolomite had occurred, the more coarsely crystalline dolomites, which record more extensive recrystallization of an initial finely crystalline dolomite (eg., Land et al., 1975), should be the most depleted in Sr, which is not the case for the zone 2A dolomites (Fig. 20).

In neomorphosed early dolomites, the least altered dolomites typically have higher Sr contents along with more 'pristine', enriched ^{18}O values (Graber and Lohmann, 1989; Montanez et al., 1988). In the zone 2A replacement dolomites there is no correlation between Sr and ^{18}O compositions. In addition, neomorphism of an unstable carbonate precursor should produce an inverse relationship between Sr contents and Mn and Fe contents (Veizer, 1983), which also is not the case for the zone 2A replacement dolomites (Fig. 30).

Therefore, the low Sr contents in the zone 2A replacement dolomites was imparted during dolomite precipitation, rather than from neomorphic replacement of an existing dolomite. There are no published distribution coefficients for Sr^{2+} partitioning between dolomite and solution (D_{Sr}^{dol}) for temperatures less than 250°C, which precludes rigorous application of distribution coefficients to estimate Sr/Ca ratios of the dolomitizing fluid. However, Sr^{2+}, which has an ionic radius larger than Ca^{2+}, should preferentially substitute for the calcium sites of the dolomite, and D_{Sr}^{dol} should thus be approximately 0.5 $D_{Sr}^{calcite}$ (Behrens and Land, 1972; Jacobson and Usdowski, 1976; Kretz, 1982). Reported $D_{Sr}^{calcite}$ values range between 0.027 to 0.20 for temperatures between 20 and 200°C (Holland et al., 1964a; 1964b; Bodine et al., 1965; Katz et al., 1972; Lorens,

1981; Pingitore and Eastman, 1986; Stoessell et al., 1987). Therefore, by assuming $D_{Sr}^{dol} \approx 0.5\ D_{Sr}^{calcite}$, yields D_{Sr}^{dol} values of 0.014 to 0.10, which agree with those established experimentally for dolomite at 250-300°C ($D_{Sr}^{dol} = 0.025$; Katz and Matthews, 1977).

Using these distribution coefficients yields estimated Sr/Ca (weight) ratios of 6×10^{-4} to 1×10^{-2} for the dolomitizing fluids from which zone 2A and 2B dolomite formed. These Sr/Ca ratios are considerably lower than for modern seawater (Sr/Ca = 2×10^{-2}, Drever, 1982) or saline formation waters (White et al., 1963; Carpenter et al., 1974; Kharaka et al., 1977; 1980a; 1980b; Starinsky et al., 1983; Chaudhuri et al., 1987; Morton and Land, 1987; Land et al., 1988), and the salinities indicated by the zone 2B dolomite fluid inclusions (23.3 to 26.3 wt % NaCl equiv.) rule out precipitation from Sr-depleted meteoric waters. The estimated Sr/Ca ratios of the zone 2A dolomitizing fluid lie between Sr/Ca ratios yielded from host limestone dissolution (Sr/Ca = 3×10^{-4} to 5×10^{-4}) and Sr/Ca ratios defined for a fluid in equilibrium with the host limestone, based on the Sr contents of the host limestone and marine cement from Table 1 using $D_{Sr}^{calcite}$ (Sr/Ca = 2×10^{-4} to 1.8×10^{-2}). This implies that the system was relatively closed with respect to total Sr during zone 2A replacement dolomitization of limestone. Mattes and Mountjoy (1980) and Chaudhuri et al. (1983) postulated a similar interpretation for the low total Sr contents in burial dolomite. This conclusion is compatible with the $^{87}Sr/^{86}Sr$ ratios for the zone 2A dolomites, which are identical to marine $^{87}Sr/^{86}Sr$ values (Table 1, Fig. 23), indicating that the Sr was derived from marine carbonate.

Zone 2B dolomite cement, which postdates secondary porosity development and major MVT ore deposition, has similar total Sr and $^{87}Sr/^{86}Sr$ composition as the zone 2A replacement dolomite, indicating that the total Sr composition of the diagenetic fluid

continued to be buffered by the host carbonate. Some workers have suggested that the Zn^{2+} and Pb^{2+} in MVT mineralizing fluids are derived from interaction of formation waters with clastic sediments (chiefly shale) undergoing diagenetic alteration (Jackson and Beales, 1967; Billings et al., 1969; Carpenter et al., 1974; Macqueen, 1976). Experimental work confirms that these metals are easily mobilized from clastic sedimentary rocks by brines compositionally similar to formation waters, at burial diagenetic temperatures (Long and Angino, 1982; Lentini and Shanks, 1983). However, this water-rock interaction should similarly enrich the fluid in radiogenic Sr. The zone 2B dolomite cements contain marine $^{87}Sr/^{86}Sr$ values, indicating that the Sr composition and $^{87}Sr/^{86}Sr$ ratios of the fluids that immediately postdate ore deposition was dominated by Sr derived from host carbonate, and that the zone 2B dolomite cement may chiefly reflect reprecipitation of zone 2A dolomite host that was dissolved during secondary porosity development.

Zones 3 and 4 dolomite cement are enriched in total Sr relative to the zone 2A and 2B dolomites which may reflect an increase in Sr/Ca of the diagenetic fluid. However, the $\delta^{18}O$ data suggests that there was a 40 to 60°C temperature increase (fig. 28). Because $D_{Sr}^{calcite}$ increases with temperature (Stoessel et al., 1987), $D_{Sr}^{dolomite}$ should similarly increase, resulting in higher total Sr contents for zones 3 and 4 dolomites, even if the Sr/Ca ratio of the fluid did not greatly change.

The higher $^{87}Sr/^{86}Sr$ ratios for zones 3 and 4 dolomite cement (Table 1, Fig. 23) record influx of radiogenic Sr-enriched fluids, indicating that dissolution of the host carbonate no longer dominated the solution Sr composition, and that water-rock interaction with clastic sedimentary rocks was increasingly important. Shales and clay minerals have high Rb/Sr ratios and correspondingly high $^{87}Sr/^{86}Sr$ ratios ($^{87}Sr/^{86}Sr$ =

0.713 to > 0.730; Steele and Pushkar, 1973; Perry and Turekian, 1974; Chaudhuri and Brookins, 1979; Steuber et al, 1984; 1987; Morton, 1985; Emery et al., 1987); other than shales derived from mafic volcanics or young, non-radiogenic rocks (Dasch, 1969). Thus, formation water interacting with siliciclastics undergoing diagenetic reactions (via clay mineral transformations, detrital K-feldspar dissolution; albitization of plagioclase), will also be enriched in radiogenic Sr (Perry and Turekian, 1974; Steuber et al., 1984; 1987; Morton, 1985; Chaudhuri et al., 1987). Possible sources of radiogenic Sr include off-shelf basinal shales, basal arkosic clastic sediments of the Chilhowee Group, and Precambrian granitic basement rocks of the Blue Ridge that were overthrust on top the platform margin facies of the Shady Dolomite during late Paleozoic thrusting.

The high Sr content of the calcites may, in part, reflect the higher D_{Sr} value for calcite relative to dolomite (Behrens and Land, 1972; Jacobson and Usdowski, 1976; Kretz, 1982). The enrichment in $^{87}Sr/^{86}Sr$ is compatible with water-rock interaction with clastic sediments undergoing diagenesis, or from Precambrian rocks of the Blue Ridge basement, which was overthrust on top of the Shady Dolomite. The high U content of these calcites (≈ 20 ppm, S.L. Dorobek, pers. comm., 1989) is compatible with derivation from this basement source.

ORIGIN OF LATE DIAGENETIC SEQUENCE

Zone 1 Replacement Dolomite

This nonluminescent dolomite is poorly developed and is confined to rare relict cores within zone 2A dolomite. Zone 1 dolomite, which is generally overgrown and partially replaced by zone 2A dolomite, probably was nonstoichiometric and metastable. It is not

clear whether the similar stable isotope and trace element compositions of zone 1 and the later zone 2A dolomite reflects the original chemistry of zone 1 dolomite or overprinting by later zone 2A dolomite. The lack of a well preserved precursor geochemistry obscures recognition of the diagenetic environment in which zone 1 dolomite formed.

Zone 2A Replacement Dolomite

The zone 2A replacement dolomite is late burial, because it postdates calcite cementation, is associated with tectonic fractures and stylolites, and forms anhedral replacement mosaics indicative of elevated precipitation temperatures. The depleted ^{18}O and enriched ^{13}C composition of zone 2A dolomite and its low total Sr contents also suggest a burial origin. The burial signature of the geochemistry reflects that imparted during primary precipitation rather than neomorphic overprinting of a metastable, near-surface dolomite precursor during burial (Land et al., 1975; Land, 1980; 1985). This is supported by the geochemical similarity of zone 2A dolomites in dolomite fronts in limestone, and zone 2A dolomites in completely dolomitized rocks. If some of the zone 2A dolomites were neomorphically replaced early dolomites, they should have retained some memory of the precursor dolomite composition and thus differ geochemically from the burial dolomites that replaced limestone directly. Secondly, even though facies location would exert a strong control on the distribution of potential early dolomitization environments and the chemistry of the dolomites, the zone 2A replacement dolomites are geochemically and isotopically similar, despite differences in carbonate facies in which they occur. This suggests that all the dolomites are cogenetic and thus are burial.

The depleted $\delta^{18}O$ values for the zone 2A dolomite relative to marine calcite (Fig. 15) reflect elevated precipitation temperatures, and did not arise from diagenetic overprinting

or influence of ^{18}O depleted meteoric waters. The zone 2A replacement dolomite and zone 2B dolomite cement have identical $\delta^{18}O$ values, which implies similar elevated precipitation temperatures from fluids of similar enriched ^{18}O composition.

The enriched $\delta^{13}C$ values of zone 2A dolomites relative to marine values reflects ^{13}C fractionation between HCO_3^- (derived from dissolution of host limestone) and precipitation of dolomite at elevated temperatures. Zone 2A replacement dolomites were not a neomorphically-replaced, near-surface dolomite precursor because their ^{13}C values would likely overlap those of the marine calcites. This is due to the difficulty in completely overprinting the initial ^{13}C composition of a dolomite because of the low amount of dissolved HCO_3^- in the fluid relative to the dolomite (Land, 1985; Banner et al., 1988).

The well-defined Mn and Fe covariation of the zone 2A dolomite (Fig. 22) further supports the contention that zone 2A dolomite formed by replacement of limestone during burial rather than from neomorphism of a metastable, Ca-rich dolomite precursor. It is unlikely that the stoichiometry, ^{18}O, ^{13}C, and Sr compositions of the dolomite precursor could be reset to essentially similar values in the zone 2A dolomite, while retaining this statistically significant Mn and Fe covariation. The increasing Mn and Fe contents in the more coarsely crystalline zone 2A dolomites (Fig. 20) records increasing Mn^{2+} and Fe^{2+} contents in the burial fluid, perhaps due to successively decreasing pH (and possibly Eh) during zone 2A replacement dolomitization, immediately prior to burial dissolution.

The uniformly low Sr contents of the zone 2A replacement dolomites, indicate that the Sr/Ca ratios of the fluid was governed by host limestone dissolution during dolomite replacement, which is supported by $^{87}Sr/^{86}Sr$ ratios in the zone 2A dolomites that are similar to those of marine calcite.

Burial Dissolution and Zn-Pb Mineralization

Immediately following zone 2A replacement dolomitization, the burial fluids became undersaturated with respect to calcite and dolomite, which caused extensive dissolution of the host carbonate coeval with tectonic and hydraulic fracturing, and resulted in development of considerable porosity and permeability. The open voids were partially supported by overpressured fluids, as attested by the common cement-supported rock fabrics consisting largely of void-filling dolomite cement. Burial dissolution had little effect on limestones protected by shale and shaly carbonate aquitards, which were subjected to only minor, fabric-selective leaching.

Some host dolomite dissolution likely was due to acid produced by MVT ore deposition reactions (Anderson, 1983) with reprecipitation as dolomite cement away from the site of ore deposition. Zn^{2+} and Pb^{2+} may have been transported to the site of ore deposition by fluids containing low H_2S, which was generated by $SO_4^=$ reduction at or near the site of ore deposition, given the low solubility of sphalerite and galena in fluids containing H_2S (Anderson, 1983);

$$SO_4^= + 2H^+ + CH_4 = H_2S + CO_2 + 2H_2O \qquad 1)$$

and this H_2S resulted in ore mineral precipitation;

$$Zn^{2+} + H_2S = ZnS + 2H^+. \qquad 2)$$

However, acid generated during ore precipitation cannot have resulted in all of the observed secondary porosity in the Shady Dolomite, as much of this porosity is not associated with sites of MVT ore deposition. Sulfate reduction also would produce ^{13}C depleted CO_2, reflecting that of the CH_4 from which it was derived ($\delta^{13}C$ = -100 to -20 ‰, Schoell, 1980; 1984; Rice, 1983; Whiticar et al., 1986) and the dolomite $\delta^{13}C$ compositions (Table 1, Fig. 15) appear to be incompatible with this process.

If H_2S and the the ore metals in the same mineralizing fluid, either as metal-chloride complexes (for example, Kharaka et al, 1983b; 1986) or metal-organic complexes (Giordano and Barnes, 1981; Barnes and Boucier, 1983; Giordano, 1985; Drummond and Palmer, 1986), then ^{13}C depleted CO_2 might not be associated with MVT mineralization. Consequently, the ^{13}C composition of the zone 2B dolomite cements would resemble that of the host carbonate (Fig. 15), and are thus compatible with this process.

Organic acids (chiefly acetic), which are abundant in formation waters (Carothers and Kharaka, 1978; 1980), could also have formed much of the secondary porosity. These organic acids are more effective at dissolving carbonate than carbonic acid (Meshri, 1986). This would have produced H^+ and pore water HCO_3^- similar in $\delta^{13}C$ composition to that of the host carbonate, provided that acetate was not extensively decarboxylated or oxidized (Lundegard et al., 1984; Meshri, 1986).

Dissolution may also have resulted from thermal decarboxylation of organic acids to yield CH_4 and CO_2 (Carothers and Kharaka, 1978; 1980; Kharaka et al., 1983a), producing carbonic acid. The restricted range of ^{13}C compositions of the zone 2B dolomite cements, which immediately postdate dissolution, however, are incompatible with thermal decarboxylation, which should produce HCO_3^- with a wide range of $\delta^{13}C$ values (see Carothers and Kharaka, 1980). Furthermore, dolomite cementation did not likely result from increasing P_{CO2} due to thermal decarboxylation in formation waters in which the pH was buffered by high acetic acid concentrations (cf. Surdam et al., 1984; 1989; Spirakis and Heyl, 1988), as the ^{13}C composition of the dolomite chemistry should have been depleted relative to the host carbonate.

Dissolution could not have been due to oxidation of organic acids (cf. Shock, 1988),

as this would produce CO_2 similar in $\delta^{13}C$ composition to that of the organic acid (≈ -25 ‰, average $\delta^{13}C$ composition of organic matter in marine sediments; Hudson, 1977; Ohmoto and Rye, 1979; Deines, 1980). The narrow range of $\delta^{13}C$ values of the zone 2A and 2B dolomites that bracket the dissolution stage and their similarity to the host carbonate (Table 1, Fig. 15) thus appear incompatible with decarboxylation (or oxidation) of organic acids as the major source of HCO_3^-. Thus, the burial dissolution resulted from sulfide precipitation, but chiefly from dissociation of organic acids.

Zone 2B Dolomite Cement

Zone 2B dolomite cement is late and postdates tectonic fracturing, secondary porosity development and MVT ore deposition. Zone 2B dolomite may, in part, be coeval with zone 2A dolomite. Precipitation of zone 2B dolomite cement followed burial dissolution, indicating cessation of acid influx and saturation of the burial fluids due to host dolomite dissolution. Based on primary fluid inclusions in zone 2B dolomite cement and in sphalerite (which postdates zone 2A but predates zone 2B dolomite), and the associated hydrocarbons, the zone 2A and 2B dolomite precipitation temperatures are estimated at 100 to 175°C. This implies that the diagenetic fluids were enriched in ^{18}O (0 to +8 ‰ SMOW, see Fig. 28), compatible with ^{18}O values reported for modern formation waters (Clayton et al., 1966; Kharaka et al., 1973; 1977; 1980b; Dutton, 1987; Morton and Land, 1987; Land et al., 1988).

The Sr and ^{18}O, $^{87}Sr/^{86}Sr$ composition of the zone 2B dolomite cements are similar to those of the zone 2A replacement dolomites, suggesting that the composition of the burial fluid was, in part, buffered by dissolution of the zone 2A host dolomite. The slightly depleted $\delta^{13}C$ values of the zone 2B dolomites relative to the zone 2A dolomites

may reflect addition of minor (<5%) amounts of ^{13}C depleted organically-derived CO_2 to the diagenetic fluid or influx of HCO_3^- derived from dissolution of younger Cambro-Ordovician carbonates in the thrust stack.

Zone 2B dolomite cement has identical Fe/Mn ratios as zone 2A replacement dolomite, which reflects a similar equilibria control over the fluid Mn and Fe chemistry. However, the lower Mn and Fe contents of zone 2B dolomite cement may reflect less acidic pH (and/or more oxidizing Eh) conditions prevailing following zone 2A dolomite replacement and burial dissolution, because Eh-pH stability diagrams indicate that these conditions will result in lower Mn^{2+} and Fe^{2+} contents for a fluid in equilibrium with common Mn- and Fe-bearing minerals. Total Sr contents and $^{87}Sr/^{86}Sr$ ratios are similar to those of the zone 2A replacement dolomites, indicating that Sr was derived from dissolution of the host dolomite.

Zones 3 and 4 Dolomite Cement

Zones 3 and 4 dolomite cement is associated with fractures in the host dolomite, indicating that dolomite cementation was coeval with late tectonic fracturing. Depleted $\delta^{18}O$ values in zone 3 and 4 dolomites relative to the earlier zone 2A and 2B dolomites, indicate a minimum temperature increase of 40 to 60°C, yielding temperatures of 150 to 235°C (Fig. 28), assuming that the ^{18}O composition of the fluid remained relatively constant following zone 2A and 2B precipitation. If fluids were further enriched in ^{18}O, than temperatures would need to be commensurately higher. The $\delta^{18}O$ values of the later quartz that precipitated coeval with, and immediately following zone 4 dolomite cement indicate minimum $\delta^{18}O$ values of 0 to +8 ‰.

Zone 3 dolomite cement is slightly depleted in ^{13}C, suggesting organic oxidation

during thermochemical sulfate reduction, which is supported by the low Fe contents of zone 3 dolomite and by the associated pyrite. The ^{13}C composition of zone 4 dolomite is similar to marine values and to zone 2B dolomite, and indicates a decrease in the production of ^{13}C depleted organic carbon. The Fe/Mn ratios of zone 4 dolomite are similar to those of the zone 2A and 2B dolomites (Fig. 21), indicating that pyrite precipitation no longer depleted the fluid in Fe^{2+}. The higher Sr contents of zones 3 and 4 dolomite cement may reflect a temperature increase and/or an increase in the Sr content of the fluid. $^{87}Sr/^{86}Sr$ ratios in zones 3 and 4 dolomite cement also increase, indicating that the late diagenetic fluids were enriched in radiogenic ^{87}Sr due to water-rock interaction with clastic sedimentary rocks and/or with granitic basement rocks of the Blue Ridge.

Authigenic Quartz

Precipitation of late authigenic quartz follows the last generation of dolomite, recording a change in the fluid chemistry. Inclusions of zone 4 dolomite within the early quartz growth zones indicates that the two mineral phases initially coprecipitated. The authigenic quartz precipitated at elevated temperatures, as it immediately follows zone 4 dolomite cement (estimated precipitation temperatures 150 to 235°C) and the quartz has secondary fluid inclusions which indicate hot (up to 175 to 225°C) saline (18 to 33 wt. % NaCl equiv.) fluids. The $\delta^{18}O$ composition of the quartz indicates that the late burial fluids remained enriched in ^{18}O (O to + 8 °/oo SMOW), compatible with water/rock interaction at elevated temperatures. The high salinities of the late burial fluids were likely derived from dissolution of evaporites from the overlying Rome Formation, Knox Group, and Mississippian sequence which were overthrust during Alleghenian

deformation.

Late Calcite and Dedolomite

Because the dolomites are stoichiometric (see above), the fabric selectivity of the dedolomite does not reflect replacement of nonstoichiometric dolomite zones (cf. Frank, 1981). Because dedolomite is best developed in the more inclusion-rich dolomite cores, the fabric selectivity likely reflects preferential replacement of more porous and permeable dolomite zones. The limpid, inclusion-free dolomite overgrowths were more resistant to replacement, although they were corroded where overgrown by late calcite. The association of dedolomite with cleavage traces and microfractures further supports a porosity and permeability control.

The late calcite cement and dedolomite records either an increase in the Ca/Mg ratio of the fluid and/or a temperature decrease, relative to the previous dolomites (Fig. 6, Land, 1985). However, because distribution coefficients for Mg^{2+} in calcite are not available for elevated diagenetic temperatures (> 90°C), it cannot be determined whether temperature or Ca/Mg ratio of the fluid primarily caused the shift from dolomite to calcite precipitation.

The highly variable ^{18}O and ^{13}C composition of the calcites (Fig. 15) suggests precipitation under highly variable diagenetic conditions involving inhomogeneities in the composition of the reservoir fluid, or variable mixing of different fluids. The higher Mn/Fe ratios in the calcite compared to the previous dolomites may reflect uptake of Fe^{2+} by pyrite precipitation. The high total Sr content of the calcites may have been due to the higher D_{Sr} value for calcite relative to dolomite. The elevated $^{87}Sr/^{86}Sr$ ratios indicate that the late diagenetic fluids continued to remain enriched in radiogenic Sr derived from

interaction of the fluids with clastic sediments and/or granitic basement rocks.

The calcite precipitated from saline fluids at elevated temperatures, based on their primary fluid inclusions and generally depleted ^{18}O composition. Secondary 3-phase inclusions indicate elevated burial temperatures continued after calcite cementation and dedolomitization. Vapor bubble homogenization temperatures for the 3-phase inclusions in calcite (Fig. 24E) are higher than those in quartz (Fig 24C). This likely reflects stretching of the calcite inclusions due to subsequent overheating, because fluid inclusions in calcite are considerably more susceptible to stretching and decrepitation due to overheating than are inclusions in quartz (Table 2, Tugarinov and Naumov, 1970). Total homogenization of the 3-phase inclusions in calcite is by halite dissolution, which is unaffected by stretching, Tm NaCl in calcite (Fig. 24E') is similar to Tm NaCl quartz (Fig. 24C').

REGIONAL FLUID FLOW

Based on mass balance considerations, large numbers of pore volumes of the late diagenetic fluids passed through the rocks during burial, in order to: import the Mg^{2+} needed for replacement dolomitization and dolomite cementation; transport the ore metals to the sites of MVT ore deposition (cf. Roedder, 1984); and import the K^+ required to form the quantities of authigenic K-feldspar found throughout the Valley and Ridge (Hearn et al., 1987). This late fluid migration event was coeval with late Paleozoic Alleghanian deformation, based on petrographic and paragenetic relations, and was of regional scale, indicated by the Alleghanian age for authigenic feldspar overgrowths (Hearn et al., 1987; 1988) and MVT mineralization (Kaiser and Ohmoto, 1985)

throughout the central and southern Appalachians.

The regional hydrologic flow system developed along the Appalachians during Alleghanian deformation in response to tectonic uplift and overthrusting (Hearn et al., 1987; 1988), which established a topographic gradient for gravity-driven, regional groundwater flow away from tectonic uplands through Appalachian basin sediments. Paleohydrologic modelling suggests that hydraulic head generated by topographic uplift of several kilometers could have produced up to 300 kilometers of lateral flow away from the orogenic uplands (Engelder and Bethke, 1986). The steep hydraulic gradient could generate overpressures downdip that promoted overthrusting and fracturing in the Valley and Ridge rocks (Bethke, 1986b; Engelder and Bethke, 1986).

These gravity-driven, meteoric fluids penetrated into deeply buried sedimentary rocks (Grover and Read, 1983; Dorobek, 1987), where the fluids were heated and became enriched in dissolved salts. Hearn et al. (1987) considered that the salinity of the diagenetic fluids indicated by fluid inclusions reflected residual evaporative brines generated on tidal flats. There is no evidence of former evaporites in platform margin facies of the Shady Dolomite (Pfeil and Read, 1980; Barnaby and Read, in press), and meteoric groundwaters would have flushed residual connate brines from the sequence during early meteoric diagenesis in the Early to Middle Cambrian, prior to deep burial. However, evaporites from the overlying Cambrian-Ordovician carbonates and redbeds, and locally, the Mississippian are more likely sources for much of the dissolved salts. These rocks could have expelled saline fluids during overthrusting and regional fluid flow. In addition, water-rock interaction at elevated burial temperatures would have enriched the fluids in dissolved salts. This is compatible with the inferred late fluid ^{18}O enrichment, and buffering of the fluid $\delta^{13}C$ and $^{87}Sr/^{86}Sr$ composition by marine

carbonate.

SOURCE OF MG^{2+}

The burial dolomitization model favored in this study for the bulk of the replacement dolomites has been criticized because of the perceived problem of an adequate Mg^{2+} source and transport mechanism in the deep subsurface (Morrow, 1982; Land, 1985).

Diagenesis and compaction of shale has been invoked as a Mg^{2+} source for burial dolomitization (Illing, 1959 Mattes and Mountjoy, 1980; Wong and Oldershaw, 1981; McHargue and Price, 1982; Gregg, 1988). However, shales release only minor quantities of Mg^{2+} during diagenesis (Hower et al., 1976), and most of this Mg^{2+} is consumed locally by authigenic chlorite (Hower et al., 1976; Boles and Frank, 1979, Boles, 1981; Land, 1985). Thus, the amount of dolomite that can be produced by Mg^{2+} derived from shale is volumetrically small (McHargue and Price, 1982; Morrow, 1982; Land, 1985; Gregg, 1988). Furthermore, nonferroan dolomites typical of the Shady Dolomite are rarely associated with shale diagenesis (Boles, 1981; Boles and Frank, 1979; McHargue and Price, 1982; Land, 1985; Land et al., 1987). In addition, the Sr isotope geochemistry of zone 2A and 2B dolomite is incompatible with derivation of Mg from shale, because formation waters interacting with shales should be enriched in ^{87}Sr (Steuber et al., 1984; 1987; Chaudhuri et al., 1987), whereas the $^{87}Sr/^{86}Sr$ ratios of the zone 2A and zone 2B dolomite are identical to marine values (Table 1; Fig. 23).

Pressure solution of limestone (Wanless, 1979) or stabilization of Mg-rich calcite components (Goodell and Garmon, 1969) could have provided only a small fraction of the Mg^{2+} required to form the zone 2A replacement dolomite, especially since much of the

initial Mg^{2+} in the limestone was expelled during early meteoric diagenesis.

Thus, the only likely Mg source for the zone 2A dolomites appears to be from remobilization of existing dolomite, either from dissolution-reprecipitation of a local dolomite source and/or from dissolution of dolomitic units elsewhere. It is difficult to assess the relative importance of a local precursor dolomite as a Mg^{2+} source, as the only recognized dolomite prior to zone 2A dolomite is zone 1 dolomite, which is relatively rare (<< 5% of total dolomite). The paucity of zone 1 dolomite may reflect either its low abundance, or pervasive replacement by zone 2A dolomite. However, if a dolomite precursor had been abundant, some petrographic or geochemical evidence of its former presence, other than the rare, relict zone 1 cores with a geochemical composition apparently similar to the zone 2A dolomite, would be expected. In any case, remobilization of a local dolomite source would produce no more dolomite than was initially present, and this mechanism cannot account for much of the zone 2A dolomite which visibly replaced limestone during late burial, or for zone 2B, 3, and 4 dolomite cements. Therefore, although zone 1 dolomite or an unidentified local metastable dolomite precursor cannot be eliminated as a potential Mg source for the zone 2A replacement dolomites, it probably cannot account for all of the replacement dolomite.

Some of the Mg^{2+} for zone 2A dolomite replacement was likely derived from an external dolomite source. One possibility is the Late Cambrian to Early Ordovician Knox Group, which attains thicknesses in excess of 1000 meters in eastern thrust sheets (Read, in press a), and contains large amounts of dolomite (>50%; Cooper, 1961), most of which is early diagenetic (Churnet et al., 1982; Burns et al., 1986; Montanez and Read, 1986). During late Paleozoic deformation, Knox Group carbonates were overriden by the thrust sheet containing the Shady Dolomite platform margin (Fig. 12). Tectonic loading

by this estimated 5-11 km thick thrust sheet (Gibson and Gray, 1985) would have resulted in considerable pressure solution of underlying Knox Group carbonates. The timing of this pressure solution and release or Mg^{2+} into the burial fluids is roughly synchronous with the inferred timing of dolomitization for the Shady Dolomite.

Dissolution of dolomite would produce fluids having Mg/Ca molar ratios of approximately 1, or lower, if accompanied by limestone dissolution. At the diagenetic temperatures estimated for the zone 2A dolomite replacement (100 to 175°C), fluids having Mg/Ca molar ratios between 0.3 and 0.1 are potentially dolomitizing (Fig. 6, Land, 1985). Therefore, each mole of dolomite dissolved could result in formation of up to 0.7 to 0.9 moles of replacement dolomite, assuming maximum efficiency of Mg remobilization. To completely dolomitize the Shady Dolomite outer platform of the study area (cross-sectional area $\approx 3.5 \times 10^6$ m^2) requires dissolution of $\approx 1.0 \times 10^7$ m^2 (total cross sectional area) of Knox Group dolomitic limestones, assuming they were 50 % dolomite. Parautochthonous Cambrian and Ordovician Knox Group carbonates were overthrust a minimum of 100 km by the easternmost thrust sheet of the Valley and Ridge province (Bartholomew, 1987), thus 10 % average dissolution of the Knox Group carbonates over the distance of tectonic transport is required to completely dolomitize the Shady Dolomite outer platform.

The Mg^{2+} derived from this dolomite dissolution likely was transported to the Shady Dolomite shelf margin via fracture and fault conduits by regional, gravity-driven, groundwater flow during late Paleozoic uplift. The narrow range of $\delta^{13}C$ values for the dolomites, the low Sr contents, and $^{87}Sr/^{86}Sr$ ratios similar to marine carbonate, are all compatible with derivation of Mg^{2+} from this source.

CONCLUSIONS

Outermost platform facies of the Shady Dolomite record a complex diagenetic history in diagenetic environments ranging from normal marine to meteoric to late burial coeval with tectonic deformation and uplift.

1) Geological and petrographic evidence indicates that all the dolomites are late, because they postdate early meteoric calcite cements, are associated with tectonic fractures and stylolites, form anhedral mosaics of turbid crystals with undulose extinction, indicative of elevated precipitation temperatures, are associated with Pb-Zn ore deposition, and some contain primary 2-phase inclusions.

2) Zone 1 dolomite consists of rare, relict nonluminescent dolomite cores that were replaced, corroded, and overgrown by zone 2A dolomite, the dominant replacement phase. Although pervasive replacement by zone 2A dolomite precludes direct analysis of the zone 1 dolomite geochemistry, it appears to be similar to that of the zone 2A dolomites. This may reflect either the original chemistry of zone 1 dolomite or diagenetic overprinting by zone 2A dolomite.

3) Zone 2A dolomites have depleted ^{18}O compositions relative to marine carbonate or estimated $\delta^{18}O$ values for early dolomite precipitating from marine or modified marine water, and appears to record elevated precipitation temperatures (estimated 100 to 175°C). The ^{13}C enrichment in zone 2A dolomite reflects ^{13}C fractionation between host limestone and replacement dolomite at elevated temperatures. Mn and Fe contents of zone 2A dolomite increase with crystal size and exhibit a well-defined, linear covariation, interpreted to primarily reflect a pH control. The low Sr contents of zone 2A dolomite and the marine $^{87}Sr/^{86}Sr$ ratios indicate that the Sr content of the dolomitizing fluid was

buffered by the host limestone, and that the system was relatively closed with respect to Sr.

The burial signature of the zone 2A replacement dolomite was imparted during precipitation rather than being due to diagenetic overprinting of a metastable, early diagenetic dolomite precursor; this is indicated by the restricted range of $\delta^{18}O$, $\delta^{13}C$ values, and the uniformly low Sr contents that exhibit no trend towards more pristine values expected for an early dolomite. The enriched $\delta^{13}C$ values cannot reflect diagenetic overprinting of a near-surface dolomite precursor, because it is difficult to alter the original ^{13}C composition of a near-surface dolomite ($\delta^{13}C$ similar to marine carbonate) because of the relatively low HCO_3^- contents of diagenetic fluids.

4) Following zone 2A replacement dolomitization, the sequence was subjected to dissolution coeval with tectonic fracturing. This dissolution may have been due to influx of organic acids or acid produced by Pb-Zn ore deposition. Dissolution porosity locally was occluded by MVT Pb-Zn ore minerals, and by later cements of dolomite, quartz, and calcite.

5) Zone 2B dolomite cements, which may, in part be coeval with zone 2A dolomite, also precipitated at elevated temperatures, based on their saddle dolomite morphology, primary fluid inclusions (Th = 120 to 150°C, 23 to 26 wt. % NaCl equiv.), horizontal geopetal structures in steeply-dipping beds, and depleted $\delta^{18}O$ values relative to marine carbonate. Estimated precipitation temperatures are 100 to 175°C, and diagenetic fluids were enriched in ^{18}O ($\delta^{18}O$ = 0 to +8 °/oo SMOW). The marine $\delta^{13}C$ values of zone 2B dolomite indicate that limestone dissolution at elevated temperatures no longer was involved, because the limestone was largely replaced by this time. Mn and Fe contents of zone 2B dolomite are low relative to the zone 2A dolomite which may reflect a shift to less

acidic (or higher Eh) conditions following zone 2A replacement dolomitization and dissolution. The Sr contents and marine $^{87}Sr/^{86}Sr$ ratios of zone 2B dolomite cement indicate that the fluid Sr chemistry continued to be buffered by host carbonate.

6) Zone 3 and 4 dolomite cements record higher temperature fluids (150 to 235°C), indicated by depleted $\delta^{18}O$ compositions. Their $\delta^{13}C$ values range from slightly depleted (reflecting organic input) to values in equilibrium with the host carbonate. Zone 3 dolomite is depleted in Fe due to pyrite precipitation, whereas zone 4 dolomite is enriched in Mn and Fe. Zones 3 and 4 dolomite have high Sr contents relative to the previous dolomites, their enriched $^{87}Sr/^{86}Sr$ ratios reflect influx of radiogenic Sr from siliciclastic diagenesis.

7) Although some of the Mg^{2+} needed for replacement dolomitization and dolomite cementation may have been derived from a local dolomite source, the lack of petrographic and geochemical evidence for a metastable dolomite precursor suggests that much of the Mg^{2+} was externally derived. Shales could not have provided significant amounts of Mg^{2+}, because the marine $^{87}Sr/^{86}Sr$ ratios of the replacement dolomites eliminate this possibility. Much of the Mg^{2+} for late dolomitization may have been derived from Knox Group carbonates which contain much early dolomite. These rocks were overthrust during Alleghenian deformation. Pressure solution from loading by a 5 to 11 km thick thrust sheet would have liberated considerable Mg^{2+} into solution, and this Mg^{2+} could have been transported via fault and fracture conduits to the platform margin limestones of the Shady Dolomite during regional, gravity-driven fluid flow that developed in response to tectonic uplift and deformation.

8) Secondary, halite-bearing fluid inclusions in late quartz and calcite evidence hotter (175-225° C), more saline (30 to 33 wt. % NaCl) fluids, following dolomitization.

These temperatures are compatible with the estimated maximum burial depths in excess of 5 km. The pressures and temperatures defined for the fluid inclusions indicate that the fluids were overpressured, which is compatible with other evidence suggesting fluid overpressuring.

REFERENCES

Aharon, P., Socki, R.A., and Chan, L., 1987, Dolomitization of atoll by sea water convection flow: test of a hypothesis at Niue, South Pacific: Journal of Geology, v. 95, p. 187-203.

Aïssaoui, D.M., 1988, Magnesian calcite cements and their diagenesis: dissolution and dolomitization, Mururoa Atoll: Sedimentology, v. 35, p. 821-841.

Aitken, J.D., 1971, Control of Lower Paleozoic sedimentary facies by the Kicking Horse Rim, southern Rocky Mountains, Canada: Bulletin of Canadian Petroleum Geology, v. 19, p. 557-569.

Aitken, J.D., and McIlreath, I.A., 1984, The Cathedral reef escarpment, a Cambrian great wall with humble origins: Geos, v. 13, no. 1, p. 17-19.

Anderson, G.M., 1983, Some geochemical aspects of sulfide precipitation in carbonate rocks: *in*, Kisvarsanyi, G., Grant, S.K., Pratt, W.P., and Koenig, J.W., eds., Proceedings International Conference on Mississippi Valley Type Lead-Zinc Deposits: University of Missouri-Rolla, Rolla, Missouri, p. 61-76.

Badger, R.L., and Sinha, A.K., 1988, Age and Sr isotopic signature of the Catoctin Volcanic Province: Implications for subcrustal mantle evolution: Geology, v. 16, p. 692-695.

Banner, J.L., Hanson, G.N., and Meyers, W.J., 1988, Water-rock interaction history of regionally extensive dolomites of the Burlington-Keokuk Formation (Mississippian): isotopic evidence: *in*, Shukla, V., and Baker, P.A., (eds.), Sedimentology and Geochemistry of Dolostones: Society of Economic Paleontologists and Mineralogists Special Publication No. 43, Tulsa, Oklahoma, p. 97-113.

Barnaby, R.J., and Bodnar, R.J., 1988, High-salinity overpressured fluids associated with MVT mineralization, Shady Dolomite (Cambrian), Virginia: American Association of Petroleum Geologists Bulletin, v. 72, p. 157-158.

Barnaby, R.J., and Read, J.F., in press, Carbonate ramp to rimmed shelf evolution: Lower to Middle Cambrian continental margin, Virginia Appalachians: Geological Society of America Bulletin.

Barnaby, R.J., and Rimstidt, J.D., 1989, Redox conditions of calcite cementation interpreted from Mn and Fe contents of authigenic calcites: Geological Society of America Bulletin, v. 101, p. 795-804.

Barner, H.E., and Scheuerman, R.V., 1978, Handbook of Thermochemical Data For Compounds and Aqueous Species: New York, Wiley and Sons, 156 p.

Barnes, H.L., and Boucier, W.L., 1983, Role of organic and inorganic complexes in ore metal transport at low temperatures (abstr.): Geological Society of America, Abstracts with Programs, v. 15, p. 521.

Bartholomew, M.J., 1987, Structural evolution of the Pulaski thrust system, southwestern Virginia: Geological Society of America Bulletin, v. 99, p. 491-510.

Bathurst, R.G.C., 1982, Genesis of stromatactis cavities between submarine crusts in Palaeozoic carbonate mud buildups: Journal of the Geological Society of London, v. 139, p. 165-181.

Bathurst, R.G.C., 1987, Diagenetically enhanced bedding in argillaceous platform limestones: stratified cementation and selective compaction: Sedimentology, v. 34, p. 749-778.

Behrens, E., and Land, L., 1972, Subtidal Holocene dolomite, Baffin Bay, Texas: Journal of Sedimentary Petrology, v. 42, p. 155-161.

Bein, A., and Land, L.S., 1983, Carbonate sedimentation and diagenesis associated with Mg-Ca-Chloride brines: The Permian San Andres Formation in the Texas panhandle: Journal of Sedimentary Petrology, v. 53, p. 243-260.

Bethke, C.M., 1986a, Hydrologic constraints on the genesis of the upper Mississippi valley mineral district from Illinois basin brines: Economic Geology, v. 81, p. 233-249.

Bethke, C.M., 1986b, Roles of sediment compaction, tectonic compression, and topographic relief in driving deep groundwater migration (abstr.): Geological Society of America Abstracts with Programs, v. 18, no. 6, p. 540.

Billings, G.K., Kesler, S.E., and Jackson, S.A., 1969, Relation of zinc-rich formation waters, Northern Alberta, to the Pine Point ore deposit: Economic Geology, v. 64, p. 385-391.

Bodine, M.W., Holland, H.D., and Borcsik, M., 1965, Co-precipitation of manganese and strontium with calcite: *in*, Symposium on Problems of Postmagmatic Ore Deposition II, Prague, p. 401-406.

Bodnar, R.J., and Bethke, P.M., 1984, Systematics of stretching of fluid inclusions I: Fluorite and sphalerite at 1 Atm. confining pressure: Economic Geology, v. 79, p. 141-161.

Boles, J.R., 1981, Clay diagenesis and effects on sandstone cementation (case histories from the Gulf Coast Tertiary), in, Longstaffe, J.F., (ed.): Clays and the Resource Geologist, Mineralogical Association of Canada Short Course Handbook, v. 7, p. 148-168.

Boles, J.R. and Frank, S.G., 1979, Clay diagenesis in Wilcox sandstones of southwest Texas: implications of smectite diagenesis on sandstone cementation: Journal of Sedimentary Petrology, v. 49, p. 55-70.

Bond, G.C., Nickeson, P.A., and Kominz, M.A., 1984, Breakup of a supercontinent between 625 Ma and 555 Ma: New evidence and implications for continental histories: Earth and Planetary Science Letters, v. 70, p. 325-345.

Bottinga, Y., 1969, Calculated fractionation factors for carbon and hydrogen isotope exchange in the system calcite-CO_2-graphite-methane-hydrogen and water vapor: Geochimica et Cosmochimica Acta, v. 33, p. 49-64.

Brand, U., and Veizer, J., 1981, Chemical diagenesis of a multicomponent carbonate system-2: stable isotopes: Journal of Sedimentary Petrology, v. 51, p. 987-997.

Budai, J.M., Lohmann, K.C., and Owen, R.M., 1984, Burial dedolomite in the Mississippian Madison Limestone, Wyoming and Utah thrust belt: Journal of Sedimentary Petrology, v. 54, p. 276-288.

Bullen, S.B., and Sibley, D.F., 1984, Dolomite selectivity and mimic replacement: Geology, v. 12, p. 655-658.

Burns, S.J., and Baker, P.A., 1987, A geochemical study of dolomite in the Monterey Formation, California: Journal of Sedimentary Petrology, v. 57, 128-139.

Burns, S.J., Weig, P., and Baker, P., 1986, Early diagenesis of Knox Group carbonates, eastern Tennessee: trace element and isotopic evidence (abstr.): Geological Society of America Abstracts with Programs, v. 18, no. 6, p. 554.

Butts, C., 1940, Geology of the Appalachian Valley in Virginia: Virginia Geological Survey Bulletin 52, part 1, 568 p.

Byrd, W.J., 1973, Petrology of the Cambrian Shady Dolomite in North Carolina, northeast Tennessee, and southwest Virginia [Ph.D. Dissertation]: University of North Carolina at Chapel Hill, 152 p.

Byrd, W.J., Weinberg, E.L., and Yochelson, E.L., 1973, *Salterella* in the Lower Cambrian Shady Dolomite of southwestern Virginia: American Journal of Science, v. 273-A, p. 252-260.

Carothers, W.W., and Kharaka, Y.K., 1978, Aliphatic acid anions in oil-field waters and their implications for the origin of natural gas: American Association of Petroleum Geologists Bulletin, v. 62, p. 2441-2453.

Carothers, W.W., and Kharaka, Y.K., 1980, Stable carbon isotopes of HCO_3^- in oil field waters- implications for the origin of CO_2: Geochimica et Cosmochimica Acta, v. 44, p. 323-332.

Carpenter, A.B., and Oglesby, T.W., 1976, A model for the formation of luminescently zoned calcite cements and its implications: Geological Society of America Abstracts with Programs, v. 8, p. 469-470.

Carpenter, A.B., Trout, M.L., and Pickett, E.E., 1974, Preliminary report on the origin and chemical evolution of lead- and zinc-rich oil field brines in central Mississippi: Economic Geology, v. 69, p. 1191-1206.

Chaudhuri, S., Broedel, V., and Clauer, N., 1987, Strontium isotopic evolution of oil-field waters from carbonate reservoir rocks in Bindley field, central Kansas, USA: Geochimica et Cosmochimica Acta, v. 51, p. 45-53.

Chaudhuri, S., and Brookins, D.G., 1979, The Rb-Sr systematics in acid-leached clay minerals: Chemical Geology, v. 24, p. 231-242.

Chaudhuri, S., Claurer, N., and Ramakrishnan, S., 1983, Strontium isotopic composition of gangue carbonate minerals in the lead-zinc sulfide deposits at the Brushy Creek Mine, Viburnum Trend, southeast Missouri: *in*, Kisvarsanyi, G., Grant, S.K., Pratt, W.P., and Koenig, J.W., eds., International Conference on Mississippi Valley Type Lead-Zinc Deposits, Proceedings Volume, Rolla, Missouri, University of Missouri-Rolla, p. 140-144.

Churnet, H.G., Misra, K.C., and Walker, K.R., 1982, Deposition and dolomitization of Upper Knox carbonate sediments, Copper Ridge district, east Tennessee: Geological Society of America Bulletin, v. 93, p. 76-86.

Clayton, R.N., Friedman, I., Graf, D.L., Mayeda, T.K., Meents, W.F., and Shimp, N.F., 1966, The origin of saline formation waters: I. Isotopic composition: Journal of Geophysical Research, v. 71, p. 3869-3882.

Collins, M.A., and Gelhar, L.W., 1971, Seawater intrusion in layered aquifers: Water Resources Research, v. 7, p. 971-979.

Coniglio, M., and James, N.P., 1985, Calcified algae as sediment contributors to early Paleozoic limestones: Evidence from deep-water sediments of the Cow Head Group, Western Newfoundland: Journal of Sedimentary Petrology, v. 55, p. 746-754.

Cooper, B.N., Arkle, T. Jr., and Latimer, I.S. Jr., 1961, Grand Appalachian Excursion: Guidebook no. 1, Virginia Polytechnic Institute and State University, Blacksburg, Virginia, 114 p.

Dasch, E.J., 1969, Strontium isotopes in weathering profiles, deep sea sediments, and sedimentary rocks: Geochimica et Cosmochimica Acta, v. 33, p. 1521-1552.

Dawans, J.M., and Swart, P.K., 1988, Textural and geochemical alternations in Late Cenozoic Bahamian dolomites: Sedimentology, v. 35, p. 385-403.

Deines, P., 1980, The isotopic composition of reduced organic carbon: *in*, Fritz, P., Fontes, J.Ch. (eds.), Handbook of Environmental Isotope Geochemistry, vol. 1, Elsevier, NY, p. 329-406.

Demicco, R.V., 1985, Platform and off-platform carbonates of the Upper Cambrian of western Maryland, U.S.A.: Sedimentology, v. 32, p. 1-22.

Deuser, W.G., 1970, Extreme $^{13}C/^{12}C$ variations in Quaternary dolomites from the continental shelf: Earth and Planetary Science Letters, v. 8, p. 118-124.

Dickson, J.A.D., 1965, A modified staining technique for carbonates in thin section: Nature, v. 205, p. 587.

Dorobek, S.L., 1987, Petrography, geochemistry, and origin of burial diagenetic facies, Siluro-Devonian Helderberg Group (carbonate rocks), Central Appalachians: American Association of Petroleum Geologists Bulletin, v. 71, p. 492-514.

Drever, J.I., 1982, The Geochemistry of Natural Waters: Englewood Cliffs, N.J., Prentice-Hall, Inc., 388 p.

Dromgoole, E.L., and Walter, L.M., 1987, Iron and manganese incorporation into calcite cements: implications for diagenetic studies (abstr.): Geological Society of America Abstracts with Programs, v. 19, no. 7, p. 647.

Droxler, A.W., and Schlager, W., 1985, Glacial versus interglacial sedimentation rates and turbidite frequency in the Bahamas: Geology, v. 13, p. 799-802.

Drummond, S.E., and Palmer, D.A., 1986, Thermal decarboxylation of acetate. Part II. Boundary conditions for the role of acetate in the primary migration of natural gas and the transportation of metals in hydrothermal systems: Geochimica et Cosmochimica Acta, v. 50, p. 825-833.

Dutton, A.R., 1987, Origin of brine in the San Andres Formation, evaporite confining system, Texas panhandle and eastern New Mexico: Geological Society of America Bulletin, v. 99, p. 103-112.

Emery, D., Dickson, J.A.D., and Smalley, P.C., 1987, The strontium isotopic composition and origin of burial cements in the Lincolnshire Limestone (Bajocian) of central Lincolnshire, England: Sedimentology, v. 34, p. 795-806.

Engelder, T., and Bethke, C.M., 1986, Reexamination of the Gulf Coast model used by the Rubey-Hubbert hypothesis for thrust belt tectonics (abstr.): Geological Society of America Abstracts with Programs, 1986, p. 595.

Fairchild, I.J., 1983, Chemical controls of cathodoluminescence of natural dolomites and calcites: new data and review: Sedimentology, v. 30, 579-583.

Foley, N.K, 1980, Mineralogy and Geochemistry of the Austinville-Ivanhoe District [M.S. thesis]: Virginia Polytechnic Institute and State University, Blacksburg, Virginia, 84 p.

Frank, J.R., 1981, Dedolomitization in the Taum Sauk Limestone (Upper Cambrian), southeast Missouri: Journal of Sedimentary Petrology, v. 51, p. 7-18.

Frank, J.R., Carpenter, A.B., and Oglesby, T.W., 1982, Cathodoluminescence and composition of calcite cement in the Taum Sauk Limestone (Upper Cambrian), Southeast Missouri: Journal of Sedimentary Petrology, v. 52, p. 631-638.

Friedman, I., and Murata, K.J., 1979, Origin of dolomite in Miocene Monterey Shale and related formations in the Temblor Range, California: Geochimica et Cosmochimica Acta, v. 43, p. 1357-1365.

Friedman, I., and O'Neil, J.R., 1977, Data of Geochemistry, 6th Ed., Chapter KK. Compilation of Stable Isotope Fractionation Factors of Geochemical Interest: United States Geological Survey Professional Paper 440-KK.

Frind, E.O., 1982, Seawater intrusion in continuous coastal aquifer-aquitard systems: Advances in Water Resources, v. 5, p. 89-99.

Fritz, W.H., and Yochelson, E.L., 1988, The status of *Salterella* as a Lower Cambrian index fossil: Canadian Journal of Earth Sciences, v. 25, p. 403-416.

Füchtbauer, H., and Hardie, L.A., 1976, Experimentally determined homogeneous distribution coefficients for precipitated magnesian calcites (abstr.): Geological Society of America Abstracts with Programs, v. 8, p. 877.

Garven, G., 1985, The role of regional fluid flow in the genesis of the Pine Point deposit, western Canada sedimentary basin: Economic Geology, v. 80, p. 307-324.

Garven, G., and Freeze, R.A., 1984a, Theoretical analysis of the role of groundwater flow in the genesis of stratabound ore deposits. 1. Mathematical and numerical model: American Journal of Science, v. 284, p. 1085-1124.

Garven, G., and Freeze, R.A., 1984b, Theoretical analysis of the role of groundwater flow in the genesis of stratabound ore deposits. 2. Quantitative results: American Journal of Science, v. 284, p. 1125-1174.

Gibson, R.G., and Gray, D.R., 1985, Ductile-to-brittle transition in shear during thrust sheet emplacement, southern Appalachian thrust belt: Journal of Structural Geology, v. 7, p. 513-525.

Ginsburg, R.N., Marszalek, D.S., and Scheidermann, N., 1971, Ultrastructure of carbonate cements in a Holocene algal reef off Bermuda: Journal of Sedimentary Petrology, v. 41, p. 472-482.

Giordano, T.H., 1985, A preliminary evaluation of organic ligands and metal-organic complexing in Mississippi Valley-type ore solutions: Economic Geology, v. 80, p. 96-106.

Giordano, T.H., and Barnes, H.L., 1981, Lead transport in Mississippi Valley-type ore solutions: Economic Geology, v. 76, p. 2200-2211.

Gohn, G.S., 1976, Sedimentology, Stratigraphy, and Paleogeography of Lower Paleozoic Carbonate Rocks, Conestoga Valley, Southeastern Pennsylvania [Ph.D. Dissertation]: University of Delaware, Newark, Delaware, 315 p.

González, L.A., and Lohmann, K.C., 1985, Carbon and oxygen isotopic composition of Holocene reefal carbonates: Geology, v. 13, p. 811-814.

Goodell, H.G., and Garmon, R.K., 1969, Carbonate geochemistry of Superior deep test well, Andros Island, Bahamas: American Association of Petroleum Geologists Bulletin, v. 53, p. 513-536.

Graber, E.R., and Lohmann, K.C., 1989, Basinal marine dolomicrite from the Pennsylvanian/Wolfcampian Horquilla Formation, New Mexico: Journal of Sedimentary Petrology, v. 59, p. 4-12.

Gregg, J.M., 1988, Origins of dolomite in the offshore facies of the Bonneterre Formation (Cambrian), southeast Missouri: *in*, Shukla, V., and Baker, P.A., (eds.), Sedimentology and Geochemistry of Dolostones: Society of Economic Paleontologists and Mineralogists Special Publication No. 43, Tulsa, Oklahoma, p. 67-84.

Gregg, J.M., and Sibley, D.F., 1984, Epigenetic dolomitization and the origin of xenotopic dolomite texture: Journal of Sedimentary Petrology, v. 54, p. 908-931.

Gregory, G., and Mehrtens, C., 1982, Paleoenvironmental reconstruction of the Dunham Dolomite (Lower Cambrian), northwestern Vermont (abstract): Northeastern Geological Society of America Abstracts, v. 15, p. 126.

Gregory, R.T., and Taylor, H.P., 1981, An oxygen isotope profile in a section of Cretaceous oceanic crust, Samail Ophiolite, Oman: evidence for $\delta^{18}O$ buffering of the oceans by deep (> 5 km) seawater-hydrothermal circulation at mid-ocean ridges: Journal of Geophysical Research, v. 86, p. 2737-2755.

Gross, M.G., and Tracy, J.I., Jr., 1966, Oxygen and carbon isotopic composition of limestones and dolomites, Bikini and Eniwetok Atolls: Science, v. 151, 1082-1084.

Grover, G., and Read, J.F., 1983, Paleoaquifer and deep burial related cements defined by regional cathodoluminescent patterns, Middle Ordovician Carbonates, Virginia: American Association of Petroleum Geologists Bulletin, v. 67, p. 1275-1303.

Hallam, A, 1986, Origin of minor limestone-shale cycles: Climatically induced or diagenetic?: Geology, v. 14, p. 609-612.

Hardie, L.A., 1987, Dolomitization: a critical view of some current views: Journal of Sedimentary Petrology, v. 57, p. 166-183.

Harris, A.G., 1979, Conodont color alteration, an organo-mineral metamorphic index, and its application to Appalachian basin geology: *in*, P.A. Scholle and P.R. Schluger, eds., Aspects of Diagenesis: Society of Economic Paleontologists and Mineralogists Special Publication No. 26, p. 3-16.

Harris, A.G., Harris, L.D., and Epstein, J.B., 1978, Oil and gas data from Paleozoic rocks of the Appalachian basin: maps for assessing hydrocarbon potential and thermal maturity (conodont color alteration isograds and overburden isopachs): United States Geological Survey Miscellaneous Geological Investigations Map I-917 E, scale 1:2,500,000.

Hatcher, R.D., and Odum, A.L., 1980, Timing of thrusting in the southern Appalachians, U.S.A.: Model for orogeny?: Journal of the Geological Society of London, v. 137, p. 321-327.

Hearn, P.P., Jr., Belkin, H.E., and Sutter, J.F., 1988, Tectonically induced fluid migration in sedimentary basins: a new factor to be considered in the assessment of thermal history (abstr.): Geological Society of America Abstracts with Programs, v. 20, p. A330.

Hearn, P.P., Jr., and Sutter, J.F., 1985, Authigenic potassium feldspar in Cambrian carbonates: evidence of Alleghanian brine migration: Science, v. 228, p. 1529-1531.

Hearn, P.P., Jr., Sutter, J.F., and Belkin, H.E., 1987, Evidence for late Paleozoic brine migration in Cambrian carbonate rocks of the central and southern Appalachians: implications for Mississippi Valley-type sulfide mineralization: Geochimica et Cosmochimica Acta, v. 51, p. 1323-1334.

Hitchon, B., and Friedman, I., 1969, Geochemistry and origin of formation waters in the western Canada sedimentary basin-I. Stable isotopes of hydrogen and oxygen: Geochimica et Cosmochimica Acta, v. 33, p. 1321-1349.

Holland, H.D., Holland, H.J., and Munoz, J.L., 1964(a), The coprecipitation of cations with $CaCO_3$- II. The coprecipitation of Sr^{+2} with calcite between 90° and 100° C: Geochimica et Cosmochimica Acta, v. 28, p. 1287-1301.

Holland, H.D., Kirsipu, T.W., Huebner, J.S., and Oxburgh, U.M., 1964(b), On some aspects of the chemical evolution of cave waters: Journal of Geology, v. 72, p. 36-67.

Hollister, L.S., Crawford, M.L., Roedder, E., Burruss, R.C., Spooner, E.T.C., and

Touret, J., 1981, Practical aspects of microthermometry: *in*, L.S. Hollister and M.L. Crawford, eds., Fluid inclusions: applications to petrology: Mineralogical Association of Canada Short Course Handbook, v. 6, p. 278-304.

Hower, J., Eslinger, E.V., Hower, M.E., and Perry, E.A., 1976, Mechanism of burial metamorphism of argillaceous sediment - I. Mineralogical and chemical evidence: Geological Society of America Bulletin, v. 87, p. 725-737.

Hubbert, M.K., and Rubey, W.W., 1959, Role of fluid pressure in mechanics of overthrust faulting I. Mechanics of fluid-filled porous solids and its application to overthrust faulting: Geological Society of America Bulletin, v. 70, p. 115-166.

Hudson, J.D., 1977, Stable isotopes and limestone lithification: Journal of the Geological Society of London, v. 133, p. 637-660.

Illing, L.V., 1959, Deposition and diagenesis of some upper Paleozoic carbonate sediments in western Canada: Proceedings 5th World Petroleum Congress, section 1, NY, p. 23-52.

Jackson, S.A., and Beales, F.W., 1967, An aspect of sedimentary basin evolution: the concentration of Mississippi Valley-type ores during last stages of diagenesis: Bulletin of Canadian Petroleum Geology, v. 15, p. 383-433.

Jacobson, R.L., and Usdowski, H.E., 1976, Partitioning of strontium between calcite, dolomite and liquids: an experimental study under higher temperature diagenetic conditions and the model for the prediction of mineral pairs for geothermometry: Contributions to Mineralogy and Petrology, v. 59, p. 171-185.

James, N.P., 1981, Megablocks of calcified algae in the Cow Head Breccia, western Newfoundland; vestiges of a Lower Paleozoic continental margin: Geological Society of America Bulletin, v. 92, p. 799-811.

James, N.P. and Ginsburg, R.N., 1979, The seaward margin of Belize barrier and atoll reefs: International Association of Sedimentologists Special Publication, No. 3, 191 p.

James, N.P., Ginsburg, R.N., Marszalez, D.M., and Choquette, P.W., 1976, Facies and fabric specificity of early subsea cements in shallow Belize (British Honduras) reefs: Journal of Sedimentary Petrology, v. 46, p. 523-544.

James, N.P., and Klappa, C.F., 1983, Petrogenesis of Early Cambrian reef limestones, Labrador, Canada: Journal of Sedimentary Petrology, v. 53, p. 1051-1096.

James, N.P., and Stevens, R.K., 1986, Stratigraphy and Correlation of the Cambro-Ordovician Cow Head Group, Western Newfoundland: Geological Society of Canada Bulletin 366, 143 p.

James, N.P., Stevens, R.K., Barnes, C.R., and Knight, I., in press, Evolution of a Lower Paleozoic continental margin carbonate platform, northern Canadian Appalachians: Society Economic Paleontologists and Mineralogists Special Publication No. 44.

Kaiser, C.J., and Ohmoto, H., 1985, A kinematic model for tectonic structures hosting North American Mississippi Valley-type mineralization: implications for timing and hydrology (abstr.): 1985 Geological Society of America Abstracts with Programs, p. 622.

Katz, A., 1973, The interaction of magnesium with calcite at 25 - 90° C and one atmosphere: Geochimica et Cosmochimica Acta, v. 37, p. 1563-1586.

Katz, A., and Matthews, A., 1977, The dolomitization of $CaCO_3$: an experimental study at 252° C - 295° C: Geochimica et Cosmochimica Acta, v. 41, p. 297-295.

Katz, A., Sass, E., Starinsky, A., and Holland, H.D., 1972, Strontium behavior in the aragonite-calcite transformation: an experimental study at 40-98° C: Geochimica et Cosmochimica Acta, v. 36, p. 481-496.

Kaufman, J., Cander, H.S., Daniels, L.D., and Meyers, W.J., 1988, Calcite cement stratigraphy and cementation history of the Burlington-Keokuk Formation (Mississippian), Illinois and Missouri: Journal of Sedimentary Petrology, v. 58, p. 312-326.

Kelts, K., and McKenzie, J., 1984, A comparison of anoxic dolomite from deep-sea sediments: Quaternary Gulf of California and Messinian Tripoli Formation of Sicily: *in*, Garrison, R.E., Kastner, M., and Zenger, D.H., eds., Dolomites of the Monterey Formation and Other Organic-rich Units: Society of Economic Paleontologists and Mineralogists Pacific Section Special Publication, v. 41, p. 119-140.

Kendall, A.C., 1977, Fasicular-optic calcite: a replacement of bundled acicular carbonate cements: Journal of Sedimentary Petrology, v. 47, p. 1056-1062.

Kharaka, Y.K., Berry, F.A.F., and Friedman, I., 1973, Isotopic composition of oil-field brines from Kettleman North Dome oil field, California, and their geologic implications: Geochimica et Cosmochimica Acta, v. 37, p. 1899-1908.

Kharaka, Y.K., Callendar, E., and Wallace, R.H., 1977, Geochemistry of geopressured-geothermal waters from the Frio Clay in the Gulf Coast region of Texas: Geology, v. 5, p. 241-244.

Kharaka, Y.K., Carothers, W.W., and Rosenbauer, R.J., 1983a, Thermal decarboxylation of acetic acid: implications for origin of natural gas: Geochimica et Cosmochimica Acta, v. 47, p. 397-402.

Kharaka, Y.K., Law, L.M., and Specht, D.J., 1983b, Hydrodynamics, geochemistry

and metal transport of Gulf Coast brines, (abstr.): Geological Society of America Abstracts with Programs, v. 15, p. 612.

Kharaka, Y.K., Law, L.M., Carothers, W.W., and Goerlitz, D.F., 1986, Role of organic species dissolved in formation waters from sedimentary basins in mineral diagenesis: *in*, Gautier D.L., (ed.), Society of Economic Paleontologists and Mineralogists Special Publication No. 38, p. 111-122.

Kharaka, Y.K., Lico, M.S., and Carothers, W.W., 1980a, Predicted corrosion and scale-formation properties of geopressured geothermal waters from the northern Gulf of Mexico basin: Journal of Petroleum Technology, February, 1980, p.319-324.

Kharaka, Y.K., Lico, M.S., Wright, V.A., and Carothers, W.W., 1980b, Geochemistry of formation waters from Pleasant Bayou No. 2 Well and adjacent areas in coastal Texas: *in*, Proceedings of the 4th geopressured-geothermal energy conference, University of Texas, Austin, p. 168-193.

Kitano, Y., Kanamori, N., and Oomari, T., 1971, Measurement of distribution coefficients of strontium and barium between carbonate precipitate and solution-abnormally high values of distribution coefficients at early stages of carbonate formation: Geochemical Journal, v. 4, p. 183-206.

Knauth, L.P., and Epstein, S., 1976, Hydrogen and oxygen isotope ratios in nodular and bedded cherts: Geochimica et Cosmochimica Acta, v. 40, p. 1095-1108.

Kobluk, D.R., 1985, Biota preserved within cavities in Cambrian *Epiphyton* mounds, Upper Shady Dolomite, southwestern Virginia: Journal of Paleontology, v. 59, p. 1158-1172.

Kretz, R., 1982, A model for the distribution of trace elements between calcite and dolomite: Geochimica et Cosmochimica Acta, v. 46, p. 1979-1981.

Kulander, B.R., and Dean, S.L., 1986, Structure and tectonics of central and southern Appalachian Valley and Ridge and Plateau provinces, West Virginia and Virginia: American Association of Petroleum Geologists Bulletin, v. 70, p. 1674-1684.

Kupecz, J.A., and Land, L.S., 1988, Pre-Middle Ordovician dolomitization of the Lower Ordovician Ellenburger Group, and its post-Middle Ordovician modification (abstr.): Geological Society of America Abstracts with Programs, v. 20, p. A391.

Land, L.S., 1980, The isotopic and trace element geochemistry of dolomite: the state of the art: *in*, Zenger, D.H., Dunham, J.B., and Ethington, R.L. (eds.), Concepts and Models of Dolomitization, Society of Economic Paleontologists and Mineralogists Special Publication No. 28, p. 87-110.

Land, L.S., 1985, The origin of massive dolomite: Journal of Geological Education, v. 33, p. 112-125.

Land, L.S., Macpherson, G.L., and Mack, L.E., 1988, The geochemistry of formation waters, Miocene, offshore Louisiana: Gulf Coast Association of Geological Societies Transactions, v. 38, p. 503-511.

Land, L.S., Milliken, K.L., and McBride, E.F., 1987, Diagenetic evolution of Cenozoic sandstone, Gulf of Mexico sedimentary basin: Sedimentary Geology, v. 50, p. 195-225.

Land, L.S., Salem, M.R.I., and Morrow, D.W., 1975, Paleohydrology of ancient dolomites: geochemical evidence: American Association of Petroleum Geologists Bulletin, v. 59, p. 1602-1625.

Lentini, M.R., and Shanks, W.C., III, 1983, Experimental study of brine-arkose interaction at 200° C and 500 bars: origin of metalliferous oil field brines and Mississippi Valley type ore deposits: *in*, Kisvarsanyi, G., Grant, S.K., Pratt, W.P., and Koenig, J.W., (eds.), International Conference on Mississippi Valley Type Lead-Zinc Deposits, Proceedings Volume: Rolla, Missouri, University of Missouri-Rolla, p. 140-144.

Lohmann, K.C., and Meyers, W.J., 1977, Microdolomite inclusions in cloudy prismatic calcites: a proposed criterion for former high-magnesium calcites: Journal of Sedimentary Petrology, v. 47, p. 1078-1088.

Long, D.T., and Angino, E.E., 1982, The mobilization of selected trace metals from shales by aqueous solutions: effects of temperature and ionic strength: Economic Geology, v. 77, p. 646-652.

Lorens, R.B., 1981, Sr, Cd, Mn and Co distribution in calcite as a function of calcite precipitation rate: Geochimica et Cosmochimica Acta, v. 45, p. 553-561.

Lundegard, P.D. and Land, L.S., 1989, Carbonate equilibria and pH buffering by organic acids- response to changes in P_{CO2}: Chemical Geology, v. 74, p. 277-287.

Lundegard, P.D., Land, L.S., and Galloway, W.E., 1984, Problem of secondary porosity: Frio Formation (Oligocene), Texas Gulf coast: Geology, v. 12, p. 399-402.

Macqueen, R.W., 1976, Sediments, zinc and lead, Rocky Mountain belt, Canadian Cordillera: Geoscience Canada, v. 3, p. 71-81.

Matsuhisa, Y., Goldsmith, J.R., and Clayton, R.N., 1979, Oxygen isotopic fractionation in the system quartz-albite-anorthite-water: Geochimica et Cosmochimica Acta, v. 43, p. 1131-1140.

Mattes, B.W., and Mountjoy, E.W., 1980, Burial dolomitization of the Upper Devonian Miette buildup, Jasper National Park, Alberta: *in*, Zenger, D.H., Dunham, J.B., and Ethington, R.L. (eds.), Concepts and Models of Dolomitization, Society of Economic Paleontologists and Mineralogists Special Publication No. 28, p. 259-297.

McHargue, T.R., and Price, R.C., 1982, Dolomite from clay in argillaceous or shale-associated marine carbonates: Journal of Sedimentary Petrology, v. 52, p. 873-886.

McIlreath, I.A., 1977, Accumulation of a Middle Cambrian, deep-water limestone debris apron adjacent to a vertical, submarine carbonate escarpment, Southern Rocky Mountains, Canada, *in*, Deep-Water Carbonate Environments (H.E. Cook and P. Enos, eds.): Society of Economic Paleontologists and Mineralogists Special Publication No. 25, p. 113-124.

McIlreath, I.A., and James, N.P., 1984, Carbonate Slopes, *in*, Walker, R.G., ed., Facies Models: Geoscience Canada, Reprint Series 1, p. 245-257.

McKenzie, J.A, 1981, Holocene dolomitization of calcium carbonate sediments from the coastal sabkhas of Abu Dhabi, UAE: a stable isotope study: Journal of Geology, v. 89, p. 185-198.

Meshri, I.D., 1986, On the reactivity of carbonic and organic acids and generation of secondary porosity: *in*, Gautier, D.L., (ed.), Roles of Organic Matter in Sediment Diagenesis: Society of Economic Paleontologists and Mineralogists Special Publication No. 38, p. 123-128.

Meyers, W.J.,1978, Carbonate cements: their regional distribution and interpretation in Mississippian limestones of southwestern New Mexico: Sedimentology, v. 25, p. 371-400.

Mitchell, J.T., Land, L.S., and Miser, D.E., 1987, Modern marine dolomite cement in a north Jamaican fringing reef: Geology, v. 15, p. 557-560.

Montanez, I.P., and Read, J.F., 1986, Tidal-flat and shallow subsurface evaporative dolomitization (abstr.): American Association of Petroleum Geologists Bulletin, v. 70, p. 622.

Montanez, I.P., Read, J.F., and Sinha, A.K., 1988, Origin of dolomites in cyclic peritidal, Upper Knox carbonates Appalachians: evidence from trace elements, stable and radiogenic isotopes (abstr.): Society of Economic Paleontologists and Mineralogists Midyear Meeting Abstracts, v. 5, p. 38.

Morrow, D., 1982, Diagenesis 2, dolomite- part 2, dolomitization models and ancient dolomites: Geoscience Canada, v. 9, p. 95-107.

Morton, J.P., 1985, Rb-Sr evidence for punctuated illite/smectite diagenesis in the Oligocene Frio Formation, Texas: Geological Society of America Bulletin, v. 96, p. 114-122.

Morton, R.A, and Land, L.S., 1987, Regional variations in formation water chemistry, Frio Formation (Oligocene), Texas Gulf Coast: American Association of Petroleum

Geologists Bulletin, v. 71, p. 191-206.

Muehlenbachs, K., 1986, Alteration of the oceanic crust and the ^{18}O history of seawater: *in*, J.W. Valley, H.P. Taylor, Jr., and J.R. O'Neil, (eds.), Stable Isotopes in High Temperature Geological Processes, Mineralogical Society of America, Reviews in Mineralogy, v. 16, p. 425-443.

Muehlenbachs, K., and Clayton, R.N., 1976, Oxygen isotope composition of the oceanic crust and its bearing on seawater: Journal of Geophysical Research, v. 81, p. 4365-4369.

Mullins, H.T., Neumann, A.C., Wilbur, R.J., and Boardman, M.R., 1980, Nodular carbonate sediment on Bahamian slopes: Possible precursors to nodular limestones: Journal of Sedimentary Petrology, v. 50, p. 117-131.

Murata, K.J., Friedman, I., and Madsen, B.M., 1969, Isotopic composition of diagenetic carbonates in Miocene marine formations of California and Oregon, United States Geological Survey Professional Paper 614-B, 24 p.

Mussman, W.J., Montanez, I.P., and Read, J.F., 1988, Ordovician Knox paleokarst unconformity, Appalachians: *in*, N.P. James and P.W. Choquette, (eds.), Paleokarst, New York, Springer-Verlag, p. 211-228.

Naumov, G.B., Ryzhenko, B.N, and Khodakovsky, I.L., 1974, Handbook of Thermodynamic Data, United States Geological Survey, National Technical Information Service.

Nelson, A., and Read, J.F., (submitted), Updip to downdip cementation and dolomitization patterns in a Mississippian aquifer, Appalachians: Journal of Sedimentary Petrology.

Niemann, J.C., and Read, J.F., 1988, Regional cementation associated with unconformity-sourced aquifers and burial fluids, Kentucky: Journal of Sedimentary Petrology, v. 58, p. 688-705.

Ohmoto, H., and Rye, R.O., 1979, Isotopes of sulfur and carbon: *in*, Barnes, H.L., ed., Geochemistry of Hydrothermal Ore Deposits, 2nd Ed., New York, John Wiley and Sons, p. 509-567.

Palmer, A.R., 1981, Subdivision of the Sauk sequence, *in*: Second International Symposium on the Cambrian System, p. 160-162.

Palmer, A.R., and James, N.P., 1979, The Hawke Bay event: A circum-Iapetus regression near the Lower to Middle Cambrian boundary: *in*, Wones, D.R., ed., Proceedings, Caledonides in the U.S.A.: Virginia Polytechnic Institute and State University, Department of Geological Sciences, Memoir no. 2, p. 15-18.

Patterson, J.G., 1987, Tectonic Evolution of Distal Portions of the Late Proterozoic-Early Paleozoic Continental Margin to Ancestral North America [Ph.D. Dissertation]: Virginia Polytechnic Institute and State University, Blacksburg, VA, 191 p.

Patterson, R.J., and Kinsman, D.J.J., 1982, Formation of diagenetic dolomite in coastal sabkha along the Arabian (Persian) Gulf: American Association of Petroleum Geologists Bulletin, v. 66, p. 28-43.

Perry, E.C., 1967, The oxygen isotope chemistry of ancient cherts: Earth and Planetary Science Letters, v. 3, p. 62-66.

Perry, E.C., Ahmad, S.N., and Swilius, T.M., 1978, The oxygen isotope composition of 3,800 m.y. old metamorphosed chert and iron formation from Isukasai, west Greenland: Journal of Geology, v. 86, p. 223-239.

Perry, E.C., and Tan, F.C., 1972, Significance of oxygen and carbon isotope variations in early Precambrian cherts and carbonate rocks of southern Africa: Geological Society of America Bulletin, v. 83, p. 647-664.

Perry, E.A., and Turekian, K.K., 1974, The effect of diagenesis on the redistribution of strontium isotopes in shales: Geochimica et Cosmochimica Acta, v. 38, p. 929-935.

Pfeil, R.W., 1977, Stratigraphy and Sedimentology, Cambrian Shady Dolomite, Virginia [M.S. thesis]: Virginia Polytechnic Institute and State University, Blacksburg, Virginia, 137 p.

Pfeil, R.W., and Read, J.F., 1980, Cambrian carbonate platform margin facies, Shady Dolomite, southwestern Virginia, U.S.A.: Journal of Sedimentary Petrology, v. 50, p. 91-116.

Phillips, W.J., 1972, Hydraulic fracturing and mineralization: Journal of the Geological Society of London, v. 128, p. 337-360.

Pierson, B.J., 1981, The control of cathodoluminescence in dolomite by iron and manganese: Sedimentology, v. 28, p. 601-610.

Pingitore, N.E., Jr., and Eastman, M.P., 1986, The coprecipitation of Sr^{2+} with calcite at 25° C and 1 atm: Geochimica et Cosmochimica Acta, v. 50, p. 2195-2203.

Prezbindowski, D.R., and Larese, R.E., 1987, Experimental stretching of fluid inclusions in calcite-implications for diagenetic studies: Geology, v. 15, p. 333-336.

Pusey, W.C., 1973, How to evaluate potential oil and gas source rocks: World Oil, v. 176, p. 71-74.

Radke, B.M., and Mathis, R.L., 1980, On the formation and occurrence of saddle dolomite: Jour. Sed. Pet., v. 50, p. 1149-1168.

Read, J.F., (in press a), Evolution of Cambro-Ordovician passive margin, U.S. Appalachians: Decade of North American Geology Synthesis, Appalachian-Ouachita volume, Geological Society of America, Boulder, Colorado.

Read, J.F., (in press b), Controls on evolution of Cambrian-Ordovician passive margin, U.S. Appalachians: Society Economic Paleontologists and Mineralogists Special Publication No. 44.

Read, J.F., and Pfeil, R.W., 1983, Fabrics of allochthonous reefal blocks, Shady Dolomite (Lower to Middle Cambrian), Virginia Appalachians: Journal of Sedimentary Petrology, v. 53, 761-778.

Reinhardt, J., 1974, Stratigraphy, sedimentology and Cambro-Ordovician paleogeography of the Frederick Valley, Maryland: Maryland Geological Survey, Report of Investigations, v. 23, 74 p.

Reinhardt, J., 1977, Cambrian off-shelf sedimentation, central Appalachians, *in*, Deep-Water Carbonate Environments (H.E. Cook and P. Enos, eds.): Society of Economic Paleontologists and Mineralogists Special Publication No. 25, p. 83-112.

Rice, D.D., 1983, Relation of natural gas composition to thermal maturity and source rock type in San Juan Basin, northwestern New Mexico and southwestern Colorado: American Association of Petroleum Geologists Bulletin, v. 67, p. 1199-1218.

Robie, R.A., Hemingway, B.S., and Fisher, J.R., 1978, Thermodynamic properties of minerals and related substances at 298.15 K and 1 bar (10^5 Pascals) pressure and at higher temperatures: United States Geological Survey Bulletin no. 1452, 456 p.

Rodgers, J., 1968, The eastern edge of the North American continent during the Cambrian and Early Ordovician, *in*, Zen, E-an, et. al., eds., Studies of Appalachian geology: Northern and Maritime: New York, John Wiley and Sons, p. 141-149.

Roedder, E., 1984, Fluid Inclusions: Mineralogical Society of America Reviews in Mineralogy, v. 12, 644 p.

Roehl, P.O., 1981, Dilation brecciation: proposed mechanism of fracturing, petroleum expulsion, and dolomitization in Monterey Formation, California (abstr.): American Association of Petroleum Geologists Bulletin, v. 65, p. 980-981.

Saller, A.H., 1984, Petrologic and geochemical constraints on the origin of subsurface dolomite: an example of dolomitization by normal seawater: Geology, v. 12, p. 217-220.

Saller, A.H., 1986, Radiaxial calcite in Lower Miocene strata, subsurface Enewetak Atoll: Journal of Sedimentary Petrology, v. 56, p. 743-762.

Samman, N.F., 1975, Sedimentation and Stratigraphy of the Rome Formation in East

Tennessee [Ph.D. dissert.]: University of Tennessee, 337 p.

Schmidt, V., and McDonald, D.A., 1979, The role of secondary porosity in the course of sandstone diagenesis: *in*, Scholle, P.A., and Schluger, P.R., (eds.), Aspects of Diagenesis, Society of Economic Paleontologists and Mineralogists Special Publication No. 26, p. 175-208.

Schoell, M., 1980, The hydrogen and carbon isotopic composition of methane from natural gases of various origins: Geochimica et Cosmochimica Acta, v. 44, p. 649-661.

Schoell, M., 1984, Wasserstoff- und Kohlenstoffisotope in organischen substanzen, Erdölen und Erdgasen: Geologisches Jahrbuch Reihe D, H 67.

Schroeder, J., 1972, Fabrics and sequences of submarine carbonate cements in Holocene Bermuda Cup reefs: Geologisches Rundschau, v. 61, p. 708-730.

Shearman, D.J., Mossop, G., Dunsmore, H., and Martin, M., 1972, Origin of gypsum veins by hydraulic fracture: Trans. Inst. Min. Metall., v. 81, p. B149-B155.

Shinn, E.A., 1969, Submarine lithification of Holocene carbonate sediments in the Persian Gulf: Sedimentology, v. 12, p. 109-144.

Shock, E.A., 1988, Organic acid metastability in sedimentary basins: Geology, v. 16, p. 886-890.

Sibley, D.F., 1982, The origin of common dolomite fabrics: clues from the Pliocene: Journal of Sedimentary Petrology, v. 52, p. 1087-1100.

Sibley, D.F., and Gregg, J.M., 1987, Classification of dolomite rock textures: Journal of Sedimentary Petrology, v. 57, p. 967-975.

Simpson, E.L., 1987, Sedimentology and Tectonic Implications of the Late Proterozoic to Early Cambrian Chilhowee Group in Southern and Central Virginia [Ph.D. dissert.]: Virginia Polytechnic Institute and State University, Blacksburg, Virginia, 298 p.

Simpson, E.L., and Eriksson, K.A., 1989, Sedimentology of the Unicoi Formation in southern and central Virginia: evidence for late Proterozoic to Early Cambrian rift-to-passive margin transition: Geological Society of America Bulletin, v. 101, p. 42-54.

Simpson, E.L., and Sundberg, F.A., 1987, Early Cambrian age for synrift deposits of the Chilhowee Group of southwestern Virginia: Geology, v. 15, p.123-126.

Spirakis, C.S., and Heyl, A.V., 1988, Possible effects of thermal degradation of organic matter on carbonate paragenesis and fluorite precipitation in Mississippi Valley-type

deposits: Geology, v. 16, p. 1117-1120.

Starinsky, A., Bielski, M., and Lazar, B., 1983, Strontium isotope evidence on the history of oilfield brines, Mediterranean Coastal Plain, Israel: Geochimica et Cosmochimica Acta, v. 47, p. 687-695.

Steele, J.D., and Pushkar, P., 1973, Strontium isotope geochemistry of the Scioto River Basin and $^{87}Sr/^{86}Sr$ ratios of the underlying lithologies: Ohio Journal of Science, v. 73, p. 331-338.

Stoakes, F.A., 1980, Nature and control of shale basin fill and its effect on reef growth and termination: Upper Devonian Duvernay and Ireton Formations of Alberta, Canada: Bulletin of Canadian Petroleum Geology, v. 28, p. 345-410.

Stoessell, R.K., Klimentidis, R.E., and Prezbindowski, D.R., 1987, Dedolomitization in Na-Ca-Cl brines from 100° C to 200° C at 300 bars: Geochimica et Cosmochimica Acta, v. 51, p. 847-855.

Stueber, A.M., Pushkar, P., and Hetherington, E.A., 1984, A strontium isotopic study of Smackover brines and associated solids, southern Arkansas: Geochimica et Cosmochimica Acta, v. 48, p. 1637-1649.

Stueber, A.M., Pushkar, P., and Hetherington, E.A., 1987, A Strontium isotopic study of formation waters from the Illinois basin, U.S.A.: Applied Geochemistry, v. 2, p. 477-494.

Supko, P.R., 1977, Subsurface dolomites, San Salvador, Bahamas: Journal of Sedimentary Petrology, v. 47, p. 1063-1077.

Suppe, J., and Wittke, J.H., 1977, Abnormal pore-fluid pressures in relation to stratigraphy and structure in the active fold-and-thrust belt of northwestern Taiwan: Petroleum Geology of Taiwan, v. 14, p. 11-24.

Surdam, R.C., Boese, S.W., and Crossey, L.J., 1984, The chemistry of secondary porosity: *in*, McDonald, D.A., and Surdam, R.C., (eds.), Clastic Diagenesis: American Association of Petroleum Geologists Memoir 37, p. 127-149.

Surdam, R.C., Crossey, L.J., Hagen, E.S., and Heasler, H.P., 1989, Organic-inorganic interactions and sandstone diagenesis: American Association of Petroleum Geologists Bulletin, v. 73, p. 1-23.

Sverjensky, D.A., 1981, Isotopic alteration of carbonate host rocks as a function of water to rock ratio- an example from the upper Mississippi valley zinc-lead district: Economic Geology, v. 76, p. 154-157.

Tugarinov, A.I., and Naumov, V.B., 1970, Dependence of the decrepitation temperature of minerals on the composition of their gas-liquid inclusions and hardness: Doklady

Akademii Nauk SSSR, v. 195, p. 112-114.

Van der Voo, R., 1979, Age of Alleghenian folding in the central Appalachians: Geology, v. 7, p. 297-298.

Veizer, J., 1983, Chemical diagenesis of carbonates: theory and application of trace element technique: *in*, Stable Isotopes in Sedimentary Geology, Society of Economic Paleontologists and Mineralogists Short Course No. 10, Dallas, 1983, p. 3:1-3:100.

Veizer, J., and Compston, W., 1974, $^{87}Sr/^{86}Sr$ composition of seawater during the Phanerozoic: Geochimica et Cosmochimica Acta, v. 38, p. 1461-1484.

Veizer, J., Holser, W.T., and Wilgus, C.K., 1980, Correlation of $^{13}C/^{12}C$ and $^{34}S/^{32}S$ secular variations: Geochimica et Cosmochimica Acta, v. 44, p. 579-587.

Wallace, M.W., 1987, The role of internal erosion and sedimentation in the formation of stromatactis mudstones and associated lithologies: Journal of Sedimentary Petrology, v. 57, p. 695-700.

Wanless, H.R., 1979, Limestone response to stress: pressure solution and dolomitization: Journal of Sedimentary Petrology, v. 49, p. 437-462.

Ward, W.C., and Halley, R.B., 1985, Dolomitization in a mixing zone of near-seawater composition, Late Pleistocene, northeastern Yucatán Peninsula: Journal of Sedimentary Petrology, v. 55, p. 407-420.

Wehr, F., and Glover, L., 1985, Stratigraphy and tectonics of the Virginia-North Carolina Blue Ridge: Evolution of a late Proterozoic-early Paleozoic hinge zone: Geological Society of America Bulletin, v. 96, p. 285-295.

Weinberg, E.L., 1971, Sulfide mineralization, southwestern Virginia, *in* Guidebook to Appalachian Tectonics and Sulfide Mineralization of Southwestern Virginia: Guidebook no. 5, Virginia Polytechnic Institute and State University, Blacksburg, Virginia, p. 6-23.

White, D.E., Hem, J.D., and Waring, G.A., 1963, Chemical composition of sub-surface waters: in, Data of Geochemistry (6th ed.): United States Geological Survey Professional Paper 440-F, p. F1-F67.

Whiticar, M.J., Faber, E., and Schoell, M., 1986, Biogenic methane formation in marine and freshwater environments: CO_2 reduction vs. acetate fermentation- isotopic evidence: Geochimica et Cosmochimica Acta, v. 50, p. 693-709.

Willoughby, R.H., 1977, Paleontology and Stratigraphy of the Shady Formation near Austinville, Virginia [M.S. thesis]: Virginia Polytechnic Institute and State University, Blacksburg, Virginia, 189 p.

Willoughby, R.H., 1987, The Lower-Middle Cambrian unconformity in the Pine Ridge road cut on interstate 75 in Anderson County, Tennessee (abstract): Geological Society of America Abstracts with Programs, v. 19, p. 137.

Wong, P.K., and Oldershaw, A., 1981, Burial cementation in the Devonian Kaybob reef complex, Alberta, Canada: Journal of Sedimentary Petrology, v. 51, p. 507-520.

Woodward, H., 1957, Chronology of Appalachian folding: American Association of Petroleum Geologists Bulletin, v. 41, p. 2312-2327.

Zenger, D.H., 1983, Burial dolomitization in the Lost Burro Formation (Devonian), east-central California, and the significance of late diagenetic dolomitization: Geology, v. 11, p. 519-522.

APPENDIX I: ICP TECHNIQUES

APPENDIX I

For ICP analyses, ultrasonically cleaned, unstained rock chips were microsampled using a binocular microscope and a bench mounted milling machine equipped with dental drills. The sample chips were examined under cathodoluminescence both before and after drilling, in order to ascertain that individual dolomite and calcite generations, based on cathodoluminescent petrography, were isolated for analysis. Following drilling, the samples were reground to the depth of maximum drill penetration, repolished, and examined under cathodoluminescence to ensure that the sample consisted solely of the desired generation of diagenetic carbonate.

The analytical technique for ICP analysis was designed to utilize small samples. Sufficient sample size, however, was required so that after dissolution and dilution to the required minimum 11 ml volume for ICP analysis of the 5 elements (Ca, Mg, Fe, Mn, Sr), their concentrations were well above instrument detection limits. Using 0.0140 to 0.0160 g of carbonate best fit the above requirements, as this quantity could easily be obtained by microsampling, and upon dilution to the 11 ml, yielded minimum trace element concentrations that were over an order of magnitude above detection limits.

All glassware, centrifuge tubes, and sample bottles were cleaned by soaking in heated 20% HNO_3 for at least 2 hours, and then repeatedly rinsed with distilled deionized water. Quartz distilled water was used for sample dissolution, and for preparing standards and blanks. The HCl used for sample dissolution and preparation of standards and blanks was 'Baker Instra-Analyzed'® specifically intended for trace metal analysis.

The weighed carbonate sample was placed into 15 ml, polyethylene centrifuge tubes and 10 ml of 0.2 N HCl was added and the tubes were tightly capped. This weak acid

was used to minimize contamination by leaching of clays or other admixed detrital or authigenic minerals, although noncarbonate phases were largely avoided by selective sampling. Dissolution time was for 4 hours, under constant agitation. The samples were then further acidified by adding 1 ml of 3.5 N HCl, to bring the acidity to 0.5 N. This ensured that the elements would remain in solution until ICP analysis. The acidified sample was then immediately centrifuged for 4 minutes and decanted into 15 ml polyethylene sample bottles with screw closures. These aliquots were submitted for ICP analysis. Insoluble residues remaining in the centrifuge tube were dislodged by adding quartz distilled water, agitated, and then filtered using 2.5 cm diameter Whatman GF/F glass microfibre filters on a vacuum filter apparatus. The filters were then oven dried and reweighed, the weight of the accumulated insoluble residue was nearly always less than 2-3 % of the sample weight and was thus ignored, only in the few samples where it was greater than 4% of the sample weight was the weight of the insoluble residues deducted from the sample weight.

ICP analysis was conducted at the Soil Testing and Plant Analysis Laboratory at Virginia Tech under the direction of J. Friedricks and N. Phillips. Ca, Mg, Fe, and Mn were determined using a Jarrell-Ash ICAP 9000 Simultaneous Spectrometer; Sr was analysed using a Jarrell-Ash Atomscan 2400 Sequential Spectrometer. The ICP calibration required a standard solution somewhat more concentrated than the highest anticipated values for the samples, and a blank. A multielement solution standard for ICP spectroscopy was custom-made by SPEX Industries, Inc. (3880 Park Ave., Edison, NJ 08820), it was designed to match as closely as possible the TDS, elemental ratios, and acid matrix (HCl) of the dissolved carbonate samples. The Multielement solution standard prepared by SPEX contained: 10750 ppm Ca; 6500 ppm Mg; 1000 ppm Fe; 500

ppm Mn; and 25 ppm Sr; acidified to 1.0 N HCl. For ICP calibration and analysis, 4.0 ml of this standard solution and 4.6 ml of HCl were diluted to 100 ml with quartz distilled water, resulting in a solution containing: 430 ppm Ca; 260 ppm Mg; 40 ppm Fe; 20 ppm Mn; and 1 ppm Sr. The samples, calibration standards, and blanks all contained 0.5 N HCl.

The matrix of this solution, in terms of acid normality and total dissolved solid content, was closely matched to that of the dissolved carbonate samples. This eliminated possible interferences from the acidity (Walsh and Howie, 1986) or from extreme variations in the total dissolved solid (TDS) content (cf., Fig. 4, Church, 1981). ICP analyses of successive dilutions of the calibration standard indicated that the analytical accuracy for all the trace elements was generally within 3%, for TDS contents above 50% of that of the calibration standard, and that in more dilute samples with correspondingly lower TDS, the elemental concentrations were increasingly over-reported. By restricting the weight of the dissolved carbonate to 0.0140 to 0.0160 g, the total dissolved solid contents of the aliquots ranged between 60 to 80% of that of the calibration standard, and thus eliminated this source of possible error.

The raw ICP analytical data was converted to the elemental concentration in the carbonates, by calculating the dilution factor for each sample, based on its weight (less the insoluble residue, if applicable). Wherever possible, multiple analyses of each sample were conducted, in order to assess the reproducibility. Possible sources of error included sample weighing, amount of acid used in dissolution, and ICP instrument error. The accuracy of the analyses was determined by submitting blind standard solutions, the ICP analyses were generally within 3% of the known concentration, and never more than 6% in error. Blind blanks were routinely inserted within sample sets, and their results were

consistently below detection limits.

Analytical precision was determined by submitting replicate samples (minimum of 5) of B.C.S. No. 368 dolomite standard with each sample set. Thirty nine replicate analyses of this standard yielded the following results (± 1σ variation): Ca = 216,000±7,800 ppm (±3.6%); Mg = 126,150±4,400 ppm (±3.5%); Fe = 1060±100 ppm (±9.5%); Mn = 491±19 ppm (±3.9%), and Sr = 77±2 ppm (±2.6%). Comparison of the analytical results from this study with the certificate of analysis (Table 1) shows that Ca, Mg, Mn, and Sr values exhibit fairly good agreement, and lie within the standard deviation of the data. To a large extent, the analytical differences and the higher standard deviation for most of the elements in this study (except Sr) reflects the different analytical technique used, and the very small sample size (0.0140 to 0.0160 g) which is more susceptible to errors in measurement than larger size samples.

The Fe contents for B.C.S. No. 368 dolomite yielded by this method are considerably lower than the reported value, and reflect the use of dilute (0.2 N) HCl to selectively leach the carbonate, while attempting to leave the noncarbonate phases as unaffected as possible, whereas the values reported in the certificate of analysis reflect the Fe content of the bulk sample. The selective leaching of B.C.S. No. 368 dolomite in dilute acid yielded ≈3% insoluble residue. It is probable that this residue contains detrital and authigenic Fe-bearing minerals (including pyrite and Fe-oxyhydroxides), which were incompletely dissolved by the procedure, accounting for the lower Fe contents. Variable leaching of admixed Fe-bearing minerals also likely accounts for the higher standard deviation for Fe relative to the other elements.

Regarding the limits of detection for the trace element analyses, replicate analyses (n=5) of the carbonate samples containing some of the lowest measured trace element

concentrations still yielded good reproducibility, for example; Mn = 59±2 ppm; Fe = 84±17 ppm; Sr = 40±1 ppm; Mg = 1241±36 ppm, indicating that the detection limits are considerably lower.

APPENDIX II: ICP TRACE ELEMENT DATA

APPENDIX II: ICP TRACE ELEMENT DATA (PPM)

SAMP ID	SAMPLE DESCRIPTION (N)[1]		MN	FE	SR	MG
A458-7-(4)-1	MARINE CALCITE CEMENT (4)		60	78	161	2615
A452-6-1	MARINE CALCITE CEMENT (3)		45	62	195	2324
A458-7-(3)-1	MARINE CALCITE CEMENT (5)		59	76	139	2390
A458-7-1	MARINE CALCITE CEMENT (5)		66	68	151	2695
A583-51-1	MARINE CALCITE CEMENT (4)		153	299	175	2088
A458-7-I	HOST LIMESTONE (3)		64	112	172	2124
A458-7-II	HOST LIMESTONE (3)		107	96	171	2134
A456-6-I	HOST LIMESTONE (3)		122	114	144	1897
A583-51-I	HOST LIMESTONE (3)		193	415	203	2492
A583-52-II	HOST LIMESTONE (3)		68	578	183	2918
A623-6	ZONE 2A REPL. DOLOMITE (1)	MAR CEM	310	1674	61	
A623-6-1	ZONE 2A REPL. DOLOMITE (1)	MAR CEM	304	1798	63	
A623-6-2	ZONE 2A REPL. DOLOMITE (2)	MAR CEM	324	1546	65	
I265-8B-1	ZONE 2A REPL. DOLOMITE (2)	MAR CEM	661	2590	39	
I265-8B-2	ZONE 2A REPL. DOLOMITE (1)	MAR CEM	606	2428	40	
I265-19-1	ZONE 2A REPL. DOLOMITE (1)	MAR CEM	156	571	37	
A229-4-1	ZONE 2A REPL. DOLOMITE (5)	XF, FENEST	107	410	28	
A229-22-1	ZONE 2A REPL. DOLOMITE (4)	XM, THROMB	173	632	37	
A679-10-1	ZONE 2A REPL. DOLOMITE (3)	XF, THROMB	161	565	32	
A679-10-2	ZONE 2A REPL. DOLOMITE (1)	XF, THROMB	164	558	38	
A679-11-1	ZONE 2A REPL. DOLOMITE (2)	XF, THROMB	229	824	34	
A679-11-2	ZONE 2A REPL. DOLOMITE (2)	XF, THROMB	227	861	35	
A679-11-3	ZONE 2A REPL. DOLOMITE (2)	XF, THROMB	242	883	38	
A679-11-4	ZONE 2A REPL. DOLOMITE (2)	XF, THROMB	215	846	34	
A679-21-1	ZONE 2A REPL. DOLOMITE (2)	XF, THROMB	178	722	43	
A679-9-1	ZONE 2A REPL. DOLOMITE (2)	XF, THROMB	130	396	39	
A679-9-2	ZONE 2A REPL. DOLOMITE (2)	XF, THROMB	125	410	42	
I265-2-1	ZONE 2A REPL. DOLOMITE (2)	XF, GS	159	932	48	
I265-2-2	ZONE 2A REPL. DOLOMITE (2)	XF, GS	195	1098	43	
I265-2-3	ZONE 2A REPL. DOLOMITE (2)	XF, GS	146	904	53	
I265-2-4	ZONE 2A REPL. DOLOMITE (2)	XF, GS	157	789	55	
I265-3-1	ZONE 2A REPL. DOLOMITE (1)	XF, FENEST	227	1189	34	
I265-3-2	ZONE 2A REPL. DOLOMITE (2)	XF, FENEST	268	1194	34	
I265-3-3	ZONE 2A REPL. DOLOMITE (2)	XF, FENEST	278	1236	36	
A679-6-3	ZONE 2A REPL. DOLOMITE (2)	XF, GS	193	768	36	
A679-6-4	ZONE 2A REPL. DOLOMITE (1)	XF, GS	157	636	40	
A679-6-5	ZONE 2A REPL. DOLOMITE (2)	XF, GS	154	637	40	
A206-10-1	ZONE 2A REPL. DOLOMITE (2)	XF, REEF	337	1289	38	
A206-10-2	ZONE 2A REPL. DOLOMITE (2)	XF, REEF	335	1284	38	
A206-1-1	ZONE 2A/ZONE 1 REPL DOL (1)	XF, REEF	416	1611	39	
A206-4-1	ZONE 2A REPL. DOLOMITE (1)	XM, REEF	378	1561	37	
A206-4-2	ZONE 2A REPL. DOLOMITE (1)	XM, REEF	383	1097	36	

A206-6-1	ZONE 2A/ZONE 1 REPL DOL (1)	XM, REEF	287	1110	37
A206-6-2	ZONE 2A/ZONE 1 REPL DOL (1)	XM, REEF	330	1129	40
A257-1A-1	ZONE 2A/ZONE 1 REPL DOL (1)	XF, REEF	284	1010	51
A257-1B-1	ZONE 2A REPL. DOLOMITE (1)	XF, REEF	296	998	36
A257-1B-2	ZONE 2A REPL. DOLOMITE (1)	XF, REEF	291	919	36
A257-1B-3	ZONE 2A/ZONE 1 REPL DOL (1)	XF, REEF	271	960	36
A257-1B-4	ZONE 2A/ZONE 1 REPL DOL (1)	XF, REEF	269	962	33
A257-1B-5	ZONE 2A/ZONE 1 REPL DOL (1)	XF, REEF	265	974	36
A257-2A-1	ZONE 2A/ZONE 1 REPL DOL (1)	XF, REEF	287	1073	45
A257-2A-2	ZONE 2A/ZONE 1 REPL DOL (1)	XF, REEF	347	1061	44
A257-2A-3	ZONE 2A/ZONE 1 REPL DOL (1)	XF, REEF	281	1026	45
A257-2C-1	ZONE 2A/ZONE 1 REPL DOL (1)	XF, REEF	266	1004	44
A257-2C-2	ZONE 2A/ZONE 1 REPL DOL (1)	XF, REEF	253	932	42
A257-3-1	ZONE 2A REPL. DOLOMITE (2)	XF, REEF	226	764	36
A257-3-2	ZONE 2A REPL. DOLOMITE (1)	XF, REEF	234	820	33
I295-4	ZONE 2A REPL. DOLOMITE (2)	XC, GS	904	4517	29
I295-4-3	ZONE 2A REPL. DOLOMITE (2)	XC, GS	967	4984	31
A229-36-1	ZONE 2A REPL. DOLOMITE (3)	XC, GS	545	2498	32
A652-8-1	ZONE 2A REPL. DOLOMITE (2)	XC, ?	719	3490	34
A652-8-2	ZONE 2A/ZONE 1 REPL DOL (2)	XC, ?	542	2610	39
A652-8-3	ZONE 2A REPL. DOLOMITE (2)	XC, ?	575	2862	37
A652-9-1	ZONE 2A/ZONE 1 REPL DOL (1)	XC, ?	770	4178	
A679-30-1	ZONE 2A REPL. DOLOMITE (2)	XM, GS	521	2278	36
A679-38-1	ZONE 2A REPL. DOLOMITE (2)	XC, GS	625	3064	42
A679-45-1	ZONE 2A REPL. DOLOMITE (3)	XC, ?	1170	5870	26
A679-45-2	ZONE 2A REPL. DOLOMITE (3)	XC, ?	1100	5136	27
A679-6-2	ZONE 2A REPL. DOLOMITE (2)	XC, GS	659	3018	34
I295-10-1	ZONE 2A/ZONE 1 REPL DOL (1)	XC, GS	551	2391	37
I295-10-2	ZONE 2A REPL. DOLOMITE (2)	XC, GS	623	2612	41
I295-11-1	ZONE 2A/ZONE 1 REPL DOL (1)	XC, GS	558	2693	36
I295-11-2	ZONE 2A/ZONE 1 REPL DOL (2)	XC, GS	599	2841	43
I295-11-3	ZONE 2A/ZONE 1 REPL DOL (2)	XC, GS	633	3154	40
I295-11-4	ZONE 2A/ZONE 1 REPL DOL (2)	XC, GS	538	2443	45
I295-5-1	ZONE 2A REPL. DOLOMITE (1)	XC, GS	569	3067	36
I295-5-2	ZONE 2A REPL. DOLOMITE (3)	XC, GS	579	3442	37
I295-6-1	ZONE 2A REPL. DOLOMITE (1)	XC, GS	995	5058	31
A616-9-1	ZONE 2A REPL. DOLOMITE (5)	XM, NOD	699	2273	62
A623-26-2	ZONE 2A REPL. DOLOMITE (4)	XF, NOD	327	1874	45
I297-2-2	ZONE 2A REPL. DOLOMITE (3)	XM, NOD	895	3067	65
A616-8-2	ZONE 2A REPL. DOLOMITE (2)	XM, NOD	374	1754	42
A618-11A-2	ZONE 2A REPL. DOLOMITE (5)	XM, NOD	215	1682	40
A652-19-2	ZONE 2A REPL. DOLOMITE (2)	XM, NOD	907	4914	48
A591-113-1	ZONE 2A REPL. DOLOMITE (5)	XM, NOD	287	2582	57
I297-2-1	ZONE 2A REPL. DOLOMITE (2)	XM, NOD	977	3300	72
A652-19-1	ZONE 2A REPL. DOLOMITE (2)	XM, NOD	593	3461	43
A92-9B-1	ZONE 2A REPL. DOLOMITE (4)	XM, NOD	474	2121	43
A616-11A-1	ZONE 2A REPL. DOLOMITE (5)	XM, NOD	394	2228	34

A623-26-1	ZONE 2A REPL. DOLOMITE (4)	XF, NOD	337	1968	43	
A591-113-2	ZONE 2A REPL. DOLOMITE (4)	XM, NOD	266	2431	61	
A682-12-1	ZONE 2B DOLOMITE CEMENT (1)		147	596	31	
A682-12-2	ZONE 2B DOLOMITE CEMENT (1)		129	522	33	
A682-12-7	ZONE 2B DOLOMITE CEMENT (1)		175	734	34	
A583-28-1	ZONE 2B DOLOMITE CEMENT (1)		150	506	40	
A458-24-1	ZONE 2B DOLOMITE CEMENT (1)		146	613	41	
A458-24-2	ZONE 2B DOLOMITE CEMENT (1)		239	1024	44	
A591-82-1	ZONE 2B DOLOMITE CEMENT (1)		98	239	48	
A591-82-2	ZONE 2B DOLOMITE CEMENT (1)		101	302	43	
A591-82-3	ZONE 2B DOLOMITE CEMENT (1)		100	355	40	
A583-27-1	ZONE 2B DOLOMITE CEMENT (2)		154	732	35	
A591-33A	ZONE 2B DOLOMITE CEMENT (3)		132	550	44	
A652-5A	ZONE 2B DOLOMITE CEMENT (2)		263	1288	42	
A257-2C-3	ZONE 2B DOLOMITE CEMENT (1)		290	1020	45	
A583-28-3	ZONE 3 DOLOMITE CEMENT (2)		241	66	96	
A583-28-4	ZONE 3 DOLOMITE CEMENT (2)		230	3	100	
A583-28-5	ZONE 3 DOLOMITE CEMENT (2)		233	1	90	
A583-28-6	ZONE 3 DOLOMITE CEMENT (4)		248	13	112	
A583-28-8	ZONE 3 DOLOMITE CEMENT (3)		253	0	107	
A583-18-1	ZONE 3 DOLOMITE CEMENT (3)		335	727	56	
A583-18-2	ZONE 3 DOLOMITE CEMENT (5)		271	671	100	
A591-21-1	ZONE 3 DOLOMITE CEMENT (4)		269	788	131	
A591-83-1	ZONE 3 DOLOMITE CEMENT (5)		235	800	113	
A591-117A	ZONE 4 DOLOMITE CEMENT (5)		739	3979	87	
I265-27-2	ZONE 4 DOLOMITE CEMENT (3)		1319	9316	133	
A623-17A	LATE O-Y CALCITE (5)	PURP	3013	1018	121	2400
A624-12A	LATE O-Y CALCITE (5)	PURP	4805	1469	91	2320
A652-15A	LATE O-Y CALCITE (2)	PINK	1629	265	193	2190
A616-16-1	LATE O-Y CALCITE (5)	PINK/PURP	2341	596	174	3262
A623-13-1	LATE O-Y CALCITE (5)	PINK/PURP	1739	236	151	2011
A622-9B-1	LATE O-Y CALCITE (4)	PINK/PURP	1866	495	114	2017
A458-8-1	LATE O-Y CALCITE (5)	PURP	3129	956	155	1715
A624-22A	LATE DULL CALCITE (5)	PURP	407	873	510	1710
A591-92A	LATE DULL CALCITE (5)	PINK	74	93	214	1240

[1]Data reported as average of (N) duplicate samples.

For zone 2A replacement dolomite, ZONE 2A/ZONE 1 = zone 1 dolomite cores present, XF = finely crystalline, XM = medium crystalline, XC = coarsely crystalline. Precursor lithology of dolomites identified as MAR CEM = marine cement, FENEST = fenestral carbonate, THROMB = thrombolite, GS = grainstone, REEF = shelf edge algal reef, NOD = nodular bedded carbonate, ? = fabric destructive, coarse dolomite. For late calcite, O-Y = bright orange-yellow luminescence, DULL = dull luminescence; stain color indicated in next column.

APPENDIX III: ICP ANALYSIS OF BCS NO. 368 DOLOMITE STANDARD

APPENDIX III: SUMMARY OF ICP ANALYSIS OF British Chemical Standard No. 368 Dolomite

	this study (ppm)	certificate of analysis (ppm)
Ca	216000±7800 (±3.6%)	219850±850
Mg	126150±4400 (±3.5%)	126150±850
Fe	1060±100 (±9.5%)	1760±75
Mn	491±19 (±3.9%)	474±9
Sr	77±2 (±2.6%)	67±15

Error shown is 1σ standard deviation

In this study, 39 samples of B.C.S. No. 368 were analysed.

APPENDIX IV: STABLE ISOTOPE DATA

APPENDIX IV: STABLE ISOTOPE DATA

SAMP. ID.	SAMPLE DESCRIPTION[1]		$\delta^{13}C$	$\delta^{18}O$
A458-7 (2)-2	MARINE CALCITE CEMENT		0.39	-7.24
A458-7 (3)-2	MARINE CALCITE CEMENT		0.70	-6.82
A458-7 (3)-3	MARINE CALCITE CEMENT		0.68	-6.28
A458-7 (4)-1	MARINE CALCITE CEMENT		0.21	-7.49
A458-7 (4)-3	MARINE CALCITE CEMENT		0.43	-6.59
A458-7 (4)-5	MARINE CALCITE CEMENT		0.42	-6.40
A624-1-1	MARINE CALCITE CEMENT		0.54	-6.08
A624-1-3	MARINE CALCITE CEMENT		0.20	-8.73
A624-1-5	MARINE CALCITE CEMENT		0.45	-10.02
A624-1-7	MARINE CALCITE CEMENT		0.02	-8.19
A624-7-1	MARINE CALCITE CEMENT		0.66	-7.11
A583-51-1	MARINE CALCITE CEMENT		0.31	-7.47
A583-52-1	MARINE CALCITE CEMENT		0.61	-7.36
A583-52-2	MARINE CALCITE CEMENT		0.28	-6.35
A583-60-1	MARINE CALCITE CEMENT		0.59	-6.99
A583-60-2	MARINE CALCITE CEMENT		0.58	-6.89
A452-6-1	MARINE CALCITE CEMENT		0.68	-7.30
A452-6-4	MARINE CALCITE CEMENT		0.74	-6.56
A452-6-3	MARINE CALCITE CEMENT		0.80	-6.73
I265-13B-1	ZONE 2A REPL. DOLOMITE	XF, CAL	1.45	-8.97
I265-13A	ZONE 2A REPL. DOLOMITE	XF, CAL	1.30	-9.37
A679-6-1	ZONE 2A REPL. DOLOMITE	XF, GS	1.55	-9.28
A679-6-2	ZONE 2A REPL. DOLOMITE	XF, GS	1.46	-9.30
A623-6-1	ZONE 2A REPL. DOLOMITE	MAR CEM	1.25	-7.93
A229-4-1	ZONE 2A REPL. DOLOMITE	XF, FENEST	1.60	-8.86
I265-3	ZONE 2A REPL. DOLOMITE	XF, FENEST	1.05	-8.92
A257-1B-1	ZONE 2A REPL. DOLOMITE	XF, REEF	1.24	-8.31
A257-1B-2	ZONE 2A REPL. DOLOMITE	XF, REEF	1.28	-8.34
A257-3-1	ZONE 2A REPL. DOLOMITE	XF, REEF	1.30	-8.60
A206-1-1	ZONE 2A/ZONE 1 REPL. DOL.	XF, REEF	1.02	-9.29
A257-1A-1	ZONE 2A/ZONE 1 REPL. DOL.	XF, REEF	1.03	-7.44
A257-2A-2	ZONE 2A/ZONE 1 REPL. DOL.	XF, REEF	1.16	-8.48
A257-1B-4	ZONE 2A/ZONE 1 REPL. DOL.	XF, REEF	1.30	-8.29
A257-2C-2	ZONE 2A/ZONE 1 REPL. DOL.	XF, REEF	1.03	-7.86
A679-11	ZONE 2A REPL. DOLOMITE	XF, THROMB	1.45	-10.23
A679-10	ZONE 2A REPL. DOLOMITE	XF, THROMB	1.62	-8.14
A623-26-1	ZONE 2A REPL. DOLOMITE	XF, NOD	1.24	-8.72
A206-4-1	ZONE 2A REPL. DOLOMITE	XM, REEF	1.15	-8.78
A206-6-1	ZONE 2A/ZONE 1 REPL. DOL.	XM, REEF	1.01	-9.02
A679-30-1	ZONE 2A REPL. DOLOMITE	XM, GS	1.45	-8.69
A229-22-1	ZONE 2A REPL. DOLOMITE	XM, THROMB	1.17	-8.48
A92-9B-1	ZONE 2A REPL. DOLOMITE	XM, NOD	1.29	-9.20

A591-113-2	ZONE 2A REPL. DOLOMITE	XM, NOD	1.40	-9.64
A618-11A-2	ZONE 2A REPL. DOLOMITE	XM, NOD	0.81	-8.62
A652-19-1	ZONE 2A REPL. DOLOMITE	XM, NOD	1.82	-8.61
I297-2-1	ZONE 2A REPL. DOLOMITE	XM, NOD	1.19	-6.93
I295-4-1	ZONE 2A REPL. DOLOMITE	XC, GS	1.50	-8.11
I295-4-2	ZONE 2A REPL. DOLOMITE	XC, GS	1.58	-8.36
A679-38-1	ZONE 2A REPL. DOLOMITE	XC, GS	1.44	-8.68
A652-9-1	ZONE 2A/ZONE 1 REPL. DOL.	XC, ?	1.38	-9.06
I295-11-3	ZONE 2A/ZONE 1 REPL. DOL.	XC, GS	1.50	-8.50
I295-6-1	ZONE 2A REPL. DOLOMITE	XC, GS	1.16	-9.38
I295-5-1	ZONE 2A REPL. DOLOMITE	XC, GS	1.19	-9.89
I295-11-4	ZONE 2A/ZONE 1 REPL. DOL.	XC, GS	1.47	-8.39
A679-45-1	ZONE 2A REPL. DOL.	XC, ?	1.13	-9.33
A583-28-8	ZONE 2B DOLOMITE CEMENT		0.91	-9.45
A583-28-9	ZONE 2B DOLOMITE CEMENT		0.91	-9.17
A682-12-1	ZONE 2B DOLOMITE CEMENT		0.40	-7.80
A682-12-2	ZONE 2B DOLOMITE CEMENT		0.82	-7.58
A682-12-3	ZONE 2B DOLOMITE CEMENT		0.78	-7.38
A591-117-4	ZONE 2B DOLOMITE CEMENT		0.67	-10.30
A591-33-1	ZONE 2B DOLOMITE CEMENT		1.10	-8.66
A458-24-A	ZONE 2B DOLOMITE CEMENT		0.93	-9.63
A591-82-A	ZONE 2B DOLOMITE CEMENT		1.04	-9.20
A583-27-1	ZONE 2B DOLOMITE CEMENT		0.75	-7.36
A583-28-1	ZONE 3 DOLOMITE CEMENT		-0.52	-13.11
A583-28-2	ZONE 3 DOLOMITE CEMENT		-0.37	-13.14
A583-28-3	ZONE 3 DOLOMITE CEMENT		-0.71	-13.25
A583-28-4	ZONE 3 DOLOMITE CEMENT		-0.01	-13.15
A583-28-5	ZONE 3 DOLOMITE CEMENT		-0.26	-13.62
A583-28-6	ZONE 3 DOLOMITE CEMENT		-0.59	-13.51
A583-28-7	ZONE 3 DOLOMITE CEMENT		-0.37	-13.04
A682-12-5	ZONE 3 DOLOMITE CEMENT		0.37	-13.71
A583-18-1	ZONE 3 DOLOMITE CEMENT		0.45	-13.75
A583-18-3	ZONE 3 DOLOMITE CEMENT		0.55	-13.39
A591-117-2	ZONE 4 DOLOMITE CEMENT		0.68	-13.24
A591-117-3	ZONE 4 DOLOMITE CEMENT		0.63	-13.57
A591-124-1	ZONE 4 DOLOMITE CEMENT		0.92	-11.30
A591-124-2	ZONE 4 DOLOMITE CEMENT		0.76	-13.83
A624-21-1	ZONE 4 DOLOMITE CEMENT		0.45	-13.44
A624-21-2	ZONE 4 DOLOMITE CEMENT		0.86	-12.50
I265-27-2	ZONE 4 DOLOMITE CEMENT		0.38	-13.45
A624-39-1	LATE O-Y CALCITE		-0.17	-9.88
A624-22-4	LATE O-Y CALCITE		-0.16	-8.81
A624-22-5	LATE O-Y CALCITE		-0.17	-7.30
A624-22-6	LATE O-Y CALCITE		-0.36	-7.26
A623-3-1	LATE O-Y CALCITE		-0.35	-14.69
A623-3-2	LATE O-Y CALCITE		-0.33	-14.46
A623-4-1	LATE O-Y CALCITE		-0.35	-9.50

A623-17-1	LATE O-Y CALCITE	-0.84	-11.73
A624-12-A-1	LATE O-Y CALCITE	-3.80	-7.51
A652-15-A	LATE O-Y CALCITE	-4.67	-9.07
A624-12-A-2	LATE O-Y CALCITE	-3.86	-7.62
A616-16-1	LATE O-Y CALCITE	-1.83	-8.80
A622-13-1	LATE O-Y CALCITE	-2.53	-6.79
A622-9B-1	LATE O-Y CALCITE	-0.41	-8.82
A458-8-1	LATE O-Y CALCITE	-1.39	-8.83
A458-8-A	LATE O-Y CALCITE	-1.91	-10.31
A458-8-B	LATE O-Y CALCITE	-0.80	-7.81
A458-8-C	LATE O-Y CALCITE	-1.83	-13.95
A616-16-A	LATE O-Y CALCITE	-0.84	-6.58
A616-16-B	LATE O-Y CALCITE	-1.40	-11.15
A616-16-C	LATE O-Y CALCITE	-0.81	-6.75
A616-16-D	LATE O-Y CALCITE	-1.47	-11.46
A624-22-2	LATE DULL CALCITE	-0.08	-10.47
A624-22-3	LATE DULL CALCITE	-0.26	-10.96
A591-92-A	LATE DULL CALCITE	-0.99	-16.57
NBS 19	ISOTOPE STANDARD	2.08	-2.11
	(ACCEPTED VALUE)	(1.92)	(-2.19)
A591-21	AUTHIGENIC QUARTZ		+20.16
A591-92	AUTHIGENIC QUARTZ		+20.24

Carbonate data reported relative to PDB, quartz relative to SMOW.

[1]For zone 2A replacement dolomite, ZONE 2A/ZONE 1 = zone 1 dolomite cores, XF = finely crystalline, XM = medium crystalline, XC = coarsely crystalline. Precursor lithology of dolomites identified as CAL = cryptalgal laminite, GS = grainstone, MAR CEM = marine cement, FENEST = fenestral carbonate, REEF = shelf edge algal reef, THROMB = thrombolite, NOD = nodular bedded carbonate, ? = fabric destructive, coarse dolomite. For late calcite, O-Y = bright orange-yellow luminescence, DULL = dull luminescence.

APPENDIX V: $^{87}Sr/^{86}Sr$ DATA

APPENDIX V: $^{87}Sr/^{86}Sr$ DATA

SAMPLE NO.	DESCRIPTION [1]	$^{87}Sr/^{86}Sr$ [2]
A452-6	MARINE CALCITE CEMENT	0.70869±4
A458-7	MARINE CALCITE CEMENT	0.70957±2
A583-60	MARINE CALCITE CEMENT	0.70959±3
A624-7	MARINE CALCITE CEMENT	0.70975±4
A623-6	ZONE 2A DOL. (MAR. CEM)	0.70900±4
A679-6	ZONE 2A DOL. (XF, GS)	0.70966±3
I265-2	ZONE 2A DOL. (XF, GS)	0.70951±3
A257-2A	ZONE 2A DOL. (XF, REEF)	0.70938±3
I295-4	ZONE 2A DOL. (XC, GS)	0.70971±4
A229-36	ZONE 2A DOL. (XC, GS)	0.70950±3
A591-117-2	ZONE 2B DOLOMITE CEMENT	0.70933±4
A583-28-1	ZONE 2B DOLOMITE CEMENT	0.70966±4
A591-33	ZONE 2B DOLOMITE CEMENT	0.70944±3
A623-54	ZONE 2B DOLOMITE CEMENT	0.70963±3
A583-28-2	ZONE 3 DOLOMITE CEMENT	0.71072±3
A583-18	ZONE 3 DOLOMITE CEMENT	0.71033±3
A591-117-3	ZONE 4 DOLOMITE CEMENT	0.71025±4
I265-27	ZONE 4 DOLOMITE CEMENT	0.71445±4
A623-17	LATE CALCITE (O-Y)	0.71075±4
A624-12	LATE CALCITE (O-Y)	0.70963±4
A624-22	LATE CALCITE (DULL)	0.71111±3
A591-92S	LATE CALCITE (DULL)	0.71234±3

[1] XF, XC = finely and coarsely crystalline dolomite, respectively. MAR. CEM. = dolomitized marine cement, GS = dolomitized grainstone, REEF = dolomitized reef. For late calcite cements, luminescence in parantheses, O-Y = bright orange yellow.

[2] NBS SRM 987 = 0.71022, Sr isotopic precisions (1σ) occur in the last decimal place.

The vita has been removed from the scanned document